Influence of Potassium and Sodium Salts, Calcium and Phosphorus on Agglomeration Behaviour of Biomass and Quartz Sand under Combustion and Gasification Atmospheres

Thesis submitted for the degree of Doctor of Philosophy

Zimeng He

School of Chemical Engineering and Advanced Materials

Faculty of Engineering, Computer & Mathematical Sciences

The University of Adelaide, Australia

March 2020

Table of Contents

Preface

All the work presented in this thesis was carried out within the School of Chemical Engineering & Advanced Materials at the University of Adelaide between 2015 and 2019. The four following journal papers contain the main body of work of this thesis:

Paper I: He, Z.; Saw, W. L.; van Eyk, P. J.; Nathan, G. J.; Ashman, P. J., Interactions between Quartz Sand and Wood Doped with either K or Na Salts under Steam Gasification and Combustion Atmospheres. Industrial & Engineering Chemistry Research 2020, 59, (4), 1712-1722.

Paper II: He, Z.; Saw, W. L.; van Eyk, P. J.; Nathan, G. J.; Ashman, P. J., Effect of Calcium and Phosphorus on Interactions between Quartz Sand and K-Salt-Doped Wood under Both Steam Gasification and Combustion Atmospheres. Energy & Fuels 2020, 34, (3), 3210-3222.

Paper III: He, Z.; Lane, D. J.; Saw, W. L.; van Eyk, P. J.; Nathan, G. J.; Ashman, P. J., Ash–Bed Material Interaction during the Combustion and Steam Gasification of Australian Agricultural Residues. Energy & Fuels 2018, 32, (4), 4278-4290.

Paper IV: He, Z.; Saw, W. L.; Lane, D. J.; van Eyk, P. J.; de Nys, R.; Nathan, G. J.; Ashman, P. J., The ash-quartz sand interaction behaviours during steam gasification or combustion of a freshwater and a marine species of macroalgae. Fuel 2020, 263, 116621.

Abstract

Alkali metals (potassium and sodium) are usually present as inorganic salts or organic-associated elements in biomass and are major contributors to bed agglomeration. This thesis investigated interactions between quartz sand and wood doped with individual alkali salts, together with the effects of Ca and P on such interactions. The interactions behaviours of several agricultural residues and macroalgae with different compositions of alkali salts, Ca and P were assessed. The effect of the reaction atmosphere was also evaluated.

All the tests were conducted in a lab-scale, fixed-bed reactor at 900 °C under either a steam gasification (50% v/v steam) or a combustion (5% v/v O_2) atmosphere, respectively. Techniques, including scanning electron microscope in combination with energy dispersive spectroscopy (SEM-EDS), X-ray diffraction (XRD), acid digestion, water leaching and Atomic Absorption Spectrophotometer (AAS) analyses, were applied.

Significant bed agglomerates were observed for wood doped with alkali carbonate, acetate or sulfate, especially during steam gasification. In contrast, the formation of alkali silicates was much lower for alkali chloride-doped wood, especially during combustion, when only insignificant agglomerates were formed. The reactions between gaseous alkali metals and quartz sand contributed to the agglomerates' formation, especially for K salts.

The formation of alkali silicates in the agglomerates decreased significantly with the increase of Ca content, while molten alkali phosphate ash formed agglomerates via a melting-induced mechanism. The co-existence of Ca and P generated K-Ca phosphates, and the influence of the K-Ca phosphates on the interaction behaviours and the K retention in agglomerates varied significantly with the K salts species.

Compared with the combustion atmosphere, steam exacerbated bed agglomeration for the coating-induced mechanism but not for the melting-induced mechanism. Steam affected biomass ash-quartz sand interactions both by increasing the alkali metals' retention and the fractions of alkali silicates with high melting points in the

agglomerates and by facilitating the gas-solid phase reactions.

The interaction behaviours of several agricultural residues and macroalgae were consistent with those of individual alkali salt-doped wood. A high P and low Ca content in *Oedogonium intermedium* (ODN) resulted in the co-existence of both melting-induced and coating-induced mechanisms. Fuel-derived molten alkali silicates formed the wheat straw agglomerates via a melting-induced mechanism. For grape marc, cotton stalk and *Derbesia tenuissima* (Deb), alkali metals reacted with Si in the quartz sand to form agglomerates, with K-Ca phosphates distributed within these agglomerates. Steam significantly increased the size of the grape marc and Deb agglomerates. Except for Deb during combustion, the size of the agglomerates of the tested biomass increased significantly by increasing the reaction time under both atmospheres.

This thesis contributes to the comprehensive understanding of biomass ash-quartz sand interactions for various types of biomass with different inorganic compositions during steam gasification or combustion.

DECLARATION

I certify that this work contains no material which has been accepted for the award of any other degree or diploma in my name, in any university or other tertiary institution and, to the best of my knowledge and belief, contains no material previously published or written by another person, except where due reference has been made in the text. In addition, I certify that no part of this work will, in the future, be used in a submission in my name, for any other degree or diploma in any university or other tertiary institution without the prior approval of the University of Adelaide and where applicable, any partner institution responsible for the joint-award of this degree.

I acknowledge that copyright of published works contained within this thesis resides with the copyright holder(s) of those works.

I also give permission for the digital version of my thesis to be made available on the web, via the University's digital research repository, the Library Search and also through web search engines, unless permission has been granted by the University to restrict access for a period of time.

21/03/2020

Zimeng He   Date

ACKNOWLEDGEMENT

Guo and Gule Li, for their help and accompany. I would like to acknowledge the staff in the Chemical Engineering workshop, especially Jason Peak, for helping me to build my reactor. I would like to thank the ladies in the Chemical Engineering Office, Michelle Fitton, Sue Earle and Monica Dinan, for their administrative assistance. I would like to thank Alison Jane Hunter for her assistance in proofreading my thesis.

Finally, I want to express my gratitude to my family members for their support, especially to my mother. Without all her support, encouragement and love, I could not finish this tough journey.

Chapter 1. Introduction

1.1 Background

Growing concerns about the environmental issues attributed to the utilization of fossil fuels as an energy resource have driven people to search for alternative renewable fuels. Biomass, as a biofuel, has low net carbon dioxide intensity and is increasingly regarded as a critical renewable future energy resource worldwide. Among various types of biomass, agricultural residues are a low cost and abundant biomass, while macroalgae have high productivity and tolerate various cultivation conditions [1, 2]. These make them promising biofuels that meet the increasing demand for energy. Thermochemical conversion processes, such as gasification and combustion, are efficient technologies for the transformation of biomass to energy. However, the high ash and alkali metals content of agricultural residues and macroalgae lead to several ash-related issues during the gasification or combustion process [3, 4]. Agglomeration, one of the ash-related issues typically occurring in fluidized bed reactors, generally results from the adhesion of bed materials to the coating layer formed from reactions between alkali metals with Si or P either from the bed material or the feedstock. The adhesion of bed materials causes the formation of large agglomerates that then lead to the defluidization of fluidized bed reactors, which severely limits the utilization of agricultural residues and macroalgae as the feedstock in fluidized bed reactors [5]. Therefore, it is critical to investigate the interactions between the bed material and the ash of agricultural residues and macroalgae to achieve a better understanding of the agglomeration mechanisms.

Most of the studies on agglomeration have only focused on raw biomass [6, 7]. However, the composition of different water-soluble alkali salts or organic-associated alkali metals, the major contributors to agglomeration, within biomass is complex. In addition, other inorganic elements, such as Ca and P, in biomass have significant impacts on agglomeration behaviours in the presence of alkali salts. This investigation into the interactions between bed material and individual alkali metals in biomass, together with the effects of Ca and P on these interactions, will contribute significantly to a better understanding of the agglomeration behaviours of various types of biomass, with different compositions of inorganic matter.

Bed agglomeration characteristics of fluidized bed reactors are affected by both the particle physics and the ash-bed material interactions [8]. The ash-bed material interactions of agglomeration, which are very important for understanding agglomeration mechanisms, can be studied in a fixed-bed reactor without the effect of particle physics. Furthermore, most investigations into bed agglomeration have only been performed on agglomerates obtained after the bed has been defluidised [9]. Therefore, investigation of the time-dependent formation process of the coating layer for agglomeration is important to better understand the agglomeration mechanism, which is easily achieved in a fixed-bed reactor. Therefore, the biomass ash-bed material interaction behaviours in the present work were assessed in a fixed-bed reactor. The time-dependent layer formation process was investigated.

The reaction atmosphere of combustion or gasification plays a vital role in bed agglomeration. The steam gasification atmosphere affects the morphology of the agglomerates and the generation of alkali silicates significantly, when compared with other atmospheres [10]. Understanding of the effect of the reaction atmosphere (steam gasification vs combustion) on the biomass ash-bed material interaction behaviour contributes to some practical utilizations, such as dual fluidized bed gasifiers, which have both steam gasification and combustion atmospheres.

The principal aim of the thesis is to provide a comprehensive, fundamental understanding of the biomass ash-quartz sand interaction behaviours and the time-dependent layer formation process for agglomerates. The interaction behaviours between quartz sand and individual alkali metals in biomass, together with the effects of Ca and P on these interactions, were also assessed and compared with the interaction behaviours of several agricultural residues and macroalgae with different inorganic compositions. This thesis also contributes to a better understanding of the difference between the biomass ash-quartz sand interaction behaviours under a steam gasification or a combustion atmosphere.

1.2 Scope and structure of the thesis

Chapter 2 gives a review of the important literatures, which identifies the research gaps of this thesis. The emphasis of the review is on the following areas: bed

agglomeration of agricultural residues and macroalgae, the time-dependent layer formation process of biomass, interactions between quartz sand and individual alkali salts in biomass, and the effects of Ca or P, or both, along with the steam gasification atmosphere on biomass bed agglomeration. The limitations in the literature, which directs the work presented in the subsequent chapters, are also discussed at the end of this chapter.

Chapter 3 presents the interaction behaviour between quartz sand and wood doped with individual alkali salts (K or Na carbonate, acetate, chloride, sulfate and phosphate) in biomass (first journal publication). The time-dependent layer formation process and the gas-solid phase reactions between gaseous alkali metals and the bed material were assessed for different individual alkali salts in wood samples. The impact of the steam gasification atmosphere on the formation of various types of alkali silicates in the agglomerates was compared with that of the combustion atmosphere.

Chapter 4 presents the effect of Ca and P, two important inorganic elements in biomass, on the interaction behaviour between quartz sand and wood doped with individual K salts (K_2CO_3, K_2SO_4 and KCl) in biomass under a steam gasification or a combustion atmosphere (second journal publication). The effect of either Ca or P on the agglomerates' formation was assessed. The impact of the co-existence of Ca and P and the formation of Ca phosphates on interaction behaviours was also evaluated.

Chapters 5 and 6 present the interaction behaviours between quartz sand and several agricultural residues (grape marc, wheat straw and cotton stalk) or macroalgae (*Oedogonium intermedium* (denoted as ODN) and *Derbesia tenuissima* (denoted as Deb)) with various compositions of alkali metals, Ca and P (the third and fourth journal publications, respectively). The time-dependent layer formation process was assessed for the biomass. The effect of the steam gasification atmosphere on the formation of agglomerates was evaluated for the biomass and compared with that of the combustion atmosphere.

Chapter 7 presents conclusions from the body of work, along with

recommendations for future work in this area of research.

References cited in Chapters 1, 2 and 7 are given at the end of the thesis. Other references cited in each journal papers are provided within the journal paper themselves.

Chapter 2. Literature Review

2.1 Bed agglomeration of Agricultural residues and macroalgae

2.1.1 Agricultural residues

Climate change, depletion of fossil fuels and the drastic increase in global population call for more sustainable and eco-friendly energy resources [11-13]. Agricultural residues, as typical second generation biofuels, are important sources of renewable energy and widely distributed all over the world. The advantage of agricultural residues is their low price, no demand for additional arable land and high level of production. Utilisation of agricultural residues as energy resource reduces the consumption of valuable woody biomass and the short growth period of agricultural residues promises continuity of energy production [14]. The production of agricultural residues is approximately 10^{10} Mt worldwide, equivalent to an energy value of 47 EJ [15]. Therefore, agricultural residues are promising energy resources to replace fossil fuels.

Australia has abundant resources of agricultural residues, such as wheat straw, grape marc and cotton stalk. Wheat straw is one of the major agricultural residues worldwide [14]. Wheat straw and grape marc, are the residues from wheat production and the wine industry, respectively. Wheat can produce approximately 2.5-5 t/ha of straw, while 10-15% of the grape material ends up as grape marc during winery process. Australia is one of the world's largest cotton producers. Cotton stalk, the residues left after cotton harvest, is a promising energy resource, as it has appropriate properties and a similar structure to woody fuels [16]. During 2015-2016, in Australia, the production of wheat for grain and grape for wine were approximately 22Mt and 1.6Mt, respectively, while approximately 0.3M ha cotton was planted. To sum up, wheat straw, grape marc and cotton stalk are anticipated to play important roles as future sources of bioenergy.

Even though the production of agricultural residues is enormous in many countries, their major utilisations are usually limited to animals feeding, being burned in the field or being disposed of as landfill [17, 18]. The improper management of agricultural residues causes pollution problems [13, 19]. Therefore, it is essential and pressing to develop more efficient and environmentally friendly techniques that

utilise agricultural residues.

2.1.2 Macroalgae

Macroalgae are important third generation biofuels. They have a high photosynthetic efficiency (6-8%) and a high growth rate [20-23]. They can be cultivated in wastewater or seawater, without the need of extra fertilizer or competition for arable land or fresh water for irrigation [21, 24]. The life cycle of macroalgae is short and they can be harvested up to five times a year [21]. Macroalgae are very environmentally friendly and biodegradable [2]. They can be used to treat wastewater [22]. Compared with microalgae, macroalgae is simple to harvest due to its plant like characteristics and its high carbohydrates content makes it suitable for biofuel production [23]. Consequently, macroalgae are promising renewable energy resources to meet the increasing demand for energy worldwide.

The utilisation of macroalgae as energy resources is quite limited. The industry surrounding macroalgae is mainly aimed at food products for human consumption [25]. To explore macroalgae energy alone is not economically practicable, as the investment in macroalgae cultivation and processing is high [23, 26, 27]. The concept of utilising biomass cultivated for wastewater treatment, or biomass residues left after the extraction of high value products, as energy resources is more economically feasible. A freshwater macroalgae species, *Oedogonium intermedium* (denoted as ODN), can be cultivated to remove multiple harmful components from wastewater [28]. A marine species, *Derbesia tenuissima* (denoted as Deb), has a relatively high lipid content and can be used for bio-oil production [29]. The residues of Deb after bio-oil production can still be utilised as energy resources [26]. Both ODN and Deb have broad distribution and high productivity (specific information can be found in the fourth journal publication in Chapter 6). Therefore, they are promising macroalgae species for bioenergy production.

2.1.3 Fluidized bed gasification or combustion

Biochemical and thermochemical routes are two major processes that convert agricultural residues and macroalgae into bioenergy [22, 24, 30]. Thermochemical

processes include pyrolysis, combustion, gasification and hydrothermal treatments. Compared with other processes, thermochemical conversion processes have the following advantages: all of the biomass can be converted, higher conversion rates and the compatibility with a wide range of biomass [24, 30, 31]. Therefore, thermochemical processes are more efficient and flexible than biochemical processes for agricultural residues and macroalgae. Gasification or combustion in fluidized bed reactors are typical thermochemical processes to convert biomass into energy. The advantages of fluidized bed gasification or combustion processes are their high flexibility, uniform distribution of temperature, high conversion efficiency and adaptation to various types of biomass with different properties. [32, 33]. Therefore, fluidized bed gasification and combustion are suitable techniques to convert agricultural residues and macroalgae into bioenergy.

There are some challenging problems for the utilisation of agricultural residues or macroalage in fluidized bed gasification or combustion processes. Agricultural residues are normally rich in alkali metals [3]. Macroalgae generally have a much higher ash content (13.1–42.8% (mean 26.6%)) and alkali metals and halogen content (0.5–11%) than terrestrial biomass [4, 23]. The inorganic elemental composition of agricultural residues and macroalgae easily causes bed agglomeration and limits their utilisation as feedstock in fluidized bed reactors. Therefore, the agglomeration behaviour of agricultural residues and macroalgae during fluidized bed gasification or combustion needs to be investigated before appropriate countermeasures can be proposed.

2.1.4 Bed agglomeration

Agglomeration is a common ash-related problem occurring in fluidized bed reactors. Agglomeration causes defluidisation of the bed and can even cause an unscheduled shutdown of the whole reactor [34]. The frequent shutdown and start-up of reactors can reduce the profit and the lifespan of the plant [35]. Agglomeration is usually induced by the formation of sticky liquids, which increase inter-particle forces and adhere bed materials to form large agglomerates. The sticky liquids are further strengthened by sintering. In fluidized bed reactors, if the inter-particle forces of

the bed material developing through the formation of sticky liquids are increased to the same order of magnitude as the gravitational force on the particles of the bed material, the bed tends to attain defluidisation [34]. Many types of biomass feedstock have the problem of agglomeration in fluidized bed reactors. The agglomeration behaviour depends significantly on the inorganic elemental composition of feedstock. The inorganic elemental composition of agricultural residues and macroalgae is complicated due to the complexity of their species. Therefore, the agglomeration behaviour of various types of agricultural residues and macroalgae with different inorganic elemental compositions needs to be assessed for their utilisation in fluidized bed reactors.

Alkali metals play vital roles in biomass bed agglomeration [36]. Two major biomass bed agglomeration mechanisms are identified: one is a melting-induced mechanism, which is fuel-derived partially molten alkali silicate or phosphate ash that adheres bed particles together to form agglomerates; the other one is a coating-induced mechanism, which is where alkali metals from the fuel react with Si from the bed material to form alkali silicate [3]. Ohman et al. [37] have found that both Ca and K influence the bed agglomeration significantly, as K increases the amount of melt in the coating layer, while Ca decreases it. Brus et al. [7] have also identified the agglomeration behaviour for biomass with different K, Ca or Si compositions: for woody biomass with a high Ca and a low K content, an alkali silicate coating layer forms, followed by the diffusion of Ca into the coating layer; for biomass with a high K content, the coating layer is formed by alkali silicate, followed by viscous-flow sintering and agglomeration; for biomass with a high K and reactive Si content, a coating layer is formed by the adhesion of the bed material to the partially molten fuel-derived ash particles of alkali silicate. Other bed agglomeration formation processes have also been suggested, such as the adhesion of bed particles to high temperature burning char particles [38], reactions between the bed material and alkali metals from the attached ash particles, or the diffusion of these alkali metals into the coating layer on the surface of the bed material [39, 40]. Compared with agricultural residues, fewer studies have been performed for algae fuels, which are limited to certain algae species [41-45]. Many types of agricultural residues and macroalgae are rich in P [4, 46], which tends to form the partially molten alkali

phosphate ash that induces bed agglomeration via a melting-induced mechanism [47]. For both agricultural residues and macroalgae, alkali metals are the major contributors to bed agglomeration. The agglomeration behaviour of alkali metals is significantly affected by other inorganic elements in agricultural residues and macroalgae, such as Ca, P or Si. However, the alkali metals in agricultural residues and macroalgae are present as different types of alkali salts or organic-associated alkali metals. The impact of the composition of alkali salts in these fuels on the bed agglomeration behaviour is different. In addition, the effect of other inorganic elements on the agglomeration behaviour of agricultural residues and macroalgae with different alkali salts' compositions is different. This knowledge is critical for a better understanding of the agglomeration behaviour of alkali metals in agricultural residues and macroalgae. Therefore, more work need to be done to evaluate the agglomeration behaviour of agricultural residues and macroalgae with different alkali salts' compositions.

2.1.5 Time-dependent layer formation

Although biomass bed agglomeration behaviour has been investigated by many studies, most of the studies have been performed on the agglomerates after the bed has been defluidised [9]. Little work has been done to assess the time-dependent coating layer formation process of bed agglomeration, which is essential for the better understanding of bed agglomeration. The layer formation process for different bed materials, including quartz sand, olivine, ilmenite, manganese ore, Na-Feldspar and K-Feldspar, has been assessed [48-55]. He et al. [48, 49] have evaluated the time-dependent layer formation process of woody fuels with quartz sand as the bed material during combustion in a fluidised bed reactor. They have discovered that, at an early stage of layer formation, K from the fuel reacts with the quartz sand to form a K silicate coating layer with a high K/Ca ratio. The Ca rich ash particles then attach to the sticky inner K silicate coating layer, which forms the inhomogeneous outer coating layer. Then, Ca from the outer coating layer gradually diffuses into the inner coating layer. The growth of the inner layer is fast at the initial stage, with a rise in the Ca/Si ratio and a decline in the K/Ca ratio, while both the growth of the inner layer and the changes in these ratios become much slower

after several weeks. The formation of the final Ca silicate inner coating layer prohibits further reactions between K and the quartz sand, which reduces the agglomeration tendency. Investigation into the time-dependent layer formation process for agricultural residues and macroalgae with quartz sand as the bed material is necessary to achieve a better understanding of the bed agglomeration behaviour of these fuels. This information is available for some woody biomass, but the difference in the ash chemistry between woody biomass with agricultural residues or macroalgae requires more work to be done on the time-dependent layer formation process of biomass.

2.2 Interactions between quartz sand and individual alkali salts in biomass

2.2.1 Alkali metals in biomass

Alkali (K and Na) metals play essential roles in biomass bed agglomeration. Potassium (K) is an essential inorganic matter in biomass. Most of the K in biomass is highly mobile and is present as water soluble salts, while small amounts of K are organic-associated [56, 57]. Some herbaceous and agricultural biomass have a high K content [46]. The behaviour of sodium (Na) during thermochemical processes is similar to that of K but the content of Na in biomass is generally much lower than that of K [56]. Salt-tolerated biomass, such as straws and algae, are rich in Na [57]. Alkali metals (K and Na) often associate with sulfur (S), phosphorus (P) and chlorine (Cl) in biomass, as water-soluble salts. Algae is usually rich in S [57]. Some herbaceous and agricultural biomass are rich in P [46]. Most of Cl in biomass is water soluble and associated with K or Na [56]. Wood has quite a low Cl content, while salt-tolerated biomass, such as algae, straws and herbaceous biomass, is generally rich in Cl [46, 57, 58]. The composition of alkali metals in biomass is complicated and it varies significantly with the biomass species. The assessment of the agglomeration behaviour of individual alkali salts or organic-associated alkali metals in biomass is important to better understand the agglomeration behaviour of biomass with different alkali salts compositions.

Generally, alkali sulfate is formed first during biomass ash transformation [36]. However, as most biomass has a lack of S, alkali metals are generally present as

alkali chloride, which is released at around 800 °C. The amount of gaseous alkali chloride normally determines the amount of alkali metals released to the gas phase, rather than the content of alkali metals [36]. At 700-900 °C, K_2CO_3 is decomposed, which can be accelerated by steam such that K is released as KOH [59, 60]. For biomass that is lacking in Cl, KOH is the most stable K salts in the gas phase [61]. Generally, K is incorporated into silicates at 800-900 °C. The retention of K in silicates is inhibited by Ca and Mg, which are more likely to be incorporated into silicates than K [59]. Transformation of K in biomass is mainly affected by Cl and Si, while K prefers to be released as KCl, rather than retained in the ash as K silicates [59]. Only small amounts of K are released below 700 °C, which come from the organic-associated K [59, 60]. The extra amount of organic-associated K could also decompose into K_2CO_3 [62]. The behaviour of Na is similar to that of K [63]. The difference between K and Na during thermochemical processes is that K can interact with char to form intercalates, which then transform to K_2CO_3 or oxides, while the intercalation of Na with char is insignificant [62]. In addition, K can be more readily incorporated into silicates than Na, while Na is more likely to form sulfates [62]. These factors give rise to the higher release of Na than that of K above 800 °C [62]. The behaviours of different individual alkali salts or organic-associated alkali metals during biomass ash transformation are different, which implies that the agglomeration behaviour of these individual alkali salts or organic-associated alkali metals in biomass is different.

2.2.2 Reactions between quartz sand and pure individual alkali salts

The interactions between pure alkali salts in biomass and quartz sand have been assessed [64-68]. Many studies have identified that pure K_2CO_3 or Na_2CO_3 salt reacts with quartz sand during both gasification and combustion for some conditions [64-68]. No reactions take place between pure K_2SO_4 or Na_2SO_4 salt and quartz sand under either a steam atmosphere or a combustion atmosphere [64, 65, 67], while Ma et al. [67] have found that pure K_2SO_4 reacts with quartz sand under an H_2/N_2 (5 vol% H_2) atmosphere. Sevonius et al. [65] have discovered that under an H_2O/air (20% H_2O) atmosphere, pure NaCl salt has some reactions with the quartz sand to form alkali silicate. For pure KCl salt, some studies have found that

13

it reacts with quartz sand to a limited extent for some conditions, when steam is present [67, 68]. However, no reactions happen between pure KCl salt and quartz sand for a combustion atmosphere [67]. Some alkali salts can be hydrolysed by steam to form alkali hydroxide [69]. Alkali hydroxide can react with the quartz sand to form the agglomerates. The reaction between alkali chloride and quartz sand can be improved when alkali chloride is hydrolysed by steam [70]. However, the hydrolysis of alkali chloride needs quite a high temperature, which competes with the evaporation of alkali chloride [71]. The above results show that the interactions between quartz sand and pure alkali salts vary significantly with both the salt species and the reaction atmosphere. However, alkali salts in biomass not only react with quartz sand, but also react with the organic components of biomass during gasification or combustion, which affects the behaviour of the alkali salts. Therefore, interactions between quartz sand and pure alkali salts are different from interactions between quartz sand and those alkali salts that are present in biomass.

Alkali salts need to be dissociated before they can react with the organic components of fuels. Compared with alkali carbonate and sulfate, alkali chloride and alkali phosphate are relatively inert to react with the organic components of fuels [72]. Generally, alkali salts of weak acids or can be decomposed to salts of weak acids can easily be dissociated and react with the organic components of the fuels to form intermediates [69]. Conversely, alkali salts of strong acids, such as alkali chloride, cannot easily form intermediates [69]. Both K_2CO_3 and Na_2CO_3 interact with the organic components of the fuels and produce some intermediates as reactive sites, which can react with CO_2 or H_2O to facilitate gasification [73-78]. Some studies have demonstrated that the intermediates are more likely to be alkali oxides or peroxides [79, 80]. Both KCl and NaCl react with some organic groups of the fuels and K or Na becomes organic-associated [81-84]. Alkali sulfate also forms intermediates, such as oxides [72, 80]. Another possible mechanism is that it can be reduced by the organic components of the fuels to form alkali sulfide, which further transforms to alkali hydroxide under steam atmospheres [71, 85]. Although alkali phosphates are weak acid salts, they tend to form glassy compounds, which coat the surface of carbon particles to prevent their reactions with the reaction gas [69]. These intermediates are generated from reactions between alkali salts and the

14

organic components of biomass, such as alkali oxides, alkali hydroxide or organic-associated alkali metals, and can react with the quartz sand to form agglomerates. This affects the interactions between the quartz sand and alkali salts that are present in biomass significantly. Assessment of the interactions between quartz sand and individual alkali metals that are present in biomass is unlikely to be performed by evaluating raw biomass, as the inorganic elemental composition of raw biomass is complex. Therefore, doping these individual alkali salts with a low-ash content biomass, such as wood, is a valid method to achieve this assessment.

2.2.3 Reactions between quartz sand and fuel doped with individual alkali salts

Studies into the reactions between quartz sand and the individual alkali salts that are present in biomass are quite limited, although several studies have evaluated the reactions between quartz sand and alkali salt-doped coal during thermochemical conversion processes. Qi et al. [86] have found the slagging degree of Zhundong coal doped with Na_2SO_4 and NaAc is higher than that of Zhundong coal doped with NaCl. Lindner et al. [87] have showed that the amount of Na silicate that is formed by reactions between quartz sand and NaAc (sodium acetate)-doped coal is 3 to 5 times higher than that formed by reactions between quartz sand and NaCl-doped coal during combustion. Kosminski et al. [10] have discovered that NaAc-doped coal decomposes to Na_2CO_3, which reacts with silica under CO_2, N_2 and steam atmospheres, while NaCl-doped wood only reacts with silica under a steam atmosphere to a very limited extent. The above studies have mainly focused on Na salt-doped coal, while similar investigations into biomass doped with individual alkali salts, especially K salts, are still quite limited. The organic components of coal are different from those of biomass and the agglomeration behaviour of K salts in biomass is different from that of Na salts. Therefore, more work is needed to investigate the interactions between quartz sand and the individual alkali (K or Na) salts that are present in biomass. This understanding should provide a fundamental understanding of the agglomeration behaviour of biomass. Furthermore, it can be used to understand or predict the agglomeration behaviour of a wide range of biomass with different compositions of alkali salts.

2.3 Effects of Ca and P on biomass bed agglomeration

2.3.1 Effects of Ca on biomass bed agglomeration

As a common major inorganic matter in biomass, Ca is present either as organic-associated matter or as included minerals, such as calcium oxalate. It can also be introduced to reactors as an additive or bed material, such as dolomite, calcite or limestone. During thermochemical processes, Ca can be present as CaO, which participates in some reactions [88]. The presence of Ca can mitigate bed agglomeration. Firstly, Ca dilutes the ash particles to hinder the formation of large agglomerates [89]. Secondly, Ca can dissolve into low melting-point K silicates and form high melting-point K-Ca silicates [90, 91]. The Ca rich coating layer can also protect the inner coating layer from further growth and drive K to be released to the gas phase [91, 92]. Thirdly, Ca reacts with Si to form Ca silicates and enhances the release of K through the consumption of Si [89, 90, 93, 94]. The effect of Ca on biomass bed agglomeration can vary with the composition of alkali salts in biomass, which is unlikely to be investigated by utilizing raw biomass with a complicated inorganic elemental composition. An evaluation of the effect of Ca on the interactions between quartz sand and individual water-soluble K salts present in biomass is critical for better assessment of the effect of Ca on the interaction behaviours of various types of biomass, with different compositions of alkali salts.

2.3.2 Effects of P on biomass bed agglomeration

The presence of P in biomass has a significant impact on ash transformation and bed agglomeration [95]. The addition of P rich additives to fuels can promote the formation of K phosphates, Ca phosphates or K-Ca phosphates [90]. Some studies have indicated that the addition of P-based additives ($NH_4H_2PO_4$ and $Ca(H_2PO_4)_2$) to biomass decreases the release of K and reduces the formation of K silicates, because K reacts with $NH_4H_2PO_4$ to form K phosphates, K-Ca phosphates or reacts with $Ca(H_2PO_4)_2$ to form K-Ca phosphates [96, 97]. The formation of high melting-point Ca phosphates and K-Ca phosphates increases the melting point of the ash and has positive effects on the mitigation of agglomeration, while the formation of low melting-point volatile K phosphates has negative effects. During agglomeration,

P is present in the outer coating layer instead of the inner coating layer and is generally integrated with Ca as Ca phosphates [98]. The ratio of (K+Na)/(Ca+Mg) determines the influence of P on ash transformation and agglomeration [99]. Eriksson et al. [100] have demonstrated that for fuels that have high agglomeration and slagging tendencies due to the formation of K phosphates and silicates, the addition of Ca or Mg rich fuels can mitigate the agglomeration or slagging tendencies by forming high melting-point silicates or phosphates, such as K-Ca/Mg silicates/phosphates or Ca silicates/phosphates. Similar results have been identified by Steenari et al. [101]. Piotrowska et al. [47] have co-combusted bark rich in Ca, K and Si with rapeseed cake rich in K, P and Na for different mixing ratios. They have found that a combination of coating-induced (formation of K-Ca silicate) and melting-induced (formation of alkali phosphate ash) mechanisms is present for the fuel mixtures. For the co-combustion of wood with rapeseed cake, Piotrowska et al. [102] have also identified that the agglomeration mechanism is the formation of a K silicate coating layer that is attached by the P dominant ash particles. The presence of P in biomass, especially together with Ca, can have different influence on the agglomeration behaviour of biomass with different alkali salts compositions. Therefore, the study of the effect P, with or without the presence of Ca, on the interactions between quartz sand and the individual alkali salts that are present in biomass contributes to a better understanding of the agglomeration behaviour of various types of biomass with different compositions of alkali metals, Ca and P.

2.3.3 Effects of Ca phosphate on biomass bed agglomeration

When both Ca and P are present, Ca phosphate commonly forms in biomass, and it has a considerable impact on bed agglomeration. Generally, Ca phosphates are more stable than K phosphates and Ca silicates [103, 104]. Therefore, Ca phosphates will form before K phosphates and Ca silicates. The composition of the Ca phosphates formed depends on the stoichiometric ratio of CaO to P_2O_5 [105]. preferably, $Ca(PO_3)_2$, $Ca_2P_2O_7$, or $Ca_3(PO_4)_2$ are formed in biomass ash [105]. Normally, if Ca is in excess proportion to form Ca phosphates in the solid phase, then almost no P will be released. In contrast, P will be released at the gas phase if the level of Ca is insufficient [106]. The formation of Ca phosphates significantly improves the

melting point of biomass ash and decreases the amount of P to form low melting-point K phosphates, which mitigates some ash-related issues. The addition of Ca phosphates to biomass keeps K from releasing to the gas phase [107]. However, the formation of Ca phosphates decreases the amount of Ca that reacts with Si, which increases the formation of K silicate and aggravates agglomeration [103]. The formation of Ca phosphates in biomass can have different influences on biomass with different compositions of alkali salts. Therefore, evaluation of the effect of the presence of Ca phosphates on the interactions between quartz sand and the individual alkali salts that are present in biomass can contribute to an understanding of the influence of the formation of Ca phosphates on the bed agglomeration behaviour of various types of raw biomass.

2.4 Effect of steam gasification atmosphere on biomass bed agglomeration

Many studies have demonstrated that the reaction atmosphere has a remarkable influence on the agglomeration behaviour of biomass and coal [6, 108]. Ohman et al. [6] have studied the agglomeration mechanisms of several types of biomass under both gasification and combustion atmospheres. They have found that for Lucerne with a high S content, a thin and particle-rich coating layer dominated by a salt melt (K, S, Cl and K_2SO_4) induces agglomeration during combustion, while a thick and homogeneous coating layer, rich in K silicate, is formed during gasification. Kaknics et al. [108] have investigated the interactions between Miscanthus ash and bed materials during gasification or combustion. The thermodynamic calculations have indicated that S forms solid K_2SO_4 during combustion, while S is released to the gas phase and leaves more K to form K silicates during gasification. Ma et al. [109] have assessed the agglomeration behaviour of three straws under N_2/CO_2, N_2/H_2, N_2/steam and air atmospheres. The defluidisation temperatures of the three straws under the N_2/H_2 and the N_2/steam atmospheres are much lower than those under N_2/CO_2 and air atmospheres. Manzoori et al. [110] and van Eyk et al. [111] have studied the agglomeration behaviour of a low-rank coal with a high S and Na content in fluidized bed reactors during combustion. They have concluded that the agglomeration results from the adhesion of the bed material to the ash-derived molten Na sulfate eutectic.

McCullough et al. [112] have discovered that for similar low-rank coal with a high S and Na content during steam/air gasification, the agglomeration is initiated by the formation of a Na silicate coating layer. The influence of the reaction atmosphere (steam gasification vs combustion) on the agglomeration behaviour varies significantly with the biomass species. Therefore, more studies are needed for other types of biomass, especially for some agricultural residues and macroalgae. Investigation into the impact of the reaction atmosphere (steam gasification vs combustion) on the agglomeration behaviour, especially on the time-dependent layer formation process, of various types of agricultural residues and macroalgae with different inorganic elemental compositions is necessary for the utilisation of them in different gasification or combustion processes.

Steam affects the agglomeration behaviour of biomass by influencing the behaviour of alkali salts in biomass. Compared with other atmospheres, steam can decrease the melting point of some alkali salts, such as K_2CO_3, Na_2CO_3 and K_2SO_4 [113, 114]. This has noticeable impacts on bed agglomeration. Kosminski et al. [10, 115] have identified that steam reduces the melting temperature of Na_2CO_3 and more liquid Na_2CO_3 is present under a steam atmosphere than under a CO_2 or an N_2 atmosphere. Therefore, the liquid-solid phase reaction between Na_2CO_3 and quartz sand under a steam atmosphere generates more liquid silicates than the solid-solid phase reaction between Na_2CO_3 and quartz sand under a CO_2 or an N_2 atmosphere. The formation of liquid Na silicate begins at 750 °C under a steam atmosphere, while it starts at 850 °C under a CO_2 or an N_2 atmospheres. The reaction between NaCl and quartz sand only takes place under a steam atmosphere, while to a very limited extent. This work has been undertaken on coal doped with Na salts, while similar studies on biomass are limited. The biomass agglomeration behaviour depends significantly on the behaviour of alkali salts, Ca and P in biomass. Therefore, an understanding of the effect of the steam gasification atmospheres on the interactions between quartz sand and individual alkali (K or Na) salts in biomass, together with the presence of Ca and P, can contribute to a better understanding of the impact of steam gasification atmospheres on the agglomeration behaviour of raw biomass with different inorganic elemental compositions.

19

Acid digestion and water leaching are valid methods to investigate the effect of steam gasification atmospheres on biomass ash-bed material interactions. Acid digestion can quantify the alkali metals retained in the agglomerates, which suggests the agglomerates' formation tendencies. Water leaching tests can quantify the formation of alkali silicates with different silica contents. Alkali silicates with a low silica content are cold water (15-25 °C) soluble; while alkali silicates with a high silica content are hot water (90-100 °C, nearly boiling water) soluble [10]. An increase in the silica-to-alkali oxide weight ratio decreases the solubility of a silicate [116]. Alkali silicate with a ratio approximately greater than 4 is generally considered insoluble in water [117]. As alkali silicates with different silica contents melt at different temperatures, the water leaching method can indicate the melting behaviour of the coating layer under different reaction atmospheres. These two methods, together with other typical techniques for bed agglomeration, such as SEM/EDS and XRD, can provide a better understanding of the effects of the reaction atmospheres on biomass ash-bed material interaction behaviours.

2.5 Objective of thesis

The aim of this thesis is to provide a comprehensive and fundamental assessment of biomass ash-quartz sand interaction behaviours, which can be applied to various species of biomass with different compositions of inorganic matter under either a steam gasification or a combustion atmosphere. The specific objectives are:

1. To understand the interactions between quartz sand and wood doped with individual K or Na salts (acetate, carbonate, chloride, sulfate and phosphate) in a fixed-bed reactor. To evaluate the time-dependent layer formation and the gas-solid phase interactions between the gaseous K/Na generated from these alkali salts within biomass and the quartz sand, to compare all these interactions between a steam gasification and a combustion atmosphere.

2. To assess the effects of Ca or P, or both, on the interaction behaviour between the quartz sand and wood doped with a series of individual K salts (K_2CO_3, KCl or K_2SO_4) under a steam gasification or a combustion atmosphere.

3. To investigate the time-dependent layer formation process during ash-quartz sand interactions for three agricultural residues (grape marc, wheat straw and cotton stalk) with different ash-forming elements under both steam gasification and combustion atmospheres. To compare the ash-bed material interactions under both the steam gasification and the combustion atmospheres.

4. To evaluate the ash-quartz sand interaction behaviour of two species of macroalgae (*Oedogonium intermedium* (denoted as ODN) and *Derbesia tenuissima* (denoted as Deb)) by investigating the time-dependent layer formation process. To compare the macroalgae ash-quartz sand interaction behaviours under both a steam gasification and a combustion atmosphere for two species of macroalgae.

Chapter 3

Paper I

Interactions between Quartz Sand and Wood Doped with either K or Na Salts under Steam Gasification and Combustion Atmospheres

Zimeng He * [a,b], Woei L. Saw [a,b], Philip J. van Eyk [a,b], Graham J. Nathan [a,c], Peter J. Ashman [a,b]

[a] *Centre for Energy Technology, The University of Adelaide, Adelaide, South Australia 5005, Australia*
[b] *School of Chemical Engineering and Advanced Materials, The University of Adelaide, Adelaide, South Australia 5005, Australia*
[c] *School of Mechanical Engineering, The University of Adelaide, Adelaide, South Australia 5005, Australia*

Statement of Authorship

Title of Paper	An investigation into the interaction behaviour between K and Na salt-doped wood and quartz sand under a steam gasification or a combustion atmosphere
Publication Status	☐ Published ☐ Accepted for Publication ☑ Submitted for Publication ☐ Unpublished and Unsubmitted work written in manuscript style
Publication Details	The manuscript was submitted to the journal of Industrial & Engineering chemistry Research for review

Principal Author

Name of Principal Author (Candidate)	Zimeng He
Contribution to the Paper	Performed analysis on all samples, interpreted data, wrote manuscript and acted as corresponding author.
Overall percentage (%)	70
Certification:	This paper reports on original research I conducted during the period of my Higher Degree by Research candidature and is not subject to any obligations or contractual agreements with a third party that would constrain its inclusion in this thesis. I am the primary author of this paper.
Signature	Date 22.10.2019

Co-Author Contributions

By signing the Statement of Authorship, each author certifies that:

i.   the candidate's stated contribution to the publication is accurate (as detailed above);

ii.   permission is granted for the candidate in include the publication in the thesis; and

iii. the sum of all co-author contributions is equal to 100% less the candidate's stated contribution.

Name of Co-Author	Woei L.Saw
Contribution to the Paper	Supervised development of work, helped in data interpretation, reactor construction and manuscript evaluation and edition
Signature	Date 21/10/2019

Name of Co-Author	Philip J. van Eyk
Contribution to the Paper	Supervised development of work, helped in data interpretation and manuscript evaluation
Signature	Date 21/10/2019

Name of Co-Author	Graham J. Nathan
Contribution to the Paper	Supervised development of work, helped in data interpretation and manuscript evaluation and edition
Signature			Date	17/10/19

Name of Co-Author	Peter J. Ashman
Contribution to the Paper	Supervised development of work, helped in data interpretation and manuscript evaluation
Signature			Date	17-10-19

I&EC research
Industrial & Engineering Chemistry Research

Article

Interactions between Quartz Sand and Wood Doped with either K or Na Salts under Steam Gasification and Combustion Atmospheres

Zimeng He,* Woei L. Saw, Philip J. van Eyk, Graham J. Nathan, and Peter J. Ashman

Cite This: *Ind. Eng. Chem. Res.* 2020, 59, 1712−1722

Read Online

ACCESS | 📊 Metrics & More | 📖 Article Recommendations

ABSTRACT: The interactions between quartz sand and wood, which was doped with either K or Na salts, were investigated in a lab-scale, fixed-bed reactor under either a steam gasification or a combustion atmosphere at 900 °C. For the cases of the potassium/sodium phosphate salts, the interaction was found to be melting induced, while for the cases of the other salts, it was found to be coating induced. Large agglomerates were found to have already been formed during the early stages of steam gasification for the wood samples doped with potassium/sodium carbonate and acetate. However, the agglomerates obtained under the combustion atmosphere were found to be insignificant for the wood samples doped with potassium/sodium chloride. Both the reaction atmosphere and the types of salts were found to affect the formation of potassium/sodium silicates in the agglomerates and the interactions between the quartz sand with gaseous K or Na significantly.
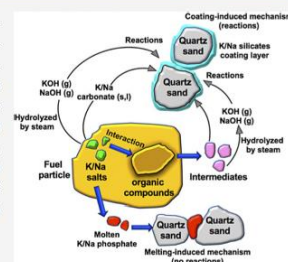
1. INTRODUCTION

Agricultural residues and algae are promising biomass fuels in fluidized bed reactors due to their low net CO_2 intensity. Furthermore, agricultural residues are a relatively low cost feedstock, while algae have both a fast growth rate and a high productivity.[1,2] However, agricultural residues and algae are normally rich in K or Na or both, which are the main contributors to agglomeration.[3,4] Agglomeration generally arises from the adhesion of bed materials to alkali silicates or phosphates that are generated from reactions between alkali metals (K and Na) with Si or P. These can lead to several problems such as defluidization or even unscheduled shut-downs in fluidized bed reactors.[5,6] In biomass, K and Na are mostly present as water-soluble inorganic salts, such as carbonate, sulfate, chloride, and phosphate, or as organic associated elements.[7,8] In addition, quartz sand, which is rich in Si, is one of the common bed materials in fluidized bed reactors.[3] Understanding of the interactions between quartz sand and individual K or Na salts within biomass is critical to having an insight into the agglomeration mechanism of biomass with various elemental compositions of inorganic matter. Therefore, the aim of this study is to assess the interactions between wood doped with various individual K or Na salts and quartz sand as the bed material, under conditions relevant for both steam gasification and combustion.

The interactions between quartz sand and typical pure K or Na salts within biomass vary with the species of salts under either a steam gasification or combustion atmosphere.[9−14] Some studies revealed that pure K_2CO_3 or Na_2CO_3 can react with quartz sand to form potassium or sodium silicates under either of these atmospheres.[9−11,14] However, the reaction temperature depends on the atmosphere, because the defluidization temperature of pure K_2CO_3 under a steam gasification atmosphere can be approximately 100 °C lower than that under a combustion atmosphere for some conditions, as has been suggested by Ma et al.[11] Pure KCl or NaCl only reacts with quartz sand to a very limited extent under a steam gasification atmosphere, while no reaction can be observed under a combustion atmosphere, as has been reported previously.[9,11,12,14] McKee concluded that alkali chloride is more active under steam atmospheres than under CO_2 atmospheres, probably due to the hydrolysis that can occur with steam.[15] Furthermore, previous studies indicated that no interaction has been detected between pure K_2SO_4 or Na_2SO_4 and quartz sand under either a steam gasification or combustion atmosphere.[10,11,14] Lang suggested that alkali phosphate forms glassy compounds that can coat the surface of carbon particles, thus inhibiting their reaction with the reaction gases.[16] However, the behavior of pure K and Na salts is different from that of the K and Na salts within biomass because the organic components of biomass can affect the behavior of these salts during thermochemical processes.[15−23] Alkali carbonate, chloride, or sulfate can react with the organic components in biomass either to form some intermediates,

such as alkali oxides, or to become organic associated.[15−22] The intermediates can interact with the quartz sand to form the coating layer. Hence it can be deduced that the interactions between K or Na salts and the organic compounds within biomass have a considerable influence on the reactions between these salts and quartz sand. Due to the complex composition of the inorganic species within biomass, it is difficult to isolate the behavior of individual K or Na salts from the evaluations of raw biomass. Consequently, the present paper has assessed the interactions between quartz sand and these individual alkali salts in the presence of organic material systematically by doping individual K and Na salts with a low-ash-content wood.

The work on understanding the interactions between quartz sand and some feedstocks doped with typical individual K or Na salts is far from complete, although some studies were conducted for several individual Na salts for agglomeration or slagging processes.[12,24,25] Lindner et al.[25] discovered that the mass of silicates produced from the reaction between quartz sand and sodium acetate (NaAc) doped coal is 3−5 times greater than that from the reaction between quartz sand and NaCl-doped coal. Qi et al.,[24] who investigated the slagging behavior between quartz sand and Zhundong coal doped with various Na salts (NaCl, Na_2SO_4, and NaAc), found that the extent of slagging follows the order NaAc/Na_2SO_4 > NaCl. Kosminski et al.[12] doped coal with NaAc or NaCl to reveal that NaAc decomposes to Na_2CO_3, which reacts with the silica sand, and that the steam gasification atmosphere reduces the melting point of Na_2CO_3. Through this pathway, more liquid sodium silicate is generated from the liquid−solid reaction between Na_2CO_3 and silica sand under the steam gasification atmosphere than under either the CO_2 or N_2 atmosphere. In contrast, NaCl only reacts with silica sand to a very limited extent to form the sodium silicate under a steam gasification atmosphere. However, most of these previous studies were performed with coal. Very limited information is available on the interactions for various K or Na salts using biomass as the feedstock, especially for K salts which are typically less prevalent in coal than in biomass. Therefore, the present investigation aims to meet this need.

The influence of the reaction atmosphere (steam gasification or combustion) on the interactions between quartz sand and various types of K or Na salts within biomass is not well understood. Steam can reduce the melting temperature of some alkali salts, such as K_2CO_3, Na_2CO_3, and K_2SO_4, thereby increasing the potential of agglomeration.[26,27] Steam affects the morphology of agglomerates, the retention of alkali metals, and the formation of alkali silicates in the agglomerates.[12,28,29] These properties influence the agglomeration of biomass significantly. The effect of steam on these properties also depends on the types of alkali salts in biomass. The retention of alkali metals in the agglomerates can be used to partially suggest the tendency towards agglomeration under the two atmospheres. In addition, a method based on the solubility of alkali silicates in water can be utilized to investigate the effect of steam on the formation of alkali silicates with different melting points in the agglomerates. Alkali silicates with a low silica content are known to be soluble in cold water (15−25 °C), while alkali silicates with a high silica content are soluble in hot water (90−100 °C, nearly boiling water).[12] That is, the solubility of a silicate is decreased with an increase in the silica-to-alkali oxide weight ratio[30] and a ratio greater than approximately 4 is generally considered to be insoluble in

water.[31] Furthermore, the melting temperature depends on this ratio. Two typical alkali silicates with a higher ratio, that is potassium tetrasilicate and sodium disilicate which can be formed in agglomerates, generally have lower melting points; while several typical alkali silicates with a lower ratio, that is potassium metasilicate/disilicate and sodium metasilicate which can be formed in agglomerates, normally have higher melting points.[12,30,31] Alkali silicates with a silica content higher than 80 wt % typically have melting points above 1100 °C.[30] Consequently, alkali silicates insoluble in water usually have very high melting points. The melting behavior of alkali silicates in agglomerates affects the agglomeration process significantly. Few studies have used the method of water leaching combining acid digestion and scanning electron microscopy/energy dispersive X-ray spectroscopy (SEM/EDS) to investigate the effect of steam on the formation of agglomerates. The influence of both the species of alkali salts and the reaction atmosphere on the formation of alkali silicates in agglomerates can help in better understanding of the agglomeration of various types of raw biomass. Therefore, this is another aim of the present study.

The solid−gas phase interactions between quartz sand and the gaseous K/Na generated from various alkali salts within biomass have received relatively little attention, although a study deduced that they are important in the formation of agglomerates.[32] Nevertheless, there is some debate over this point because other studies suggested that the solid−gas phase interaction is not a possible route for the formation of agglomerates.[33] This limited and contradictory information provides strong motivation to evaluate the solid−gas phase interactions between the quartz sand and wood doped with typical individual K or Na salts in biomass under both the steam gasification and combustion atmospheres.

More specifically, the aim of the present work is to identify the nature of the interactions between quartz sand as the bed material and wood doped with a range of alternative K or Na salts (acetate, carbonate, chloride, sulfate, and phosphate) in a fixed-bed reactor under both steam gasification and combustion atmospheres. We also aim to identify the early stages of the interactions and the solid−gas phase interactions between the quartz sand and the gaseous K/Na generated from wood samples doped with these individual alkali salts under both atmospheres.

2. EXPERIMENTAL METHODS

2.1. Feedstock and Bed Material. The feedstocks were prepared with a commercial Swedish softwood, which has been studied previously so that its proximate and ultimate analyses and inorganic elemental composition can be found elsewhere.[34] The concentration of the ash-forming elements in this wood is low. Quartz sand with a particle size range of 75−212 μm, was obtained from the Coonarr Creek mine in Bundaberg, Australia, for the bed material. The composition of the quartz sand has also been reported elsewhere[29] and is shown here in Table 1. Analytical reagent grades of K or Na salts (carbonate, acetate, chloride, sulfate, or phosphate monobasic) were used during the sample preparation, the process for which is explained in section 2.2.

2.2. Sample Preparation. Known quantities of individual K or Na salts (carbonate, acetate, chloride, sulfate, or phosphate monobasic) were completely dissolved in deionized water in a beaker. Measured quantities of wood were then added to the solution to form a well-mixed, wood−water

26

pubs.acs.org/IECR

Table 1. Composition of the Quartz Sand

wt %	quartz sand
SiO_2	99.8
Fe_2O_3	0.12
TiO_2	0.05
Al_2O_3	0.04
K_2O	<0.01
Na_2O	<0.01
MgO	<0.01
CaO	<0.01
Cr_2O_3	0.0001

slurry, which was dried at 35 °C, then further dried in an oven at 105 °C overnight. The assessments were all performed for a fixed concentration of 3 wt % K or Na in the feedstock because a preliminary investigation found that this concentration did not affect either the morphology of the agglomerates or the elemental composition of the coating layer significantly.

2.3. Interaction Tests. Each interaction test between the quartz sand and the salt-doped wood was carried out in the lab-scale, fixed-bed reactor as shown in Figure 1. A 1.4 m
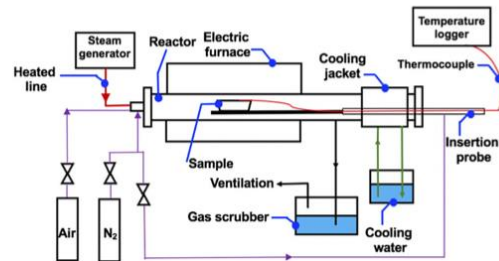

Figure 1. Schematic diagram of the lab-scale, fixed-bed reactor employed for the interaction tests between the quartz sand and the salt-doped wood.

stainless steel pipe with an inner diameter of 40.9 mm was utilized as the reactor, both ends of which were sealed. The reactor was heated in a horizontal tube furnace. Samples were placed in a water-cooled "cooling jacket", located at one end of the reactor, to be maintained a temperature below 50 °C before the tests and to allow cooling of samples after each test. Samples were inserted to, or retracted from, the center of the reactor with an insertion probe monitoring the temperature of the samples with a thermocouple located inside the insertion probe. All the reaction gases, including steam generated from a controlled evaporator mixer (CEM; Bronkhorst), high purity N_2, and industrial grade air, were introduced into the reactor from the opposite end. All flow rates, both of all the reaction gases and of the water, were controlled using mass flow controllers. A trace heater was used to maintain the steam feeding line at approximately 200 °C. The product gases from the reactor were vented to the atmosphere after passing through a gas scrubber.

Approximately 1.5 g of the salt-doped wood was first mixed uniformly with the quartz sand to a mass ratio of 3:1 (feedstock:quartz sand) in an alumina crucible. The test was started by inserting the crucible into the fixed-bed reactor and finished by retracting the crucible from the reactor to the "cooling jacket", where it was cooled with high purity nitrogen.

All the tests were performed at 900 °C for a reaction time of either 7 or 45 min using steam/N_2 (50% v/v steam) for the gasification atmosphere or air/N_2 (5% v/v O_2) for the combustion atmosphere, with a flow rate of 4 SLPM (standard liters per minute), respectively. The mass fraction of the organic residue retained in the agglomerates for a 7 min reaction time was determined by ashing the agglomerates in a muffle furnace at 550 °C for 12 h.

2.4. Solid−Gas Phase Interaction Tests. A specified quantity of the salt-doped wood (1.5 g) was loaded into an alumina crucible. A known quantity of quartz sand (∼0.5 g) was then uniformly distributed onto a high-temperature resistant metal mesh that entirely covered the top of the crucible. The method allows the gaseous K and Na released from the samples to pass through the metal mesh and react with the quartz sand above the crucible, while preventing any direct contact between the two media. The solid−gas phase test was performed at 900 °C for a reaction time of 45 min under either a steam gasification or combustion atmosphere, following the same procedure as described above.

2.5. SEM/EDS Analysis. Both the morphology and the composition of the agglomerates from the 45 min interaction test were analyzed with a scanning electron microscope (Philips model XL30) in combination with energy dispersive X-ray spectroscopy (SEM/EDS) at both the surface and the cross sections. Only the SEM/EDS analysis at the surface was performed with the samples from the 7 min interaction test and the solid−gas phase test. Samples were either mounted to a carbon tape for the surface analysis or embedded in epoxy resin and polished for the cross-sectional analysis. Furthermore, all the samples were carbon coated to reduce charging of the sample. The backscattering electron mode was employed to investigate the composition and the character of the samples. For each sample, several sections uniformly distributed over the sample were selected for EDS analysis with several spots assessed within each section. The elemental composition of the agglomerates was then averaged over all the selected spots.

2.6. Acid Digestion and Water Leaching Tests. The agglomerates obtained from the 45 min interaction tests under both atmospheres were digested with high concentration nitric acid (70%) and hydrofluoric acid (48%) for 1 week at 140 °C. These provided a measure of the total mass of K or Na retained in the agglomerates. Each sample was then diluted with 0.1 M HCl and analyzed with a Shimadzu atomic absorption spectrophotometer (AAS; AA-6300). The concentration of K or Na in the agglomerates was calculated as a fraction (%) of the mass of the K or Na retained in the agglomerates relative to the mass of the K or Na in the feedstock.

Three individual samples were prepared repeatedly from each 45 min interaction test under both atmospheres, and then leached with both cold water (15−25 °C) and hot water (90−100 °C) using magnetic stirring for 4 h to determine the K or Na content in silicates. The solutions from the cold and hot water leaching tests were further diluted with 0.1 M HCl to measure the concentration of K or Na with AAS. The concentration of K or Na in the cold and hot water leaching fractions were calculated as the fractions (%) of the mass of K or Na in cold/hot water leachates relative to the mass of the K or Na in the feedstock. The reported value is the average of the three repeated tests.
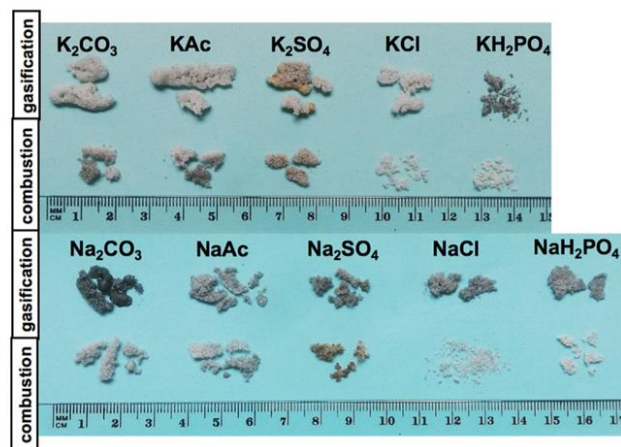
Figure 2. Agglomerates formed under both the steam gasification and combustion atmospheres at 900 °C with a reaction time of 45 min for wood samples doped with individual K or Na salts.

Figure 3. SEM cross-sectional and surface analyses of the agglomerates obtained from the interaction tests between the quartz sand and the individual K-salt-doped wood with a reaction time of 45 min at 900 °C under both the steam gasification and combustion atmospheres.

3. RESULTS

3.1. Interactions between the Quartz Sand and the Salt-Doped Wood. Figure 2 presents the images of the agglomerates formed under both steam gasification and combustion atmospheres for the wood samples doped with individual K or Na salts for a reaction time of 45 min at 900 °C, while Figures 3 and 4 present the SEM images of the cross sections and the surface of these agglomerates. The SEM images in Figures 3 and 4 show that the size of the agglomerates formed under the steam gasification atmosphere is generally larger than that of those formed under the combustion atmosphere for the wood samples doped with individual K_2CO_3, KAc, K_2SO_4, Na_2CO_3, and NaAc salts. Although Figure 2 shows that the difference in the size of the agglomerates for the wood samples doped with either Na_2CO_3

or NaAc is not great under the two atmospheres, more large molten lumps can be observed in the agglomerates formed under the steam gasification atmosphere than in those formed under the combustion atmosphere for these wood samples (Figure 2). This provides an explanation for the differences in the SEM images in Figure 4. For the wood samples doped with either potassium or sodium chloride, although agglomerates with a size of approximately 1 cm can be formed under the steam gasification atmosphere (Figure 2), fewer quartz sand particles are adhered to the silicate coating layer than that for the wood samples doped with individual alkali carbonate, acetate, and sulfate salts (Figures 3 and 4). However, the size of the agglomerates formed from the wood samples doped with either KH_2PO_4 or NaH_2PO_4 is not affected significantly by the reaction atmosphere.

28

Figure 4. SEM cross-sectional and surface analyses of the agglomerates obtained from the interaction tests between the quartz sand and the individual Na-salt-doped wood with a reaction time of 45 min at 900 °C under both the steam gasification and combustion atmospheres.

Figure 5 presents the elemental composition of the coating layer formed under both the steam gasification and combustion
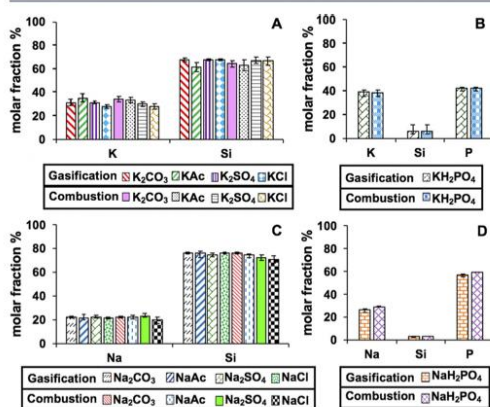
Figure 5. Elemental composition of some major ash-forming elements on a C- and O-free basis for the coating layer based on the SEM/EDS cross-sectional analysis of the agglomerates obtained from the interaction tests between the quartz sand and the salt-doped wood with a reaction time of 45 min at 900 °C under both the steam gasification and combustion atmospheres. (A) Wood samples doped with individual K_2CO_3, KAc, K_2SO_4, and KCl salts. (B) KH_2PO_4-doped wood. (C) Wood samples doped with individual Na_2CO_3, NaAc, Na_2SO_4, and NaCl salts. (D) NaH_2PO_4-doped wood .

atmospheres as determined from the SEM/EDS cross-sectional analysis for a reaction time of 45 min at 900 °C. The four cases of the K-salt-doped wood (K_2CO_3, KAc, K_2SO_4, and KCl, as shown in Figure 5A) and the four cases of the Na-salt-doped wood (Na_2CO_3, NaAc, Na_2SO_4, and NaCl, as shown in Figure 5C) have all reacted with the quartz sand to form a coating layer dominated by either K or Na silicates with an elemental composition of K:Si ≈ 33:67 (molar ratio) or Na:Si ≈ 24:76 (molar ratio), respectively. In contrast, the coating layer of the

agglomerates formed from the wood samples doped with either KH_2PO_4 or NaH_2PO_4 mainly consist of K/Na and P, as shown in Figure 5B and 5D. This suggests that these agglomerates have been formed by a different mechanism, in which the quartz sand particles have been adhered to the partially molten alkali-phosphate ash to form the agglomerates, while no reaction can be observed between the quartz sand and either the KH_2PO_4 or NaH_2PO_4. The reactions between the quartz sand and either the pure K_2SO_4 or KCl salts can be insignificant under both atmospheres for the interaction tests, especially under the combustion atmosphere, as has been suggested by others.[10,11] Therefore, the formation of the agglomerates in the present study is due to the formation of either some intermediates or some organic associated compounds resulting from the reaction between the organic components of wood with either K_2SO_4 or KCl. The formation of these intermediates and compounds has been indicated by others.[15,16,19−21,23,35] Some studies indicated that similar intermediates can also be formed for K_2CO_3.[18,22] These intermediates can react with the quartz sand to form the K-silicate coating layer. Pure K_2CO_3 salt can also react with the quartz sand to form the agglomerates, as has been revealed previously.[9−11] Lang et al.[16] concluded that KAc can decompose to K_2CO_3, and follow the same pathway as K_2CO_3. Under a steam environment, KCl, K_2SO_4, and K_2CO_3 can also be hydrolyzed by steam to form KOH, as has been reported previously.[35−37] The formed KOH can react with the quartz sand. However, Knudsen et al.[36] suggested that KCl is very stable. This means that it tends to evaporate into the gas phase rather than to be hydrolyzed by steam or to react with either the organic components of wood or the quartz sand. Therefore, the extent of any interactions between the quartz sand and the KCl-doped wood is small. Although the size of the agglomerates varies with the species of the K salts, the elemental composition of the K-silicate coating layer formed is similar, as shown in Figure 5A. The behavior of the various types of Na salts is similar to that of the corresponding K salts.

The acid digestion data in Figure 6 show that all except the chloride salts retain at least 70% of the mass of K and Na in the agglomerates formed under both atmospheres. Parts of the acid

Figure 6. Mass fractions (%) of the K and Na in the agglomerates that is dissolved in cold water, hot water, and acid relative to the K and Na introduced from the feedstock. Thes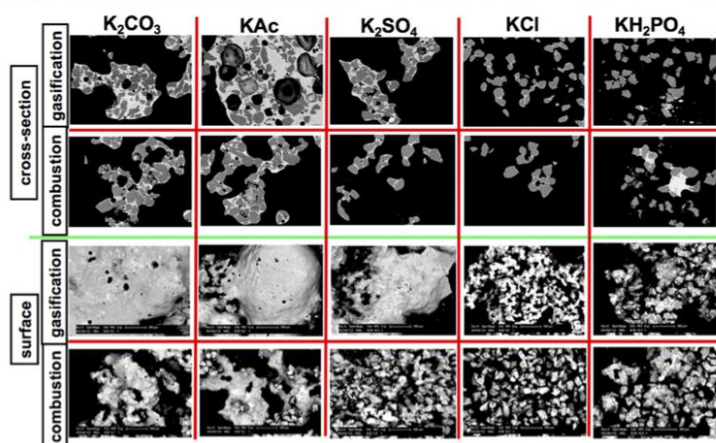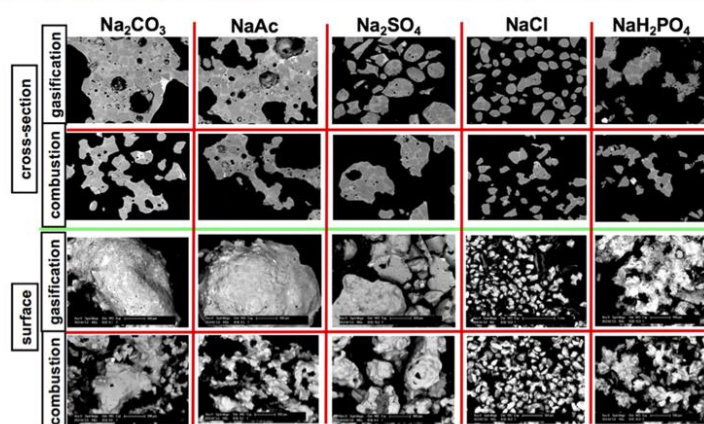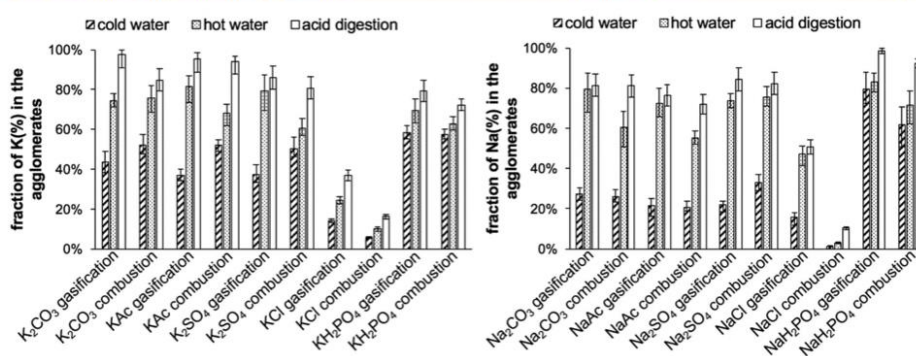e agglomerates were formed under both the steam gasification and combustion atmospheres for a reaction time of 45 min at 900 °C.

digestion data in Figure 6 have been reported in another study.[38] The mass fraction of K or Na retained in the agglomerates formed from the alkali-chloride-doped wood is much less than that in those formed from the other salt-doped wood. This is consistent with the very thin coating layer of the agglomerates formed from the wood samples doped with either KCl or NaCl observed in the SEM images. This can be explained by the fact that in comparison with other alkali salts, alkali chloride is very stable and tends to evaporate to the gas phase, rather than to react with the quartz sand to form alkali silicates, as has been suggested by Knudsen et al.[36] As shown in the SEM images in Figures 3 and 4, the size of the agglomerates formed under the steam gasification atmosphere is larger than that of those formed under the combustion atmosphere for the wood samples doped with individual K_2CO_3, Na_2CO_3, KAc, NaAc and K_2SO_4 salts. (Note that the Na_2SO_4 agglomerates formed under the steam gasification atmosphere were found to adhere to the crucible, so they became fragmented during the sample collection. This explains the lack of any obvious differences in the size of the Na_2SO_4 agglomerates for the two atmospheres in Figure 4.) Nevertheless, the mass fraction of the K or Na, which is retained as alkali silicates in the agglomerates, relative to the K or Na in the salt-doped wood samples is relatively similar for the two atmospheres. This suggests that the difference in the morphology of the agglomerates formed under the two atmospheres for these wood samples doped with alkali salts does not result wholly from the difference in the amount of alkali silicates formed in the agglomerates. Instead, a more likely explanation is the difference in the melting behavior of the alkali silicates formed under the two atmospheres, as is discussed below from the water leaching tests. In contrast, for the wood samples doped with either KCl or NaCl, a large difference can be seen in the retention of either K or Na in the agglomerates formed under the two atmospheres. In comparison with the combustion atmosphere, steam hydrolyzes KCl or NaCl to favor a reaction with the quartz sand.

Figure 6 presents the average results of the three repeated tests for the cold and hot water leaching. Parts of the water leaching data in Figure 6 have been reported in another study.[38] The fraction of K dissolved in hot water is the difference between the columns of hot water leaching and cold water leaching (Figure 6). Figure 6 shows that, for the

agglomerates formed from the wood samples doped with individual K_2CO_3, KAc, and K_2SO_4 salts, the combustion atmosphere favors silicates with a lower silica content, while the steam gasification atmosphere favors silicates with a higher silica content. In contrast, for the agglomerates formed from the wood samples doped with either Na_2CO_3 or NaAc, the mass fraction of silicates with a lower silica content is independent of the reaction atmosphere. As for the K salts, the steam gasification atmosphere favors Na silicates with a higher silica content for the agglomerates formed from the wood samples doped with individual Na_2CO_3, NaAc, and Na_2SO_4 salts. For the agglomerates formed from the wood samples doped with either KCl or NaCl, the mass fraction of either type of silicates formed under the combustion atmosphere is far less than that of those formed under the steam gasification atmosphere. This is in agreement with the smaller agglomerates formed under the combustion atmosphere for the wood samples doped with either KCl or NaCl observed in Figure 2. Some previous studies suggested that potassium/sodium metasilicate or disilicate or potassium tetrasilicate can be formed during agglomeration.[3,12,39−43] The potassium silicates soluble in hot water are deduced to be potassium tetrasilicate with a melting point of 770 °C, while the potassium silicates soluble in cold water are deduced to be potassium metasilicate or disilicate with much higher melting points (976 °C for metasilicate and 1045 °C for disilicate), based on the comparison with other studies.[3,30,31,40] The sodium silicates soluble in hot water are deduced to be sodium disilicate or a eutectic with a melting point of 874 or 789 °C, respectively, while the sodium silicates soluble in cold water are deduced to be sodium metasilicate with a melting point of 1086 °C, consistent with previous work.[3,12,30,31,39,41] Therefore, the alkali silicates formed in the present agglomerates with a higher silica content are likely to melt at a lower temperature than those with a lower silica content. For the wood samples doped with either K or Na salts, the formation of large agglomerates under the steam gasification atmosphere by these molten silicates at lower temperatures is plausible. In contrast, for the K-salt-doped wood, the combustion atmosphere facilitates the formation of more alkali silicates that melt only at higher temperatures, which can be even higher than the reaction temperature (900 °C) of the present tests. This explains the smaller sized agglomerates formed
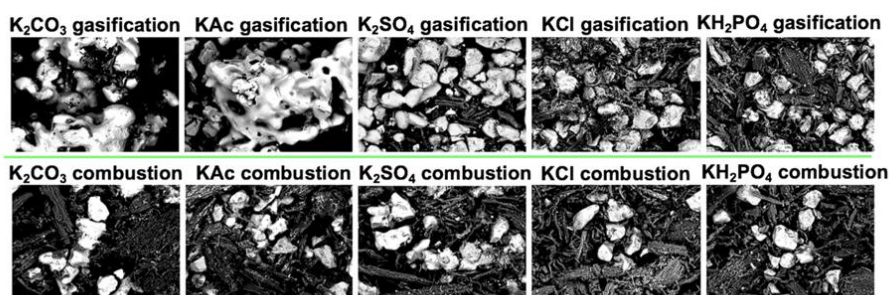
Figure 7. SEM surface analysis of the agglomerates obtained from the interaction tests between the quartz sand and the K-salt-doped wood with a reaction time of 7 min at 900 °C under both the steam gasification (top series) and the combustion atmospheres (bottom series).
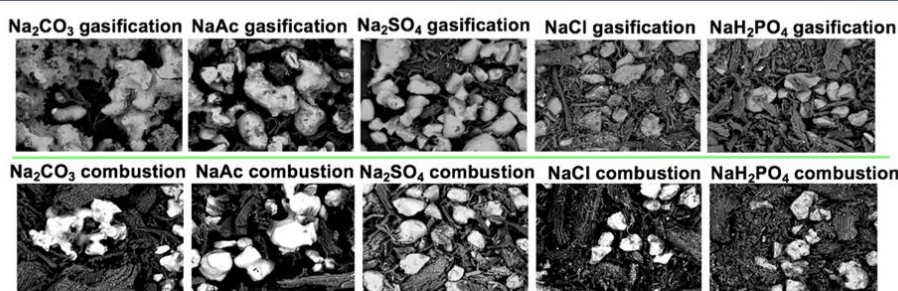
Figure 8. SEM surface analysis of the agglomerates obtained from the interaction tests between the quartz sand and the Na-salt-doped wood with a reaction time of 7 min at 900 °C under both the steam gasification (top series) and the combustion atmospheres (bottom series).

Figure 9. Mass ratios of the organic residue retained in the 7 min agglomerates formed under both the steam gasification and combustion atmospheres at 900 °C relative to the feedstock used (mg of organic residue/g of fuel) for the K-salt-doped wood and the Na-salt-doped wood.

under the combustion atmosphere than those formed under the steam gasification atmosphere for the K-salt-doped wood. For the wood samples doped with either Na_2CO_3 or NaAc, the difference in the fractions of Na silicates with higher melting points in the agglomerates formed under the two atmospheres is insignificant. This can explain the less obvious differences in the size of these agglomerates observed in Figure 2 for the Na-salt-doped wood than those for the corresponding K-salt-doped wood. For the agglomerates formed from the wood samples doped with either KH_2PO_4 or NaH_2PO_4, no alkali

silicates are formed and most of the K and Na phosphates are soluble in cold water. Consequently, for biomass with a high phosphorus content, the formation of alkali phosphates can affect the water leaching results of alkali silicates.

3.2. Early Stage of the Interactions. Figures 7 and 8 present the images of the samples obtained during an early stage (a 7 min reaction time) at 900 °C under both the steam gasification and combustion atmospheres based on the SEM surface analysis for the salt-doped wood. Char particles can be found within the samples formed during this early stage. For
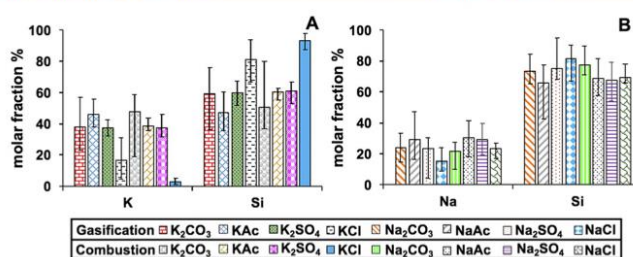
31

Figure 10. Elemental composition of some major ash-forming elements on a C- and O-free basis for the coating layer of the agglomerates obtained from the interaction tests between the quartz sand and either the K-salt-doped wood or the Na-salt-doped wood with a reaction time of 7 min at 900 °C under both the steam gasification and combustion atmospheres based on SEM/EDS surface analysis.
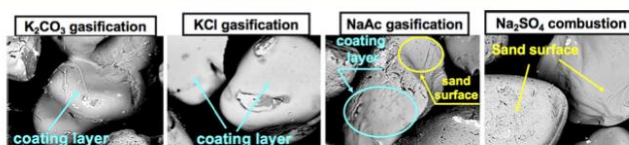

Figure 11. SEM surface analysis of selected quartz sand particles obtained from the solid−gas phase interaction tests between the quartz sand and the gaseous K/Na generated from the salt-doped wood for a 45 min reaction time at 900 °C under both the steam gasification and combustion atmospheres.

the wood samples doped with individual K_2CO_3, Na_2CO_3, KAc, and NaAc salts, many sand particles have already been incorporated into the agglomerates formed under the steam gasification atmosphere. In contrast, only a few sand particles have been adhered together within the coating layer for the agglomerates formed from the wood samples doped with either K_2SO_4 or Na_2SO_4. Any sand particles are separate for the cases of the wood samples doped with individual KCl, NaCl, KH_2PO_4, and NaH_2PO_4 salts. This implies that the formation of the agglomerates during the early stages is facilitated by the addition of individual K_2CO_3, Na_2CO_3, KAc, and NaAc salts to the wood, especially for the cases under the steam gasification atmosphere.

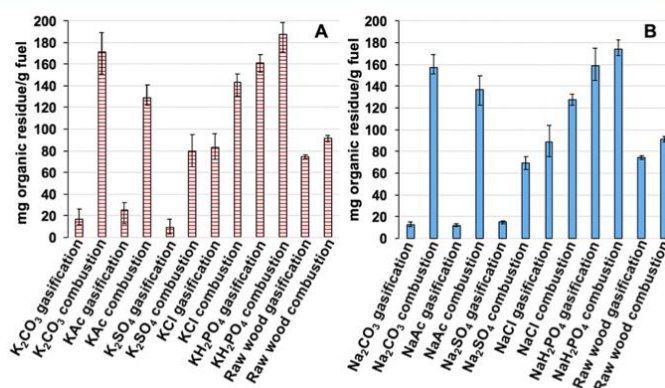Figure 9 presents the mass ratios of the organic residue retained in the 7 min samples formed under both the steam gasification and combustion atmospheres at 900 °C relative to the feedstock used for the salt-doped wood and the raw wood. The mass ratio for the raw wood produced with steam gasification is just a fraction smaller than that produced with combustion. The mass ratios produced with steam gasification for the wood samples doped with individual K_2CO_3, KAc, and K_2SO_4 salts are much smaller than that for the raw wood, while for the KCl-doped wood it is similar to that for the raw wood. In contrast, the mass ratios produced with combustion for all the K-salt-doped wood (except for the K_2SO_4-doped wood which is similar to that for the raw wood) are much greater than that for the raw wood. Generally, alkali carbonate, acetate, and sulfate salts are more likely to react with the organic components of fuel to form the intermediates than are the alkali chloride and phosphate salts under steam atmospheres for selected conditions, as has been suggested by previous researchers.[15,16,37,44] The generation of the intermediates facilitates the reactions between carbon particles and the reaction gases, as has also been deduced previously.[15,22,35,37,44,45] Therefore, for the cases of the wood samples doped with individual K_2CO_3, KAc, and K_2SO_4 salts,

steam favors the consumption of the organic components of wood and the formation of agglomerates. In contrast, KCl is very stable and favors evaporation at the gas phase, so the extent of the interactions between the KCl and the organic components of wood is small. To control the reaction temperature, the concentration of oxygen used for the combustion atmosphere (5% v/v O_2) is much lower than that for the steam gasification atmosphere (50% v/v H_2O). Therefore, it is deduced that the reactions between the organic components of wood and either the K salts or the reaction gases are limited during combustion. Furthermore, the unreacted inorganic salts can be deposited onto the char surface and inhibit the reaction between the char and the gas phase. These factors can slow down the formation of the agglomerates during combustion. For the KH_2PO_4-doped wood, the mass ratios produced with both steam gasification and combustion are much greater than those for the raw wood. This further suggests that the KH_2PO_4 salt coats the surface of carbon particles, thus inhibiting the interactions between the carbon particles and the reaction gases, consistent with Lang et al.[16] The cases of the various Na salts are similar to those of the corresponding K salts.

Figure 10 presents the elemental composition of the coating layer of the agglomerates formed during the early stages (sampled after 7 min) for the salt-doped wood (except for the phosphate-salt-doped wood) at 900 °C under both the steam gasification and combustion atmospheres, as determined from the SEM/EDS surface analysis. Almost no coating layer can be detected on the surface of the sand particles for the cases of the wood samples doped with either KH_2PO_4 or NaH_2PO_4. The coating layer for the cases of other salt-doped wood is rich in K/Na and Si. For the cases of the wood samples doped with either KCl or NaCl, the molar fractions of either K or Na detected in the coating layer are lower than those for the cases of the other salt-doped wood. These results further suggest that any reactions between the quartz sand and the wood samples
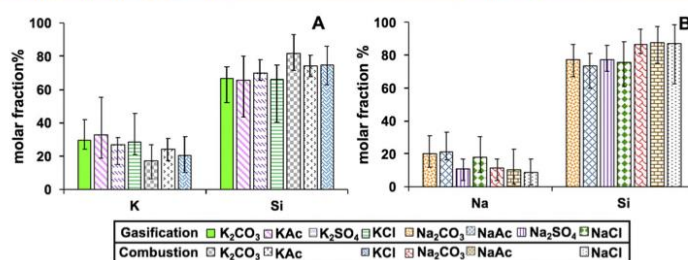
Figure 12. Elemental composition of some major ash-forming elements on a C- and O-free basis for the surface of the quartz sand particles from the solid−gas phase interaction tests between the quartz sand and the gaseous K/Na generated from the salt-doped wood for a 45 min reaction time at 900 °C under both the steam gasification and combustion atmospheres based on SEM/EDS surface analysis.

doped with either alkali chlorides or phosphates are quite limited. The larger error bars in Figure 10 than those in Figure 5 (the 45 min agglomerates) imply that the coating layer is inhomogeneous during the early stages of agglomeration, while it becomes homogeneous when the reaction time is increased.

3.3. Solid−Gas Phase Interactions. Figure 11 presents selected SEM images of the quartz sand particles obtained from the solid−gas phase interaction tests between the quartz sand and the gaseous K/Na generated from the respective cases of the salt-doped wood with a 45 min reaction time at 900 °C under both the steam gasification and combustion atmospheres. Many quartz sand particles have been coated with K silicates for the cases of the wood samples doped with either KAc or K_2CO_3 produced with both the steam gasification and combustion atmospheres, and also for the cases of the wood samples doped with either KCl or K_2SO_4 produced with the steam gasification atmosphere. However, almost no coating layer can be detected on the surface of the quartz sand particles for the cases of the wood samples doped with either KH_2PO_4 or NaH_2PO_4 produced with either atmosphere, or for the cases of the wood samples doped with either K_2SO_4 or Na_2SO_4 produced with the combustion atmosphere. For all the other cases, only some of the quartz sand particles are coated. These results suggest that the gaseous K generated from the K-salt-doped wood is more likely to react with the quartz sand than the gaseous Na generated from the Na-salt-doped wood, especially for the cases of the steam gasification atmosphere. For the alkali-phosphate-doped wood, almost no reaction takes place between the quartz sand and the gaseous K/Na for either atmosphere. Three pathways are proposed for the interactions between the quartz sand and the gaseous K/Na based on both the above results and the literature: (1) the alkali salts in the feedstock reacts with the organic components of wood to form some intermediates,[15,22,35,37,44,45] which release alkali metals in some forms to the gas phase to react with the quartz sand; (2) the alkali salts in the feedstock release alkali metals in some forms to the gas phase to react with the quartz sand;[36] and (3) the alkali metals in the feedstock are hydrolyzed by steam to form gaseous KOH or NaOH to react with the quartz sand.[35−37] For the wood samples doped with alkali sulfate, only the third pathway is possible, as no solid−gas phase interactions can be observed for the combustion atmosphere. In addition, the third pathway can explain why the solid−gas phase interactions for most cases are more significant for the steam gasification atmosphere than those for the combustion atmosphere. For the alkali-phosphate-doped wood, the gaseous

alkali metals can be in the form of alkali phosphate, which has no interactions with the quartz sand. Further work is needed to explain the greater tendency for the solid−gas phase interactions between the K-salt-doped wood and the quartz sand than that for the Na-salt-doped wood.

Figure 12 presents the elemental composition of the surface of selected quartz sand particles obtained from the solid−gas phase interaction tests between the quartz sand with the K-salt-doped wood and the Na-salt-doped wood for a 45 min reaction time at 900 °C under both the steam gasification and combustion atmospheres based on the SEM/EDS analysis. The coating layer is rich in K/Na and Si. The large error bars in Figure 12 indicate that the coating layer is not homogeneous.

4. CONCLUSION

For the cases of the wood samples doped with individual alkali (K and Na) carbonate, acetate, sulfate, and chloride salts, the alkali metals were found to react with the quartz sand to form a coating layer of alkali silicates via a coating-induced mechanism. Although the elemental composition of the coating layer is consistent for these wood samples, much less alkali silicates are generated for the alkali-chloride-doped wood because the alkali chloride tends to be released to the gas phase. Steam facilitates the formation of larger agglomerates for the wood samples doped with individual alkali carbonate, acetate, and sulfate salts than does the combustion atmosphere. However, the masses of the alkali silicates generated are similar for the two atmospheres. The difference in the size of the agglomerates formed under the two atmospheres can be explained by the presence of steam favoring the formation of more alkali silicates with a lower melting point than the the combustion atmosphere. For the alkali-chloride-doped wood, the presence of steam increases significantly both the size of the agglomerates and the formation of alkali silicates, while the agglomerates are insignificant for a combustion atmosphere. For the alkali-phosphate-doped wood, agglomerates are formed by the adhesion of the quartz sand particles to the partially molten alkali-phosphate ash via a melting-induced mechanism, while steam has an insignificant effect on this type of interaction.

The wood samples doped with either alkali carbonate or acetate facilitates the formation of larger agglomerates during the early stages of the interactions for the steam gasification atmosphere, more than do the wood samples doped with other individual alkali salts. Steam favors the reactions between the organic components of wood with individual alkali carbonate,

33

acetate, and sulfate salts. This then facilitates the consumption of the organic components and the formation of agglomerates during the early stages. No significant formation of agglomerates can be detected during the early stages for the wood samples doped with alkali chloride. The alkali phosphate salts inhibit the reactions between the carbon particles and the reaction gases, because almost no coating layer can be formed during the early stages.

The extent of the solid−gas phase interactions between the quartz sand and the gaseous K generated from the K-salt-doped wood is greater than that for the gaseous Na generated from the Na-salt-doped wood, especially for the cases of the steam gasification atmosphere. Steam hydrolyzes these alkali metals in the gas phase to form either KOH or NaOH, both of which react with the quartz sand. The effect of steam is important for the solid−gas phase interactions for the alkali-sulfate-doped wood, since no interactions can be found for the combustion atmosphere. For the alkali-phosphate-doped wood, no interactions between the quartz sand and the gaseous K/Na can be observed for either atmosphere.

■ AUTHOR INFORMATION

Corresponding Author

    Zimeng He − *The University of Adelaide, Adelaide, Australia;* ⓞ orcid.org/0000-0001-5420-3661; Email: zimeng.he@adelaide.edu.au

Other Authors

    Woei L. Saw − *The University of Adelaide, Adelaide, Australia*

    Philip J. van Eyk − *The University of Adelaide, Adelaide, Australia;* ⓞ orcid.org/0000-0003-3768-2044

    Graham J. Nathan − *The University of Adelaide, Adelaide, Australia*

    Peter J. Ashman − *The University of Adelaide, Adelaide, Australia*

Complete contact information is available at:
https://pubs.acs.org/10.1021/acs.iecr.9b05712

Notes
The authors declare no competing financial interest.

■ ACKNOWLEDGMENTS

■ REFERENCES

(1) Naik, S. N.; Goud, V. V.; Rout, P. K.; Dalai, A. K. Production of first and second generation biofuels: A comprehensive review. *Renewable Sustainable Energy Rev.* **2010**, *14* (2), 578−597.

(2) Ullah, K.; Ahmad, M.; Sofia; Sharma, V. K.; Lu, P.; Harvey, A.; Zafar, M.; Sultana, S. Assessing the potential of algal biomass opportunities for bioenergy industry: A review. *Fuel* **2015**, *143*, 414−423.

(3) Werther, J.; Saenger, M.; Hartge, E. U.; Ogada, T.; Siagi, Z. Combustion of agricultural residues. *Prog. Energy Combust. Sci.* **2000**, *26* (1), 1−27.

(4) Vassilev, S. V.; Vassileva, C. G. Composition, properties and challenges of algae biomass for biofuel application: An overview. *Fuel* **2016**, *181*, 1−33.

(5) Niu, Y.; Tan, H.; Hui, S. e. Ash-related issues during biomass combustion: Alkali-induced slagging, silicate melt-induced slagging (ash fusion), agglomeration, corrosion, ash utilization, and related countermeasures. *Prog. Energy Combust. Sci.* **2016**, *52*, 1−61.

(6) Skrifvars, B. J.; Hupa, M.; Hiltunen, M. Sintering of ash during fluidized bed combustion. *Ind. Eng. Chem. Res.* **1992**, *31* (4), 1026−1030.

(7) Zevenhoven, M.; Yrjas, P.; Skrifvars, B.-J.; Hupa, M. Characterization of Ash-Forming Matter in Various Solid Fuels by Selective Leaching and Its Implications for Fluidized-Bed Combustion. *Energy Fuels* **2012**, *26* (10), 6366−6386.

(8) Werkelin, J.; Skrifvars, B.-J.; Zevenhoven, M.; Holmbom, B.; Hupa, M. Chemical forms of ash-forming elements in woody biomass fuels. *Fuel* **2010**, *89* (2), 481−493.

(9) Narayan, V.; Jensen, P. A.; Henriksen, U. B.; Glarborg, P.; Lin, W.; Nielsen, R. G. Defluidization in fluidized bed gasifiers using high-alkali content fuels. *Biomass Bioenergy* **2016**, *91*, 160−174.

(10) Sevonius, C.; Yrjas, P.; Hupa, M. Defluidization of a quartz bed − Laboratory experiments with potassium salts. *Fuel* **2014**, *127*, 161−168.

(11) Ma, T.; Fan, C.; Hao, L.; Li, S.; Jensen, P. A.; Song, W.; Lin, W.; Dam-Johansen, K. Biomass ash induced agglomeration in fluidized bed. Part 2: Effect of potassium salts in different gas composition. *Fuel Process. Technol.* **2018**, *180*, 130−139.

(12) Kosminski, A.; Ross, D. P.; Agnew, J. B. Reactions between sodium and silica during gasification of a low-rank coal. *Fuel Process. Technol.* **2006**, *87* (12), 1037−1049.

(13) Wibberley, L. J.; Wall, T. F. Alkali-ash reactions and deposit formation in pulverized-coal-fired boilers: experimental aspects of sodium silicate formation and the formation of deposits. *Fuel* **1982**, *61* (1), 93−99.

(14) Sevonius, C.; Yrjas, P.; Lindberg, D.; Hupa, L. Impact of sodium salts on agglomeration in a laboratory fluidized bed. *Fuel* **2019**, *245*, 305−315.

(15) McKee, D. W. Gasification of graphite in carbon dioxide and water vapor—the catalytic effects of alkali metal salts. *Carbon* **1982**, *20* (1), 59−66.

(16) Lang, R. J. Anion effects in alkali-catalysed steam gasification. *Fuel* **1986**, *65* (10), 1324−1329.

(17) Kopyscinski, J.; Rahman, M.; Gupta, R.; Mims, C. A.; Hill, J. M. K2CO3 catalyzed CO2 gasification of ash-free coal. Interactions of the catalyst with carbon in N2 and CO2 atm. *Fuel* **2014**, *117*, 1181−1189.

(18) McKee, D. W.; Chatterji, D. The catalytic behavior of alkali metal carbonates and oxides in graphite oxidation reactions. *Carbon* **1975**, *13* (5), 381−390.

(19) Wang, Y.; Wu, H.; Sárossy, Z.; Dong, C.; Glarborg, P. Release and transformation of chlorine and potassium during pyrolysis of KCl doped biomass. *Fuel* **2017**, *197*, 422−432.

(20) Chen, H.; Chen, X.; Qiao, Z.; Liu, H. Release and transformation characteristics of K and Cl during straw torrefaction and mild pyrolysis. *Fuel* **2016**, *167*, 31−39.

(21) Tang, H.; Xu, J.; Dai, Z.; Zhang, L.; Sun, Y.; Liu, W.; Mostafa, M. E.; Su, S.; Hu, S.; Wang, Y.; Xu, K.; Zhang, A.; Xiang, J. Functional Mechanism of Inorganic Sodium on the Structure and Reactivity of Zhundong Chars during Pyrolysis. *Energy Fuels* **2017**, *31* (10), 10812−10821.

(22) McKee, D. W. Mechanisms of the alkali metal catalysed gasification of carbon. *Fuel* **1983**, *62* (2), 170−175.

(23) Guo, S.; Jiang, Y.; Liu, T.; Zhao, J.; Huang, J.; Fang, Y. Investigations on interactions between sodium species and coal char by thermogravimetric analysis. *Fuel* **2018**, *214*, 561−568.

(24) Qi, X.; Song, G.; Song, W.; Lu, Q. Influence of sodium-based materials on the slagging characteristics of Zhundong coal. *J. Energy Inst.* **2017**, *90* (6), 914−922.

(25) Lindner, E. R.; Wall, T. F. Sodium ash reactions during combustion of pulverised coal. *Symp. (Int.) Combust., [Proc.]* **1991**, *23* (1), 1313−1321.

(26) Song, B. H.; Kim, S. D. Catalytic activity of alkali and iron salt mixtures for steam-char gasification. *Fuel* **1993**, *72* (6), 797−803.

(27) Hüttinger, K. J.; Minges, R. Catalytic water vapour gasification of carbon. *Fuel* **1985**, *64* (4), 491−494.

(28) Kosminski, A.; Ross, D. P.; Agnew, J. B. Influence of gas environment on reactions between sodium and silicon minerals during gasification of low-rank coal. *Fuel Process. Technol.* **2006**, *87* (11), 953−962.

(29) He, Z.; Lane, D. J.; Saw, W. L.; van Eyk, P. J.; Nathan, G. J.; Ashman, P. J. Ash−Bed Material Interaction during the Combustion and Steam Gasification of Australian Agricultural Residues. *Energy Fuels* **2018**, *32* (4), 4278−4290.

(30) Weldes, H. H.; Lange, K. R. PROPERTIES OF SOLUBLE SILICATES. *Ind. Eng. Chem.* **1969**, *61* (4), 29−44.

(31) Merrill, R. C. Chemistry of the soluble silicates. *J. Chem. Educ.* **1947**, *24* (6), 262.

(32) Öhman, M.; Nordin, A.; Skrifvars, B.-J.; Backman, R.; Hupa, M. Bed Agglomeration Characteristics during Fluidized Bed Combustion of Biomass Fuels. *Energy Fuels* **2000**, *14* (1), 169−178.

(33) Gatternig, B.; Karl, J. Investigations on the Mechanisms of Ash-Induced Agglomeration in Fluidized-Bed Combustion of Biomass. *Energy Fuels* **2015**, *29* (2), 931−941.

(34) Zhu, Y.; Piotrowska, P.; van Eyk, P. J.; Boström, D.; Wu, X.; Boman, C.; Broström, M.; Zhang, J.; Kwong, C. W.; Wang, D.; Cole, A. J.; de Nys, R.; Gentili, F. G.; Ashman, P. J. Fluidized Bed Co-gasification of Algae and Wood Pellets: Gas Yields and Bed Agglomeration Analysis. *Energy Fuels* **2016**, *30* (3), 1800−1809.

(35) Hüttinger, K. J.; Minges, R. Influence of the catalyst precursor anion in catalysis of water vapour gasification of carbon by potassium: 1. Activation of the catalyst precursors. *Fuel* **1986**, *65* (8), 1112−1121.

(36) Knudsen, J. N.; Jensen, P. A.; Dam-Johansen, K. Transformation and Release to the Gas Phase of Cl, K, and S during Combustion of Annual Biomass. *Energy Fuels* **2004**, *18* (5), 1385−1399.

(37) Hashimoto, K.; Miura, K.; Xu, J.-J.; Watanabe, A.; Masukami, H. Relation between the gasification rate of carbons supporting alkali metal salts and the amount of oxygen trapped by the metal. *Fuel* **1986**, *65* (4), 489−494.

(38) He, Z.; Saw, W. L.; van Eyk, P. J.; Nathan, G. J.; Ashman, P. J. Effect of calcium and phosphorus on interactions between quartz sand and K-salt-doped wood under both steam gasification and combustion atmospheres. Submitted for publication in *Energy Fuels*.

(39) HRMA, P. Reaction between Sodium Carbonate and Silica Sand at 874°C < T < 1022°C. *J. Am. Ceram. Soc.* **1985**, *68* (6), 337−341.

(40) Anicic, B.; Lin, W.; Dam-Johansen, K.; Wu, H. Agglomeration mechanism in biomass fluidized bed combustion − Reaction between potassium carbonate and silica sand. *Fuel Process. Technol.* **2018**, *173*, 182−190.

(41) Grynberg, J.; Gouillart, E.; Chopinet, M.-H.; Toplis, M. J. Importance of the Atmosphere on the Mechanisms and Kinetics of Reactions Between Silica and Solid Sodium Carbonate. *International Journal of Applied Glass Science* **2015**, *6* (4), 428−437.

(42) Kirnbauer, F.; Koch, M.; Koch, R.; Aichernig, C.; Hofbauer, H. Behavior of Inorganic Matter in a Dual Fluidized Steam Gasification Plant. *Energy Fuels* **2013**, *27* (6), 3316−3331.

(43) Elled, A. L.; Åmand, L. E.; Steenari, B. M. Composition of agglomerates in fluidized bed reactors for thermochemical conversion of biomass and waste fuels: Experimental data in comparison with predictions by a thermodynamic equilibrium model. *Fuel* **2013**, *111*, 696−708.

(44) Yuh, S. J.; Wolf, E. E. FTIR studies of potassium catalyst-treated gasified coal chars and carbons. *Fuel* **1983**, *62* (2), 252−255.

(45) Yuh, S. J.; Wolf, E. E. Kinetic and FT-i.r. studies of the sodium-catalysed steam gasification of coal chars. *Fuel* **1984**, *63* (11), 1604−1609.

Chapter 4

Paper II

Effect of Calcium and Phosphorus on Interactions between Quartz Sand and K-Salt-Doped Wood under Both Steam Gasification and Combustion Atmospheres

Zimeng He*[†‡], Woei L. Saw[†‡], Philip J. van Eyk[†‡], Graham J. Nathan[†§], Peter J. Ashman[†‡]

[†]Centre for Energy Technology, The University of Adelaide, Adelaide, South Australia 5005, Australia
[‡]School of Chemical Engineering and Advanced Materials, The University of Adelaide, Adelaide, South Australia 5005, Australia
[§]School of Mechanical Engineering, The University of Adelaide, Adelaide, South Australia 5005, Australia

Statement of Authorship

Title of Paper	Effect of calcium and phosphorus on the interaction behaviour between K salt-doped wood and bed material under a steam gasification or a combustion atmosphere
Publication Status	☐ Published ☐ Accepted for Publication ☑ Submitted for Publication ☐ Unpublished and Unsubmitted work written in manuscript style
Publication Details	The manuscript was under revision by the author after according to the comments of the reviewers from the journal of Energy & Fuels.

Principal Author

Name of Principal Author (Candidate)	Zimeng He
Contribution to the Paper	Performed analysis on all samples, interpreted data, wrote manuscript and acted as corresponding author.
Overall percentage (%)	70
Certification:	This paper reports on original research I conducted during the period of my Higher Degree by Research candidature and is not subject to any obligations or contractual agreements with a third party that would constrain its inclusion in this thesis. I am the primary author of this paper.
Signature	Date 22.10.2019

Co-Author Contributions

By signing the Statement of Authorship, each author certifies that:

     i.   the candidate's stated contribution to the publication is accurate (as detailed above);

     ii.   permission is granted for the candidate in include the publication in the thesis; and

     iii.   the sum of all co-author contributions is equal to 100% less the candidate's stated contribution.

Name of Co-Author	Woei L.Saw
Contribution to the Paper	Supervised development of work, helped in data interpretation, reactor construction and manuscript evaluation and edition
Signature	Date 21/10/2019

Name of Co-Author	Philip J. van Eyk
Contribution to the Paper	Supervised development of work, helped in data interpretation and manuscript evaluation
Signature	Date 4/10/2019

Name of Co-Author	Graham J. Nathan
Contribution to the Paper	Supervised development of work, helped in data interpretation and manuscript evaluation and edition
Signature			Date	17/10/19

Name of Co-Author	Peter J. Ashman
Contribution to the Paper	Supervised development of work, helped in data interpretation and manuscript evaluation
Signature			Date	17-10-19

energy&fuels

Article

Effect of Calcium and Phosphorus on Interactions between Quartz Sand and K-Salt-Doped Wood under Both Steam Gasification and Combustion Atmospheres

Zimeng He,* Woei L. Saw, Philip J. van Eyk, Graham J. Nathan, and Peter J. Ashman

Read Online

ACCESS | Metrics & More | Article Recommendations

ABSTRACT: Effects of Ca and P on the interactions between quartz sand as the bed material and wood loaded with K_2CO_3, K_2SO_4, or KCl salts were studied in a lab-scale, fixed bed reactor at 900 °C under a combustion (5%, v/v, O_2) and steam gasification (50%, v/v, steam) atmosphere. The addition of calcite to these salt-loaded wood samples decreases the K retention in agglomerates and reduces the size of agglomerates. The extent of these effects depends upon the salt species. Steam increases the K retention in agglomerates. For wood loaded with salt mixtures of K_2CO_3/KH_2PO_4, K_2SO_4/KH_2PO_4, or KCl/KH_2PO_4, agglomerates dominated by K silicates are formed when the content of P in the wood samples is high, while agglomerates dominated by K phosphates are formed when the content of P in the wood samples is low. Both the addition of calcite at 1 wt % Ca to the wood samples loaded with the K salt mixtures and the addition of $Ca(PO_3)_2$ at either 0.5 or 1 wt % Ca to the wood samples loaded with K_2CO_3, K_2SO_4, or KCl salts result in the formation of K−Ca phosphates ($KCaPO_4$, $K_2CaP_2O_7$, or other phases) within the silicate coating layer. Further increasing the $Ca(PO_3)_2$ concentration to 3 wt % Ca leads to the formation of agglomerates dominated by partially molten K−Ca phosphates ($K_2CaP_2O_7$ or other phases), which is inhibited by steam. With the addition of $Ca(PO_3)_2$, the K retention in agglomerates is increased by the formation of K−Ca phosphates while decreased by the inhibition of K silicates. The domination of the two opposite effects depends upon the concentration of $Ca(PO_3)_2$ and the types of K salts.

1. INTRODUCTION

Agglomeration is a term used to describe the adhesion of bed materials by either fuel-derived partially molten ash (silicates or phosphates) or alkali silicates formed by reactions between Si from bed materials and alkali metals (K and Na) from fuels.[1,2] Understanding of agglomeration is critical to ensure continuous operation of fluidized bed reactors and to avoid unscheduled shut down of the whole reactor.[1,3] Many studies were conducted to better understand agglomeration mechanisms of raw biomass.[2,4−10] However, elemental compositions of inorganic matter in raw biomass are complicated. Alkali metals, especially K, are key inorganic elements in biomass for agglomeration and are mainly in a form of water-soluble salts, such as carbonates, chlorides, sulfates, or phosphates, in biomass.[3,11] Quartz sand, mainly consisting of Si, is usually used as a bed material in fluidized bed reactors and can easily cause bed agglomeration in fluidized bed reactors, especially when feedstock rich in alkali metals is used.[12,13] He et al.[14] investigated agglomeration behaviors of individual water-soluble alkali salts in biomass, which contributes to a better understanding of agglomeration behaviors of different species of biomass. They indicated that interactions between quartz sand and wood loaded with K_2CO_3, K_2SO_4, or KCl salts vary with K salt species.[14] The presence of calcium (Ca) and phosphorus (P) in biomass can be significant, especially in agricultural residues.[15] Interactions between quartz sand and alkali metals in biomass are also influenced significantly by the presence of Ca or P,[8,9,16] from either biomass or additives.

These are complex and poorly understood, and therefore, there is a need to assess the effects of Ca and P on interactions between quartz sand and K_2CO_3, K_2SO_4, or KCl salts systematically.

Ca is a major inorganic matter in biomass and has been found to have positive effects on the mitigation of agglomeration.[17−22] Therefore, an understanding of the effects of Ca on the agglomeration of various types of biomass is critical. Generally, Ca presents as either an organically associated element or crystalline salts in biomass.[23] Moreover, Ca can be introduced as an additive or found naturally within bed materials, such as calcite, limestone, and dolomite, during biomass gasification or combustion.[19−22,24] The addition of Ca provides a dilution effect on biomass ash, thus minimizing agglomeration activities.[20,25] Reactions between Ca and Si form high-melting-point Ca silicates, which reduce the amount of Si that reacts with K, thus inhibiting the formation of K silicates and increasing the release of K.[19,26] During the formation of the coating layer on quartz sand, He et al.[22] found that the ash particles rich in Ca stick to the K silicate coating layer. Then, the Ca/Si ratio of the layer is increased, while the

K/Ca ratio is decreased by the gradual diffusion of Ca into the layer. The Ca-rich layer prevents quartz sand from further reacting with K in biomass.[22,27] The impact of Ca on the interactions between individual K salts in biomass and quartz sand is seldom reported. This knowledge contributes to the understanding of the effect of Ca on the agglomeration of various types of biomass and needs to be acquired.

P affects the agglomeration behaviors of K salts in biomass significantly.[8,28,29] It is critical to further explore the influence of P on the agglomeration of various species of biomass with different contents of P. For fuels rich in P, agglomerates are usually formed by the adhesion of bed materials to fuel-derived phosphate ash without any reactions between the bed materials and the ash (a non-reactive mechanism).[28] An increase in the P content of biomass decreases the amount of K that reacts with Si.[8] Co-combustion of fuels rich in P and fuels with a low P content cause the co-existence of both reactive (the formation of alkali silicates) and non-reactive mechanisms.[28] The role of P on ash transformation processes is influenced significantly by Ca.[16,30−32] When the P content is increased for fuels rich in Ca, high-melting-point K−Ca phosphates are formed instead of low-melting-point K silicates. In contrast, a large amount of low-melting-temperature volatile K phosphates can be generated if fuels have a low Ca content.[30] Usually, either K phosphates or Ca silicates are considered less stable than Ca phosphates.[33,34] Stable Ca phosphates, such as $Ca_2P_2O_7$, $Ca(PO_3)_2$, or $Ca_3(PO_4)_2$, are formed when both Ca and P are present, and the compositions of the Ca phosphates depend upon the stoichiometric ratio of Ca/P.[35] The addition of Ca phosphates to biomass results in the formation of K−Ca phosphates with high melting temperatures, which increases the K retention in agglomerates and improves the fusion temperatures of ash.[36−39] Therefore, the formation of Ca phosphates can have an significant impact on the agglomeration of biomass.[33] Assessment of the effect of P, with or without the presence of Ca, on the interactions between several K salts in biomass and quartz sand is important to the knowledge of bed agglomeration of biomass. However, these effects are poorly understood, and this study aims to meet the need.

Steam can potentially influence the effects of Ca or P on the interactions between quartz sand and biomass. The effects can be assessed by the K retention in agglomerates, which identifies the formation of K silicates in agglomerates. This information partially suggests the tendency toward bed agglomeration. The solubility of K silicates in water varies with the silica contents of these silicates.[40,41] Alkali silicates can dissolve in cold water (15−25 °C) if the silica content is low, while alkali silicates can dissolve in hot water (90−100 °C), nearly boiling water, if the silica content is high.[40,42] The solubility of alkali silicates is decreased if the silica/alkali oxide weight ratio is increased, and silicates with a ratio greater than 4 normally cannot be water-soluble.[41] The melting temperature of K silicates also varies with the silica contents, thus affecting the formation of agglomerates.[40,41] Therefore, the solubility of silicates is related to their melting behaviors during agglomeration. Several studies revealed that steam gasification atmospheres aggravate agglomeration by influencing the behaviors of various types of alkali salts present within biomass.[14,42,43] However, the influence of steam gasification atmospheres on the behaviors of Ca or P during agglomeration processes is seldom reported. Therefore, another objective of this paper is evaluating how a steam gasification atmosphere

impacts the interactions between K salts and quartz sand, with the presence of Ca or P. This effect is also compared to that of a combustion atmosphere.

Both particle physics and interactions between bed materials with biomass influence agglomeration in a fluidized bed reactor.[44] In the present study, the interactions between quartz sand (the bed material) and biomass were assessed in a lab-scale, fixed bed reactor alone without considering the potential effect of particle physics, which can be evaluated in a modeling study.[44] The interactions identified in the present study contribute to the knowledge of the chemical reaction mechanisms of agglomeration in fluidized bed reactors. The fixed bed reactor has more initial solid−solid and liquid−solid contacts between particles in comparison to a fluidized bed reactor because there is no fluidization of particles in the proposed fixed bed reactor. Therefore, this has potential to aggravate agglomeration to some extent.

In light of the discussion above, the aim of this work is to assess how Ca or P influence the interactions between quartz sand (the bed material) and wood loaded with K_2CO_3, KCl, or K_2SO_4 salts relevant to the conditions of both combustion and steam gasification.

2. METHODOLOGY

2.1. Bed Material, Fuel, and Additives. A commercial Swedish softwood with a low ash content (less than 0.3%) was used to prepare the K-salt-loaded feedstock. The ultimate and proximate analyses and inorganic elemental composition of the wood were reported previously, as shown in Tables 1 and 2, respectively.[45] Quartz sand

Table 1. Proximate and Ultimate Analyses of the Swedish Softwood[45]

	Swedish softwood
moisture (%)	7.3
Proximate Analysis (wt %, db[a])	
volatile matter	85.6
fixed carbon	14.1
ash	0.3
Ultimate Analysis (wt %, db[a])	
C	51.4
H	6.2
N	<0.1
O (by difference)	42.0
S	0.01
Cl	0.02

[a]db = dry basis.

Table 2. Ash Elemental Composition of the Swedish Softwood[45]

mg/kg of dry fuel	Swedish softwood
K	359
Ca	686
Na	8
Mg	139
Al	26
Fe	24
P	40
S	56
Cl	<100
Si	91

from the Coonarr Creek mine in Bundaberg, Australia, was used as the bed material. Its particle size is between 75 and 212 μm, and its composition was described elsewhere.[6] Calcite whose size is below 250 μm was from Sibelco, Australia, and was selected as one of the two Ca additives. The other Ca additive, $Ca(PO_3)_2$, was prepared by heating $Ca(H_2PO_4)_2$ at 230 °C for 2–3 h.[32]

2.2. Feedstock Preparation. A beaker was used to dissolve a certain amount of analytical-reagent-grade K_2CO_3, K_2SO_4, or KCl salts and salt mixtures of K_2CO_3/KH_2PO_4, K_2SO_4/KH_2PO_4, or KCl/KH_2PO_4 (molar ratios of 3:1 or 1:2) with deionized water. Then, a wood–water slurry was formed by adding wood to the solution and was mixed uniformly. It was dried at 35 °C and then at 105 °C for approximately 1 day. The concentration of K in all of the prepared samples was fixed at 3 wt %. Calcite was added to the wood samples loaded with K_2CO_3, K_2SO_4, or KCl to achieve a Ca content of either 1 or 3 wt % and to the wood samples loaded with the salt mixtures of K_2CO_3/KH_2PO_4, K_2SO_4/KH_2PO_4, or KCl/KH_2PO_4 (molar ratios of 3:1 or 1:2) to achieve a Ca content of 1 wt %. $Ca(PO_3)_2$ was added to the wood samples loaded with K_2CO_3, K_2SO_4, or KCl to achieve a Ca content of 0.5, 1, or 3 wt % in the samples. Melting points of the chemical compounds used in the present paper are shown in Table 3.

Table 3. Melting Temperatures of the Compounds Used in the Present Study

chemical compound	melting temperature[34,46,47] (°C)
K_2CO_3	788–904
KCl	770–790
K_2SO_4	1067–1100
KH_2PO_4	252.6
calcite	decomposes at 825
$Ca(PO_3)_2$	983

2.3. Interaction Tests. Figure 1 presents the lab-scale, fixed bed reactor, which was used to conduct the interaction tests and was
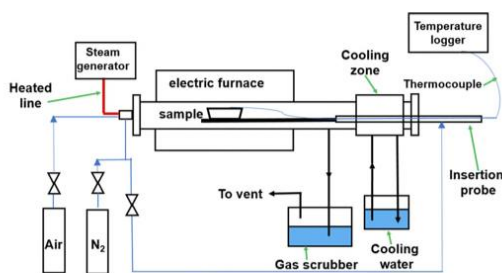

Figure 1. Schematic diagram of the reactor used for the tests.

described previously.[6] Either with or without the additives, approximately 0.5 g of quartz sand was mixed uniformly with approximately 1.5 g wood samples inside a crucible. The crucible was inserted into the center of the reactor to begin the test and was retracted from the reactor to be cooled after the test with an insertion probe. Reaction atmospheres of air/N_2 (5%, v/v, O_2) for combustion and steam/N_2 (50%, v/v, steam) for gasification were used during the tests, which were carried out for 45 min at 900 °C. For the tests with the addition of $Ca(PO_3)_2$ at 3 wt % Ca conducted during steam gasification, a reaction time of 1.5 h was also applied. Agglomerates from the tests were collected and prepared for further analyses as described in sections 2.4 and 2.5.

2.4. Scanning Electron Microscopy in Combination with Energy-Dispersive Spectroscopy (SEM/EDS) and X-ray Diffraction (XRD) Analyses. SEM/EDS (Philips model XL30) was used to analyze the cross sections of the agglomerates to obtain their elemental compositions and morphology. The cross sections were

obtained by polishing the samples, which were fixed inside a resin. After that samples were carbon-coated to reduce charging. A backscattering electron mode (BSE) was chosen to perform the SEM/EDS analysis. A significant number of spots distributed uniformly at the cross sections were analyzed with EDS for each sample. The results of all of the analyzed spots were averaged to obtain the elemental composition for each sample. Furthermore, several selected agglomerates were conducted with EDS mapping analysis to obtain the distribution of some major inorganic matter in the images of SEM cross sections. The images of SEM cross sections and EDS mapping present in this work are representative of most equivalent cases. For samples from the interaction tests between the raw wood and the quartz sand under both atmospheres, only separate quartz sand particles can be observed with SEM/EDS, while no agglomerates are formed. An XRD measurement (Rigaku MiniFlex 600) applying Cu Kα radiation was used to analyze the crystalline phases for all of the agglomerates.

2.5. Acid Digestion and Water Leaching Tests. Acid digestion (48% HF and 70% HNO_3) analysis was carried out with selected agglomerates. Then, the acid-digested samples were analyzed with a Schimadzu atomic absorption spectrophotometer (AAS, AA-6300) to obtain the K retention in these agglomerates. The procedures of the above analyses were described previously.[14] The mass of acid-soluble K relative to the mass of K introduced with the feedstock is the mass fraction (%) of K in agglomerates that is soluble in acid.

Cold water leaching at 15–25 °C and hot water leaching at 90–100 °C were performed with magnetic stirring for 4 h. The leached samples were diluted and then analyzed with AAS to obtain the concentration of K. The mass of K soluble in cold water relative to the mass of K introduced with the feedstock is the mass fraction (%) of K in agglomerates that is soluble in cold water. The difference between the mass of K soluble in hot and cold water relative to the mass of K introduced with the feedstock is the mass fraction (%) of K in agglomerates that is soluble in hot water. For each selected interaction test, three samples prepared repeatedly were analyzed. The values of the three individual samples were averaged to obtain the reported results.

3. RESULT

3.1. Effect of Ca on the Interactions. Images of agglomerates generated during both combustion and steam gasification at 900 °C are shown in Figure 2 for wood loaded with K_2CO_3, K_2SO_4, or KCl when no calcite or calcite at 1 and 3 wt % Ca was added. The interaction test matrix is shown in Table 4. The cases without the addition of calcite, as shown in panel A of Figure 2, have been discussed in a previous study.[14] For these cases without calcite, the formation of agglomerates with a size of approximately 1 cm can be observed for either K_2CO_3- or K_2SO_4-loaded wood under the two atmospheres and KCl-loaded wood under the steam gasification atmosphere. On the other hand, agglomerates with a size less than approximately 5 mm are formed for KCl-loaded wood under the combustion atmosphere. Reactions between various species of pure alkali salts and quartz sand were reported previously.[42,43,48–50] Ma et al.[50] reported that Si from quartz sand can react with pure K_2CO_3 salt but not pure K_2SO_4 salt to generate alkali silicates under either a reducing condition [H_2O/N_2 (25 vol % H_2O)] or an oxidizing condition (air). In contrast, they concluded that Si from quartz sand can only react with pure KCl salt in the presence of steam. However, Si from quartz sand have all reacted with the wood samples loaded with K_2CO_3, K_2SO_4, or KCl salts in the present study, thus forming the coating layer of K silicate. This is because the organic compounds in the wood samples have affected the behaviors of these K salts.[51–53] Panels B and C of Figure 2 show that the size of agglomerates for salt-loaded wood is
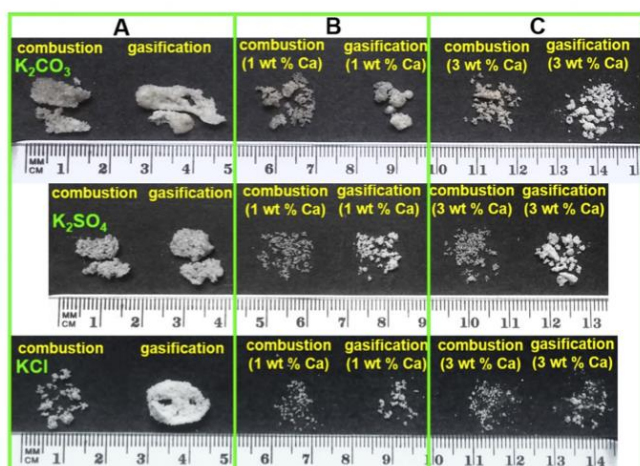
Figure 2. Images of agglomerates generated during both combustion and steam gasification at 900 °C for wood loaded with K_2CO_3, K_2SO_4, or KCl salts when no calcite or calcite at 1 and 3 wt % Ca was added: (A) no calcite was added, and calcite at (B) 1 wt % and (C) 3 wt % was added.

Table 4. Interaction Test Matrix of Section 3.1

types of K salts in wood (steam gasification and combustion)	additive
K_2CO_3	N/A
K_2CO_3	calcite at 1 wt % Ca
K_2CO_3	calcite at 3 wt % Ca
K_2SO_4	N/A
K_2SO_4	calcite at 1 wt % Ca
K_2SO_4	calcite at 3 wt % Ca
KCl	N/A
KCl	calcite at 1 wt % Ca
KCl	calcite at 3 wt % Ca

decreased significantly by calcite, especially agglomerates for K_2SO_4-loaded wood generated during combustion and agglomerates for KCl-loaded wood generated during both atmospheres. This suggests that the effect of Ca on agglomerates depends upon the composition of K salts of biomass.

Figure 3 presents selected SEM cross-sectional images and EDS mapping of agglomerates. Figure 4 shows the elemental
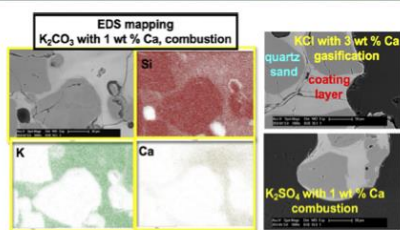
Figure 3. Selected SEM cross-sectional images and EDS mapping of agglomerates generated during both combustion and steam gasification at 900 °C for wood loaded with K_2CO_3, K_2SO_4, or KCl salts when calcite was added.

composition of the coating layer for wood loaded with K_2CO_3, K_2SO_4, or KCl salts. The coating layer referenced in section 3.1 is defined as the lighter homogeneous compounds that surround the darker particles of quartz sand (Figure 3). Adding calcite to the wood samples loaded with K_2CO_3, K_2SO_4, or KCl salts introduces Ca into the coating layer, which is dominated by K, Si, and Ca (Figure 4). However, images of EDS mapping in Figure 3 show that the distribution of Ca within the coating layer is inhomogeneous. This may result from the short reaction time of the tests or the uneven distribution of calcite in the feedstock as a result of the limitation of hand mixing before the tests. When the concentration of Ca in the samples is increased from 1 to 3 wt % Ca, insignificant changes of the elemental composition of the coating layer can be observed.

For the cases of K_2SO_4-loaded wood with the addition of calcite, some unreacted K_2SO_4 may exist in agglomerates according to the XRD results. However, almost no S can be detected in the coating layer for these cases with SEM/EDS. For some cases of the salt-loaded wood samples with the addition of calcite, some unreacted CaO can be detected in agglomerates with XRD. Phases of Ca silicates may also be formed in agglomerates, as suggested previously.[8,19,26,54] Nevertheless, no Ca silicates can be detected with XRD in agglomerates.

Mass fractions (%) presented in Figure 5 are the mass of K in agglomerates soluble in acid and cold and hot water relative to the mass of K introduced from the feedstock for wood loaded with K_2CO_3, K_2SO_4, or KCl salts. These agglomerates were generated at 900 °C under both combustion and steam gasification atmospheres with or without calcite. Acid-soluble K indicates that the total mass of K remained in agglomerates. The cases without calcite have been reported in a previous work.[14] For these cases without calcite, the K retention in agglomerates for either K_2CO_3- or K_2SO_4-loaded wood is approximately 75−100% and is much higher than that for KCl-loaded wood, which is approximately 15−40%. For wood loaded with K_2CO_3, K_2SO_4, or KCl salts, the addition of calcite

42

Figure 4. Elemental composition on a C- and O-free basis of some major inorganic elements of the coating layer generated during both combustion and steam gasification at 900 °C for wood loaded with K_2CO_3, K_2SO_4, or KCl salts when calcite was added.

Figure 5. Mass fractions (%) of K in agglomerates soluble in acid and cold and hot water relative to K introduced from the feedstock for wood loaded with K_2CO_3, K_2SO_4, o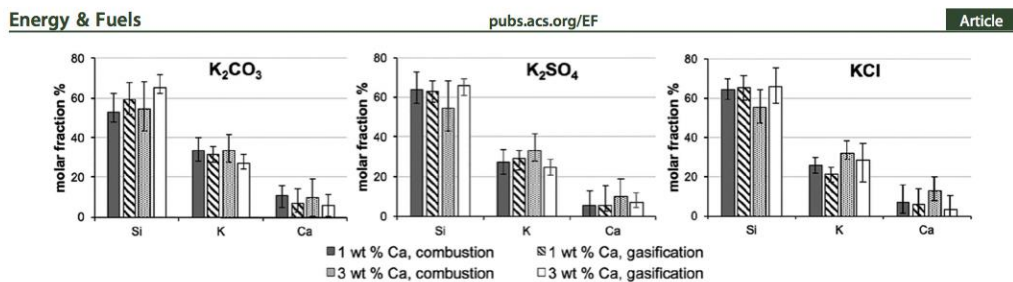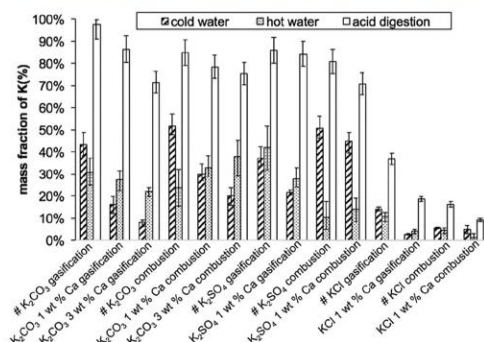r KCl salts. These agglomerates were generated during combustion and steam gasification at 900 °C when no calcite or calcite at either 1 or 3 wt % Ca was added. (#) These data were reported previously.[14]

at 1 wt % Ca decreases the K retention in agglomerates. For K_2CO_3-loaded wood, the K retention in agglomerates is further decreased when the concentration of Ca is increased from 1 to 3 wt %. Consistent with other studies,[20,27] the above results reveal that calcite decreases the formation of K silicates. Therefore, the size of agglomerates is decreased, as shown in Figure 2. In addition, for most cases of wood loaded with K_2CO_3, K_2SO_4, or KCl salts, the K retention in agglomerates generated during steam gasification is higher than that in those generated during combustion. Therefore, either with or without the addition of calcite, less silicates are formed for combustion than for steam gasification. This is consistent with the size of agglomerates (Figure 2). For the cases of wood loaded with K_2CO_3, K_2SO_4, or KCl salts, when no calcite was added, the formation of K silicates with different melting behaviors, which is deduced from the water leaching tests, has been discussed in a previous work.[14] That is, more silicates with relatively lower melting temperatures are formed with the presence of steam than that for combustion because steam increases the fraction of K soluble in hot water. This also contributes to the greater size of agglomerates generated during steam gasification than during combustion (Figure 2). For wood loaded with K_2CO_3, K_2SO_4, or KCl salts, calcite decreases the cold-water-soluble fractions for all of the cases and the hot-water-soluble fractions for some cases, as shown in

Figure 5. Therefore, for most cases, the addition of calcite decreases the formation of both types of silicates.

The addition of Ca can have a dilution effect, which influences the formation of agglomerates for wood loaded with K_2CO_3, K_2SO_4, or KCl salts. To investigate the dilution effect, the interaction tests with a 7 min reaction time (an early stage) between K_2CO_3-loaded wood and quartz sand were performed for both atmospheres when calcite at 1 wt % Ca was added. The surface analysis of SEM/EDS shows that the combustion atmosphere reduces the size of agglomerates formed during the early stage in comparison to the steam gasification atmosphere. Many CaO particles can be observed around the sand particles, while an insignificant content of Ca can be detected in the coating layer for combustion. On the other hand, with the presence of steam, the coating layer incorporates many CaO particles. However, the distribution of these CaO particles within the coating layer is inhomogeneous. The CaO particles that are either distributed around the sand particles or incorporated into the coating layer can inhibit the reactions between K and quartz sand under the two atmospheres, thus decreasing the formation tendency of agglomerates. The competition between the formation of K silicates and Ca silicates may also have an influence on the interactions. Some studies indicated that the formation of Ca silicates reduces the reaction between K and Si, thus increasing the release of K.[19,26] However, other studies suggested that the formation of Ca silicates are a slower process than that of K silicates. Generally, Ca silicates are considered to be less stable than K silicates, as reported by Billen et al.[33] In addition, Boström et al.[55] suggested that reactions between K and quartz sand can be gas–solid reactions, which are much faster than the solid–solid reactions between Ca and quartz sand. He et al.[22] reported that, in fluidized bed reactors with continuous feeding of feedstock, K silicates are formed first during an early stage of agglomeration. They also found that Ca is then gradually incorporated into the K silicate coating layer and forms Ca silicates when the reaction time is increased. Consequently, in the present study, Ca silicates may not be formed in agglomerates for wood loaded with K_2CO_3, K_2SO_4, or KCl salts because of either the short reaction time (45 min) or the limited amount of feedstock used in the fixed bed reactor. Furthermore, no Ca silicates can be detected with XRD in any agglomerates formed in this study. It is deduced that Ca can simply dissolve into the silicate coating layer without forming any Ca silicates. Nevertheless, further investigations are required.

The addition of Ca can affect the formation of agglomerates for wood loaded with K_2CO_3, K_2SO_4, or KCl salts by influencing the viscosity of the coating layer. For silicate

43

compounds, the viscosity of the liquid phase is affected by both the temperature and the elemental composition of the liquid phase. Generally, an increase in the temperature reduces the viscosity of the liquid phase, while the amount of the liquid phase is increased.[56,57] The strength or bonding force of the necks between particles is inversely proportional to the viscosity of the coating layer.[56,58] The reduction of viscosity promotes the movement of the liquid phase toward other particles and the formation of the liquid bridge between particles, which facilitates the formation of agglomerates.[13,59] An increase in the amount of the liquid phase also favors the formation of agglomerates. The melting points of K silicates in agglomerates can be as low as 764 °C, as indicated by others.[12] Therefore, without the addition of calcite at 900 °C, a high fraction of liquid K silicates with a low viscosity facilitates the formation of agglomerates for wood loaded with K_2CO_3, K_2SO_4, or KCl salts, as suggested by Lin et al.[56] The acid digestion results in Figure 5 suggest that the addition of calcite decreases the formation of the low-viscosity liquid K silicates in agglomerates, thus decreasing the tendency toward the formation of agglomerates.

3.2. Effect of P on the Interactions. Table 5 presents interaction test matrix and the compounds identified in agglomerates. Figure 6 presents selected SEM cross-sectional images of agglomerates and the elemental composition of the silicate coating layer generated during both combustion and steam gasification at 900 °C for wood loaded with salt mixtures of K_2CO_3/KH_2PO_4, K_2SO_4/KH_2PO_4, or KCl/KH_2PO_4 (molar ratios of 3:1 and 1:2). The coating layer referenced in section 3.2 is defined as both the homogeneous lighter silicate coating layer that surrounds particles of quartz sand and the K phosphate coating layer that covers quartz sand particles, as shown in Figure 6. The K silicate coating layer incorporates more particles of quartz sand than the K phosphate coating layer. Figure 6 also shows that the silicate coating layer mainly consists of K and Si, with a minor P content. For wood loaded with salt mixtures of K_2CO_3/KH_2PO_4, K_2SO_4/KH_2PO_4, or KCl/KH_2PO_4, as shown in Table 5, agglomerates dominated by the K silicate coating layer can be observed for most cases with a molar ratio of 3:1. In contrast, agglomerates dominated by the molten K phosphate coating layer can be observed for most cases with a molar ratio of 1:2. The elemental composition of agglomerates suggests that most agglomerates are formed by the reactions between K and Si for fuels with a lower P content. In contrast, molten phosphate ash incorporates bed materials to form most agglomerates for fuels with a higher P content. These are in agreement with other studies.[8,28]

Interestingly, morphology of agglomerates for both atmospheres is not affected significantly by the addition of calcite at 1 wt % Ca to the wood samples loaded with salt mixtures of K_2CO_3/KH_2PO_4, K_2SO_4/KH_2PO_4, or KCl/KH_2PO_4. However, the addition of calcite to these wood samples results in the formation of some light particles consisting of either K−Ca−Si−P or K−Ca−P, which are distributed within the darker silicate coating layer under both atmospheres. This agrees with the results reported by Piotrowska et al.[29] Figure 7 presents selected images of EDS mapping of the coating layer for wood loaded with the salt mixture of K_2CO_3/KH_2PO_4. These images show that the distribution of K within the coating layer is homogeneous. However, distributions of both Ca and P within the coating layer are inhomogeneous and are consistent with the distribution of the light particles. These results suggest that

Table 5. Interaction Test Matrix of Wood Loaded with Salt Mixtures of K_2CO_3/KH_2PO_4, K_2SO_4/KH_2PO_4, or KCl/KH_2PO_4 (Molar Ratios of 3:1 or 1:2, with/without the Addition of Calcite at 1 wt % Ca)

interaction test	K silicate coating layer	K phosphate coating layer	K−Ca silicates/phosphates
		K_2CO_3/KH_2PO_4	
3:1, combustion	√	√	N/A
3:1, gasification	√		N/A
3:1 + calcite, combustion	√		K−Ca−Si−P
3:1 + calcite, gasification	√		K−Ca−Si−P and K−Ca−P
1:2, combustion		√	N/A
1:2, gasification	√	√	N/A
1:2 + calcite, combustion	√	√	K−Ca−Si−P and K−Ca−P
1:2 + calcite, gasification	√	√	K−Ca−Si−P and K−Ca−P
		K_2SO_4/KH_2PO_4	
3:1, combustion	√	√	N/A
3:1, gasification	√		N/A
3:1 + calcite, combustion	√		K−Ca−Si−P and K−Ca−P
3:1 + calcite, gasification	√		K−Ca−Si−P and K−Ca−P
1:2, combustion		√	N/A
1:2, gasification		√	N/A
1:2 + calcite, combustion	√	√	K−Ca−Si−P and K−Ca−P
1:2 + calcite, gasification	√	√	K−Ca−Si−P and K−Ca−P
		KCl/KH_2PO_4	
3:1, combustion	√	√	N/A
3:1, gasification	√	√	N/A
3:1 + calcite, combustion	√		K−Ca−Si−P and K−Ca−P
3:1 + calcite, gasification	√		K−Ca−Si−P and K−Ca−P
1:2, combustion		√	N/A
1:2, gasification		√	N/A
1:2 + calcite, combustion		√	K−Ca−Si−P and K−Ca−P
1:2 + calcite, gasification	√	√	K−Ca−Si−P and K−Ca−P

the reaction between Ca and K phosphate leads to the formation of K−Ca phosphates that are distributed within the silicate coating layer. This agrees with the study by Eriksson et al.[16] Figure 8 presents the elemental composition of the silicate coating layer and the K−Ca−Si−P or K−Ca−P compounds. The silicate coating layer can be detected for most cases, as shown in Table 5. The K phosphate coating layer can be found for all of the cases with a molar ratio of 1:2.

The XRD analysis has identified the formation of $KCaPO_4$ in all agglomerates generated during both combustion and steam gasification for wood loaded with either K_2CO_3/KH_2PO_4 or K_2SO_4/KH_2PO_4 when calcite was added. In contrast, in agglomerates generated during both combustion and steam gasification for wood loaded with KCl/KH_2PO_4, $K_2CaP_2O_7$ and $KCaPO_4$ can be detected for the cases with
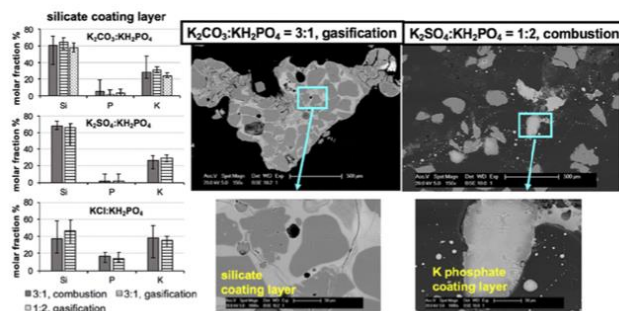
Figure 6. Selected SEM cross-sectional images of the coating layer of silicate and K phosphate generated during both combustion and steam gasification at 900 °C for wood loaded with salt mixtures of K_2CO_3/KH_2PO_4, K_2SO_4/KH_2PO_4, or KCl/KH_2PO_4 and elemental composition on a C- and O-free basis of some major inorganic elements of the silicate coating layer.
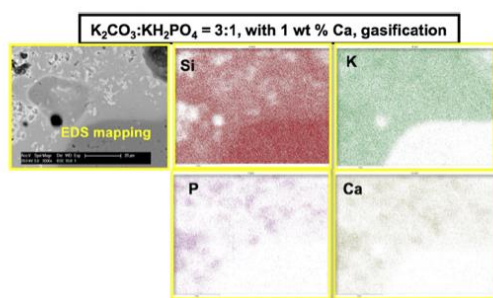
Figure 7. Selected images of EDS mapping of agglomerates.

molar ratios of 1:2 and 3:1, respectively. The presence of these K−Ca phosphate phases is consistent with the above SEM/EDS results.

The composition of the salt-loaded wood samples and the addition of calcite can influence the formation tendency of agglomerates by both the molten fraction of the coating layer

and its viscosity. Molten phosphates can be present in this study and are suggested to be miscible with molten silicates, thus reducing melting points of molten silicates.[60] This can increase the tendency toward the formation of agglomerates for wood loaded with salt mixtures of K_2CO_3/KH_2PO_4, K_2SO_4/KH_2PO_4, or KCl/KH_2PO_4 as a result of the increase in the molten fraction of the coating layer. The viscosity of either molten phosphates or silicates is suggested to be lower than that of mixtures of molten silicates and phosphates.[34] Therefore, the viscosity of the coating layer can be increased with the presence of both K phosphates and K silicates, thus decreasing the formation tendency of agglomerates for wood loaded with salt mixtures of K_2CO_3/KH_2PO_4, K_2SO_4/KH_2PO_4, or KCl/KH_2PO_4. The effect of the above two factors on the formation tendency of agglomerates requires further investigation. The addition of Ca to these wood samples loaded with the salt mixtures leads to the formation of K−Ca phosphates, such as $KCaPO_4$ and $K_2CaP_2O_7$, with melting temperatures of 1560[31] and 1143 °C, respectively.[31] The high melting -points of the two K−Ca phosphates suggest that they are in the solid phase at the temperature (900 °C) of the interaction tests. These high-melting-point K−Ca phosphates

Figure 8. Elemental composition on a C- and O-free basis of some major inorganic elements of the K silicate coating layer and K−Ca silicate/phosphate phases in agglomerates generated during both combustion and steam gasification at 900 °C for wood loaded with salt mixtures of K_2CO_3/KH_2PO_4, K_2SO_4/KH_2PO_4, or KCl/KH_2PO_4 when calcite at 1 wt % Ca was added.

45

Table 6. Interaction Test Matrix of Wood Loaded with K_2CO_3, K_2SO_4, or KCl Salts When $Ca(PO_3)_2$ at 0.5, 1, and 3 wt % Ca Was Added

interaction test	K silicate coating layer	K—Ca silicates/phosphates	Ca phosphates
K_2CO_3 + 0.5 wt % Ca, combustion	√	K—Ca—Si—P	
K_2CO_3 + 0.5 wt % Ca, gasification	√	K—Ca—Si—P	
K_2CO_3 + 1 wt % Ca, combustion	√	K—Ca—Si—P	
K_2CO_3 + 1 wt % Ca, gasification	√	K—Ca—Si—P	
K_2CO_3 + 3 wt % Ca, combustion		K—Ca—P	√
K_2CO_3 + 3 wt % Ca, gasification		K—Ca—P	√
K_2SO_4 + 0.5 wt % Ca, combustion	√	K—Ca—Si—P and K—Ca—P	
K_2SO_4 + 0.5 wt % Ca, gasification	√	K—Ca—Si—P	
K_2SO_4 + 1 wt % Ca, combustion	√	K—Ca—Si—P and K—Ca—P	
K_2SO_4 + 1 wt % Ca, gasification	√	K—Ca—Si—P	
K_2SO_4 + 3 wt % Ca, combustion		K—Ca—P	√
K_2SO_4 + 3 wt % Ca, gasification		K—Ca—P	√
KCl + 0.5 wt % Ca, combustion	√	K—Ca—Si—P and K—Ca—P	
KCl + 0.5 wt % Ca, gasification	√	K—Ca—Si—P and K—Ca—P	
KCl + 1 wt % Ca, combustion		K—Ca—P	
KCl + 1 wt % Ca, gasification	√	K—Ca—Si—P and K—Ca—P	
KCl + 3 wt % Ca, combustion		K—Ca—P	√
KCl + 3 wt % Ca, gasification		K—Ca—P	√

Figure 9. Images of agglomerates generated during both combustion and steam gasification at 900 °C for wood loaded with K_2CO_3, K_2SO_4, or KCl salts when no $Ca(PO_3)_2$ or $Ca(PO_3)_2$ at 0.5, 1, and 3 wt % Ca was added.

in the coating layer can inhibit further reactions between quartz sand and K. In addition, the formation of these K—Ca phosphates, which melt at high temperatures, reduces the fraction of molten K phosphates or K silicates, thus decreasing the formation tendency of agglomerates. However, other types of K—Ca phosphates, Ca silicates, K—Ca silicates, or some eutectics may also be formed in agglomerates. These compounds can affect both the molten fraction of the coating layer and the viscosity of the coating layer. The formation of these phases needs to be evaluated in future work.

3.3. Effect of $Ca(PO_3)_2$ on the Interactions. Table 6 presents the interaction test matrix and the compounds identified in agglomerates. Figure 9 presents images of agglomerates generated during both combustion and steam gasification at 900 °C for wood loaded with K_2CO_3, K_2SO_4, or KCl salts when no $Ca(PO_3)_2$ or $Ca(PO_3)_2$ at 0.5, 1, and 3 wt % Ca was added. Similar to section 3.1, the cases without the addition of calcite have been discussed in a previous study.[14] The addition of $Ca(PO_3)_2$ at either 0.5 or 1 wt % Ca reduces

the size of agglomerates generated during both atmospheres. This is more obvious for KCl-loaded wood than for either K_2CO_3- or K_2SO_4-loaded wood. In addition, for some cases of either K_2CO_3- or K_2SO_4-loaded wood, the size of agglomerates is further reduced when the concentration of Ca is increased from 0.5 to 1 wt %. However, when $Ca(PO_3)_2$ at 3 wt % Ca was added, the size of agglomerates is increased again for most cases of wood loaded with K_2CO_3, K_2SO_4, or KCl salts. Therefore, the effect of $Ca(PO_3)_2$ on the morphology of agglomerates depends upon both the salt species in biomass and the concentration of $Ca(PO_3)_2$.

The definition of the coating layer in section 3.3 is similar to that in section 3.1, and it is the homogeneous lighter compounds that surround the darker quartz sand particles. The coating layer formed under both atmospheres is dominated by K silicates for wood loaded with K_2CO_3, K_2SO_4, or KCl salts when $Ca(PO_3)_2$ at either 0.5 or 1 wt % Ca was added. However, for the case of KCl-loaded wood, no coating layer of silicate can be found when $Ca(PO_3)_2$ at 1 wt %

46

Ca was added for the combustion atmosphere. Selected SEM cross-sectional images and EDS mapping of the K silicate coating layer are shown in Figure 10. Figure 11 presents the
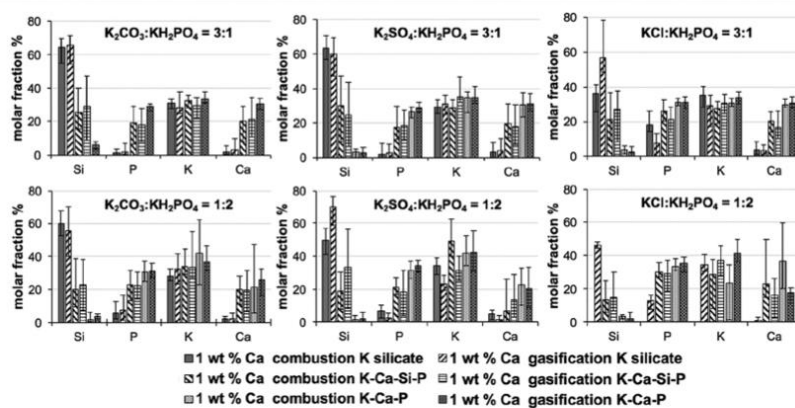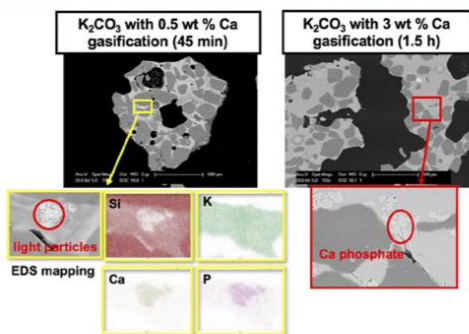

Figure 10. Selected SEM cross-sectional images and EDS mapping of agglomerates generated during both combustion and steam gas-ification at 900 °C for wood loaded with K_2CO_3, K_2SO_4, or KCl salts when $Ca(PO_3)_2$ was added.

elemental composition of the K silicate coating layer. Light particles consisting of either K−Ca−Si−P or K−Ca−P are distributed within the darker silicate coating layer for wood loaded with K_2CO_3, K_2SO_4, or KCl salts when $Ca(PO_3)_2$ at 0.5 and 1 wt % Ca was added. Images of EDS mapping in Figure 10 show that the distribution of K within the coating layer is found to be homogeneous. However, distributions of Ca and P within the coating layer are found to be inhomogeneous and are consistent with the distribution of the light particles. The

elemental composition of the light particles can be found in Figure 11. The formation of the light particles suggests that K−Ca phosphates are formed from reactions between K and $Ca(PO_3)_2$. Some light particles consisting of K−Ca−Si−P may result from the incorporation of some K silicates into the tiny spots used during EDS analysis (section 2.4).

Further increasing the $Ca(PO_3)_2$ concentration to 3 wt % Ca in the wood samples changes the interactions between salt-loaded wood and quartz sand for both atmospheres. Light particles consisting of unreacted Ca phosphates are distributed within the darker K−Ca phosphate coating layer generated during both atmospheres, as shown in Figure 10. Elemental compositions of both the Ca phosphate light particles and the K−Ca phosphate coating layer are shown in Figure 11. It is deduced that, when a large quantity of $Ca(PO_3)_2$ is present, most K in K salts reacted with $Ca(PO_3)_2$ to form K−Ca phosphates instead of K silicates. This suggests that K favors reacting with $Ca(PO_3)_2$ than with quartz sand. When $Ca(PO_3)_2$ at 3 wt % Ca was added for the 45 min tests, the size of agglomerates generated during steam gasification is smaller than that of those generated during combustion for wood loaded with K_2CO_3, K_2SO_4, or KCl salts. In addition, char particles can be observed within agglomerates generated during steam gasification. Therefore, steam inhibits the formation of the K−Ca phosphate coating layer. For the cases with the addition of $Ca(PO_3)_2$ at 3 wt % Ca, agglomerates with a similar size as the equivalent cases of combustion are formed for steam gasification by increasing the reaction time to 1.5 h (Figure 9).

The XRD analysis of agglomerates shows that the addition of $Ca(PO_3)_2$ at 1 wt % Ca to either the K_2CO_3- or K_2SO_4-loaded wood samples results in the formation of both $KCaPO_4$ and $K_2CaP_2O_7$, while only $KCaPO_4$ is detected for these samples with the addition of $Ca(PO_3)_2$ at 0.5 wt % Ca. In
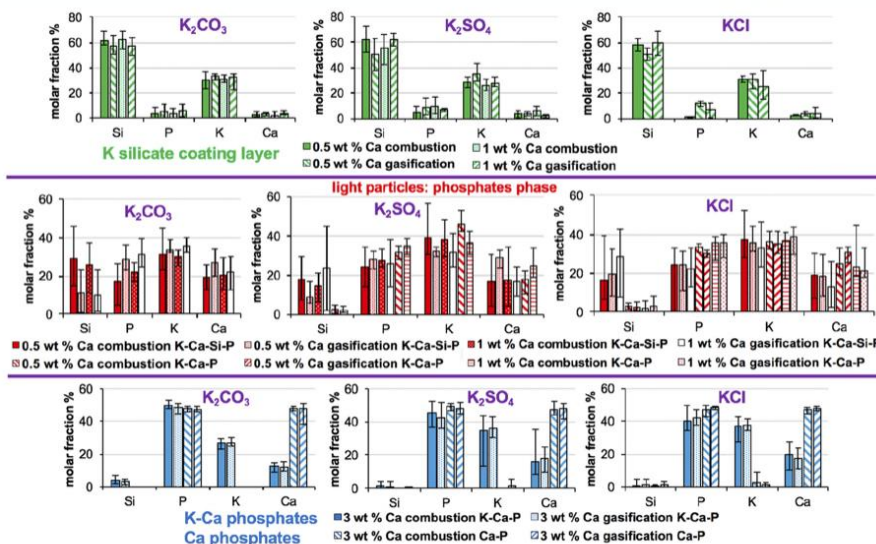

Figure 11. Elemental composition of some major inorganic elements on a C- and O-free basis of the K silicate coating layer and the phases of K−Ca silicates/phosphates and Ca phosphates in agglomerates generated during both combustion and steam gasification at 900 °C for wood loaded with K_2CO_3, K_2SO_4, or KCl salts when $Ca(PO_3)_2$ was added.
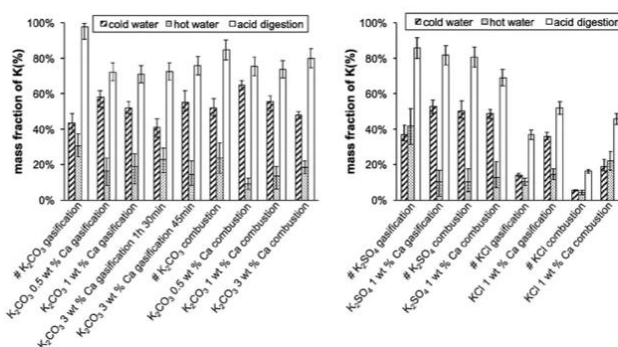
Figure 12. Mass fractions (%) of K in agglomerates soluble in acid and cold and hot water relative to K introduced from the feedstock for wood loaded with K_2CO_3, K_2SO_4, or KCl salts. These agglomerates were generated during both combustion and steam gasification at 900 °C when no $Ca(PO_3)_2$ or $Ca(PO_3)_2$ at 0.5, 1, and 3 wt % Ca was added. (#) These data were reported previously.[14]

contrast, for KCl-loaded wood, both $KCaPO_4$ and $K_2CaP_2O_7$ are detected in agglomerates with the addition of $Ca(PO_3)_2$ at either 0.5 or 1 wt % Ca. Both $K_2CaP_2O_7$ and $Ca_2P_2O_7$ are detected in agglomerates for wood loaded with K_2CO_3, K_2SO_4, or KCl salts when $Ca(PO_3)_2$ at 3 wt % Ca was added. The results suggest that, for the cases of wood loaded with K_2CO_3, K_2SO_4, or KCl salts, an increase in the addition of $Ca(PO_3)_2$ from 0.5 to 3 wt % Ca in the samples causes the gradual transformation of K−Ca phosphates from $KCaPO_4$ with a K/Ca ratio of 1 to $K_2CaP_2O_7$ with a K/Ca ratio of 2.

The addition of Ca phosphates to the wood samples loaded with K_2CO_3, K_2SO_4, or KCl salts can affect the viscosity of the coating layer. Some studies indicated that a higher affinity of P to modifier cations than that of Si increases the extent of polymerization of silicate glasses because modifier cations in silicates move to phosphates.[61,62] Therefore, it is suggested that adding P_2O_5 to silicate glasses increases the viscosity of the silicate glasses.[61] In addition, Wang et al.[36] suggested that K salts tend to react with Ca phosphates than with quartz sand. Therefore, the addition of $Ca(PO_3)_2$ at 0.5 or 1 wt % Ca to the wood samples loaded with K_2CO_3, K_2SO_4, or KCl salts reduces the formation of low-viscosity molten K silicates in agglomerates and may also increase the viscosity of the coating layer. Similar to section 3.2, the K−Ca phosphates ($KCaPO_4$ and $K_2CaP_2O_7$ with melting points of 1560 and 1143 °C, respectively[31]) with high melting temperatures formed in the coating layer can prevent K from further reacting with quartz sand. These effects of adding $Ca(PO_3)_2$ at 0.5 or 1 wt % Ca reduce the formation tendency of agglomerates. This agrees with the morphology of agglomerates, as shown in Figure 9. However, besides $KCaPO_4$ and $K_2CaP_2O_7$, other phases of K−Ca phosphates or eutectics with lower melting temperatures may also be formed. The partially molten K−Ca phosphate coating layer for wood loaded with K_2CO_3, K_2SO_4, or KCl salts when $Ca(PO_3)_2$ at 3 wt % Ca was added indicates the formation of K−Ca phosphates with lower melting temperatures, which may have low viscosities. This aggravates the formation tendency of agglomerates and is in agreement with the morphology of agglomerates (Figure 9).

Figure 12 presents mass fractions (%) of K in agglomerates soluble in acid and cold and hot water relative to K introduced from the feedstock for wood loaded with K_2CO_3, K_2SO_4, or KCl salts. These agglomerates were generated during both

combustion and steam gasification at 900 °C with and without the addition of $Ca(PO_3)_2$. Similar to section 3.1, the cases without the addition of calcite have been discussed in a previous study.[14] The K retention in agglomerates, which is the acid-soluble fraction, for either K_2CO_3- or K_2SO_4-loaded wood, is decreased when $Ca(PO_3)_2$ at 0.5 and 1 wt % Ca was added for both atmospheres (Figure 12). An increase in the addition of $Ca(PO_3)_2$ from 0.5 to 1 wt % Ca further decreases the K retention in agglomerates for K_2CO_3-loaded wood. Interestingly, an increase in the $Ca(PO_3)_2$ concentration to 3 wt % Ca increases the K retention in agglomerates for K_2CO_3-loaded wood in comparison to the cases with a lower $Ca(PO_3)_2$ concentration. These are consistent with the size of agglomerates (Figure 9), which is related to the K retention in agglomerates. The addition of $Ca(PO_3)_2$ decreases the formation of K silicates while increasing the formation of K−Ca phosphates. Similar results on the impact of Ca phosphates on K retention in biomass were reported by Wang et al.[36] When $Ca(PO_3)_2$ at 0.5 and 1 wt % Ca was added, the effect of decreasing the formation of K silicates dominates. In contrast, when $Ca(PO_3)_2$ at 3 wt % Ca was added, the effect of increasing the formation of K−Ca phosphates dominates. For KCl-loaded wood, the K retention in agglomerates is increased significantly with the addition of $Ca(PO_3)_2$ at 1 wt % Ca for both atmospheres because of an increase in the formation of K−Ca phosphates. However, adding $Ca(PO_3)_2$ at 1 wt % Ca decreases the size of agglomerates for KCl-loaded wood significantly, as shown in Figure 9. This is different from the cases of either K_2CO_3- or K_2SO_4-loaded wood, and further investigation is required. The effect of $Ca(PO_3)_2$ on the K retention in agglomerates depends upon both the salt species in biomass and the concentration of $Ca(PO_3)_2$. The impact of steam on K retention in agglomerates is insignificant for wood loaded with K_2CO_3, K_2SO_4, or KCl salts. In addition, the mass fractions of water leaching are found to not be affected by the concentration of $Ca(PO_3)_2$ added for both atmospheres. These may result from the co-existence of K silicates and K−Ca phosphates, which are both soluble in water or acid, in agglomerates. Interestingly, the mass fractions of K soluble in cold water are higher than those in hot water for most cases, as shown in Figure 12. Further work is needed to refine the method of water leaching.

4. CONCLUSION

The addition of calcite to the wood samples loaded with K_2CO_3, K_2SO_4, or KCl salts decreases both the K retention in agglomerates and the size of agglomerates. The addition of calcite mitigates the formation of agglomerates by decreasing K silicates with low melting temperatures. Reactions between K and quartz sand during the formation of agglomerates are inhibited by CaO particles. The impact of calcite on agglomerates depends upon both the salt species in biomass and the concentration of calcite.

For wood loaded with salt mixtures of K_2CO_3/KH_2PO_4, K_2SO_4/KH_2PO_4, or KCl/KH_2PO_4 with a molar ratio of 3:1, the K silicate coating layer dominates agglomerates, while the coating layer incorporates many quartz sand particles. In contrast, for wood loaded with these salt mixtures with a molar ratio of 1:2, the molten K phosphate coating layer dominates agglomerates, while the coating layer incorporates few quartz sand particles. The addition of calcite to the wood samples loaded with the salt mixtures results in the formation of K−Ca phosphate particles ($KCaPO_4$, $K_2CaP_2O_7$, or other phases), which are distributed within the coating layer. The formation of K−Ca phosphates with relatively higher melting temperatures ($KCaPO_4$ or $K_2CaP_2O_7$) reduces the formation of K silicates or K phosphates with relatively lower melting temperatures in agglomerates. The high-melting-point K−Ca phosphates can also inhibit quartz sand from further reacting with K salts. These effects decrease the formation tendency of agglomerates. However, other Ca silicates, K−Ca phosphates, K−Ca silicates, or some eutectics can also be formed, and this needs further investigation.

For wood loaded with K_2CO_3, K_2SO_4, or KCl salts, the addition of $Ca(PO_3)_2$ at either 0.5 or 1 wt % Ca leads to the formation of K−Ca phosphates ($KCaPO_4$, $K_2CaP_2O_7$, or other phases) that are distributed within the K silicate coating layer. Quartz sand particles are incorporated into molten K−Ca phosphate compounds ($K_2CaP_2O_7$ or other phases) when the $Ca(PO_3)_2$ concentration is further increased to 3 wt % Ca. The addition of $Ca(PO_3)_2$ either increases the K retention in agglomerates by the formation of K−Ca phosphates or decrease the K retention in agglomerates by the inhibition of K silicates. Therefore, the addition of $Ca(PO_3)_2$ at 0.5 or 1 wt % Ca reduces the size of agglomerates because less K silicates are formed. In contrast, the size of agglomerates is increased with the addition of $Ca(PO_3)_2$ at 3 wt % Ca because more partially molten K−Ca phosphates are formed. However, the effect of $Ca(PO_3)_2$ on KCl-loaded wood is different, and further investigation is needed. The effect of $Ca(PO_3)_2$ on the K retention in agglomerates and the size of agglomerates depends upon both the salt species in biomass and the concentration of $Ca(PO_3)_2$. The formation of $KCaPO_4$ or $K_2CaP_2O_7$ with high melting temperatures decreases the formation tendency of agglomerates. However, the potential of the formation of other K−Ca phosphates or eutectics with low melting temperatures can increase the formation tendency of agglomerates, especially when $Ca(PO_3)_2$ at 3 wt % Ca was added.

The presence of steam has insignificant effects on chemical reaction mechanisms between quartz sand, the Ca or P additives, and wood loaded with K_2CO_3, K_2SO_4, or KCl salts. For most cases of wood loaded with K_2CO_3, K_2SO_4, or KCl salts both with and without the addition of calcite, steam increases the K retention in agglomerates in comparison to the equivalent cases of combustion. In addition, steam inhibits the formation of K−Ca phosphates in agglomerates for wood loaded with K_2CO_3, K_2SO_4, or KCl salts when $Ca(PO_3)_2$ at 3 wt % Ca was added.

■ AUTHOR INFORMATION

Corresponding Author

Zimeng He − *Centre for Energy Technology and School of Chemical Engineering and Advanced Materials, The University of Adelaide, Adelaide, South Australia 5005, Australia;* orcid.org/0000-0001-5420-3661; Email: zimeng.he@adelaide.edu.au

Authors

Woei L. Saw − *Centre for Energy Technology and School of Chemical Engineering and Advanced Materials, The University of Adelaide, Adelaide, South Australia 5005, Australia*

Philip J. van Eyk − *Centre for Energy Technology and School of Chemical Engineering and Advanced Materials, The University of Adelaide, Adelaide, South Australia 5005, Australia;* orcid.org/0000-0003-3768-2044

Graham J. Nathan − *Centre for Energy Technology and School of Mechanical Engineering, The University of Adelaide, Adelaide, South Australia 5005, Australia*

Peter J. Ashman − *Centre for Energy Technology and School of Chemical Engineering and Advanced Materials, The University of Adelaide, Adelaide, South Australia 5005, Australia*

Complete contact information is available at:
https://pubs.acs.org/10.1021/acs.energyfuels.9b02992

Notes

The authors declare no competing financial interest.

■ REFERENCES

(1) Bartels, M.; Lin, W.; Nijenhuis, J.; Kapteijn, F.; van Ommen, J. R. Agglomeration in fluidized beds at high temperatures: Mechanisms, detection and prevention. *Prog. Energy Combust. Sci.* **2008**, *34* (5), 633−666.

(2) Öhman, M.; Pommer, L.; Nordin, A. Bed Agglomeration Characteristics and Mechanisms during Gasification and Combustion of Biomass Fuels. *Energy Fuels* **2005**, *19* (4), 1742−1748.

(3) Niu, Y.; Tan, H.; Hui, S. e. Ash-related issues during biomass combustion: Alkali-induced slagging, silicate melt-induced slagging (ash fusion), agglomeration, corrosion, ash utilization, and related countermeasures. *Prog. Energy Combust. Sci.* **2016**, *52*, 1−61.

(4) Lin, W.; Dam-Johansen, K.; Frandsen, F. Agglomeration in bio-fuel fired fluidized bed combustors. *Chem. Eng. J.* **2003**, *96* (1−3), 171−185.

(5) Lane, D. J.; Zevenhoven, M.; Ashman, P. J.; van Eyk, P. J.; Hupa, M.; de Nys, R.; Lewis, D. M. Algal Biomass: Occurrence of the Main Inorganic Elements and Simulation of Ash Interactions with Bed Material. *Energy Fuels* **2014**, *28* (7), 4622−4632.

(6) He, Z.; Lane, D. J.; Saw, W. L.; van Eyk, P. J.; Nathan, G. J.; Ashman, P. J. Ash−Bed Material Interaction during the Combustion

and Steam Gasification of Australian Agricultural Residues. *Energy Fuels* **2018**, *32* (4), 4278−4290.

(7) Öhman, M.; Nordin, A.; Skrifvars, B.-J.; Backman, R.; Hupa, M. Bed Agglomeration Characteristics during Fluidized Bed Combustion of Biomass Fuels. *Energy Fuels* **2000**, *14* (1), 169−178.

(8) Grimm, A.; Skoglund, N.; Boström, D.; Öhman, M. Bed Agglomeration Characteristics in Fluidized Quartz Bed Combustion of Phosphorus-Rich Biomass Fuels. *Energy Fuels* **2011**, *25* (3), 937−947.

(9) Grimm, A.; Öhman, M.; Lindberg, T.; Fredriksson, A.; Boström, D. Bed Agglomeration Characteristics in Fluidized-Bed Combustion of Biomass Fuels Using Olivine as Bed Material. *Energy Fuels* **2012**, *26* (7), 4550−4559.

(10) He, Z.; Saw, W. L.; Lane, D. J.; van Eyk, P. J.; de Nys, R.; Nathan, G. J.; Ashman, P. J. The ash-quartz sand interaction behaviours during steam gasification or combustion of a freshwater and a marine species of macroalgae. *Fuel* **2020**, *263*, 116621.

(11) Werkelin, J. Ash-forming elements and their chemical forms in woody biomass fuels. Ph.D. Thesis, Åbo Akademi University, Turku, Finland, 2008.

(12) Werther, J.; Saenger, M.; Hartge, E. U.; Ogada, T.; Siagi, Z. Combustion of agricultural residues. *Prog. Energy Combust. Sci.* **2000**, *26* (1), 1−27.

(13) Gatternig, B.; Karl, J. Investigations on the Mechanisms of Ash-Induced Agglomeration in Fluidized-Bed Combustion of Biomass. *Energy Fuels* **2015**, *29* (2), 931−941.

(14) He, Z.; Saw, W. L.; van Eyk, P. J.; Nathan, G. J.; Ashman, P. J. Interactions between Quartz Sand and Wood Doped with either K or Na Salts under Steam Gasification and Combustion Atmospheres. *Ind. Eng. Chem. Res.* **2020**, *59* (4), 1712−1722.

(15) Vassilev, S. V.; Baxter, D.; Andersen, L. K.; Vassileva, C. G. An overview of the chemical composition of biomass. *Fuel* **2010**, *89* (5), 913−933.

(16) Eriksson, G.; Grimm, A.; Skoglund, N.; Boström, D.; Öhman, M. Combustion and fuel characterisation of wheat distillers dried grain with solubles (DDGS) and possible combustion applications. *Fuel* **2012**, *102*, 208−220.

(17) Wang, L.; Hustad, J. E.; Skreiberg, Ø.; Skjevrak, G.; Grønli, M. A Critical Review on Additives to Reduce Ash Related Operation Problems in Biomass Combustion Applications. *Energy Procedia* **2012**, *20*, 20−29.

(18) Chi, H.; Pans, M. A.; Sun, C.; Liu, H. An investigation of lime addition to fuel as a countermeasure to bed agglomeration for the combustion of non-woody biomass fuels in a 20kWth bubbling fluidised bed combustor. *Fuel* **2019**, *240*, 349−361.

(19) Zhou, C.; Rosén, C.; Engvall, K. Biomass oxygen/steam gasification in a pressurized bubbling fluidized bed: Agglomeration behavior. *Appl. Energy* **2016**, *172*, 230−250.

(20) Fernández Llorente, M. J.; Escalada Cuadrado, R.; Murillo Laplaza, J. M.; Carrasco García, J. E. Combustion in bubbling fluidised bed with bed material of limestone to reduce the biomass ash agglomeration and sintering. *Fuel* **2006**, *85* (14), 2081−2092.

(21) Xiong, S.; Burvall, J.; Örberg, H.; Kalen, G.; Thyrel, M.; Öhman, M.; Boström, D. Slagging Characteristics during Combustion of Corn Stovers with and without Kaolin and Calcite. *Energy Fuels* **2008**, *22* (5), 3465−3470.

(22) He, H.; Boström, D.; Öhman, M. Time Dependence of Bed Particle Layer Formation in Fluidized Quartz Bed Combustion of Wood-Derived Fuels. *Energy Fuels* **2014**, *28* (6), 3841−3848.

(23) Zevenhoven, M.; Yrjas, P.; Skrifvars, B.-J.; Hupa, M. Characterization of Ash-Forming Matter in Various Solid Fuels by Selective Leaching and Its Implications for Fluidized-Bed Combustion. *Energy Fuels* **2012**, *26* (10), 6366−6386.

(24) Chin, K. L.; H'ng, P. S.; Maminski, M.; Go, W. Z.; Lee, C. L.; Raja-Nazrin, R. A.; Khoo, P. S.; Ashikin, S. N.; Halimatun, I. Additional additives to reduce ash related operation problems of solid biofuel from oil palm biomass upon combustion. *Ind. Crops Prod.* **2018**, *123*, 285−295.

(25) Steenari, B.-M.; Lundberg, A.; Pettersson, H.; Wilewska-Bien, M.; Andersson, D. Investigation of Ash Sintering during Combustion of Agricultural Residues and the Effect of Additives. *Energy Fuels* **2009**, *23* (11), 5655−5662.

(26) Schmitt, V. E. M.; Kaltschmitt, M. Effect of straw proportion and Ca- and Al-containing additives on ash composition and sintering of wood−straw pellets. *Fuel* **2013**, *109*, 551−558.

(27) He, H.; Ji, X.; Boström, D.; Backman, R.; Öhman, M. Mechanism of Quartz Bed Particle Layer Formation in Fluidized Bed Combustion of Wood-Derived Fuels. *Energy Fuels* **2016**, *30* (3), 2227−2232.

(28) Piotrowska, P.; Grimm, A.; Skoglund, N.; Boman, C.; Öhman, M.; Zevenhoven, M.; Boström, D.; Hupa, M. Fluidized-Bed Combustion of Mixtures of Rapeseed Cake and Bark: The Resulting Bed Agglomeration Characteristics. *Energy Fuels* **2012**, *26* (4), 2028−2037.

(29) Piotrowska, P.; Zevenhoven, M.; Davidsson, K.; Hupa, M.; Åmand, L.-E.; Barišić, V.; Coda Zabetta, E. Fate of Alkali Metals and Phosphorus of Rapeseed Cake in Circulating Fluidized Bed Boiler Part 1: Cocombustion with Wood. *Energy Fuels* **2010**, *24* (1), 333−345.

(30) Grimm, A.; Skoglund, N.; Boström, D.; Boman, C.; Öhman, M. Influence of Phosphorus on Alkali Distribution during Combustion of Logging Residues and Wheat Straw in a Bench-Scale Fluidized Bed. *Energy Fuels* **2012**, *26* (5), 3012−3023.

(31) Lindström, E.; Sandström, M.; Boström, D.; Öhman, M. Slagging Characteristics during Combustion of Cereal Grains Rich in Phosphorus. *Energy Fuels* **2007**, *21* (2), 710−717.

(32) Novaković, A.; van Lith, S. C.; Frandsen, F. J.; Jensen, P. A.; Holgersen, L. B. Release of Potassium from the Systems K-Ca-Si and K-Ca-P. *Energy Fuels* **2009**, *23* (7), 3423−3428.

(33) Billen, P.; Creemers, B.; Costa, J.; Van Caneghem, J.; Vandecasteele, C. Coating and melt induced agglomeration in a poultry litter fired fluidized bed combustor. *Biomass Bioenergy* **2014**, *69*, 71−79.

(34) Billen, P.; Van Caneghem, J.; Vandecasteele, C. Predicting Melt Formation and Agglomeration in Fluidized Bed Combustors by Equilibrium Calculations. *Waste Biomass Valorization* **2014**, *5* (5), 879−892.

(35) Billen, P.; Costa, J.; van der Aa, L.; Westdorp, L.; Van Caneghem, J.; Vandecasteele, C. An Agglomeration Index for CaO Addition (as CaCO₃) to Prevent Defluidization: Application to a Full-Scale Poultry Litter Fired FBC. *Energy Fuels* **2014**, *28* (8), 5455−5462.

(36) Wang, Q.; Han, K.; Qi, J.; Zhang, J.; Li, H.; Lu, C. Investigation of potassium transformation characteristics and the influence of additives during biochar briquette combustion. *Fuel* **2018**, *222*, 407−415.

(37) Wang, Q.; Han, K.; Gao, J.; Wang, J.; Lu, C. Investigation of Maize Straw Char Briquette Ash Fusion Characteristics and the Influence of Phosphorus Additives. *Energy Fuels* **2017**, *31* (3), 2822−2830.

(38) Zeuthen, J. H.; Jensen, P. A.; Jensen, J. P.; Livbjerg, H. Aerosol Formation during the Combustion of Straw with Addition of Sorbents. *Energy Fuels* **2007**, *21* (2), 699−709.

(39) Li, L.; Ren, Q.; Li, S.; Lu, Q. Effect of Phosphorus on the Behavior of Potassium during the Co-combustion of Wheat Straw with Municipal Sewage Sludge. *Energy Fuels* **2013**, *27* (10), 5923−5930.

(40) Merrill, R. C. Chemistry of the soluble silicates. *J. Chem. Educ.* **1947**, *24* (6), 262.

(41) Weldes, H. H.; Lange, K. R. PROPERTIES OF SOLUBLE SILICATES. *Ind. Eng. Chem.* **1969**, *61* (4), 29−44.

(42) Kosminski, A.; Ross, D. P.; Agnew, J. B. Reactions between sodium and silica during gasification of a low-rank coal. *Fuel Process. Technol.* **2006**, *87* (12), 1037−1049.

(43) Kosminski, A.; Ross, D. P.; Agnew, J. B. Influence of gas environment on reactions between sodium and silicon minerals

during gasification of low-rank coal. *Fuel Process. Technol.* **2006**, *87* (11), 953−962.

(44) Khadilkar, A. B.; Rozelle, P. L.; Pisupati, S. V. Review of Particle Physics and Chemistry in Fluidized Beds for Development of Comprehensive Ash Agglomeration Prediction Models. *Energy Fuels* **2016**, *30* (5), 3714−3734.

(45) Zhu, Y.; Piotrowska, P.; van Eyk, P. J.; Boström, D.; Wu, X.; Boman, C.; Broström, M.; Zhang, J.; Kwong, C. W.; Wang, D.; Cole, A. J.; de Nys, R.; Gentili, F. G.; Ashman, P. J. Fluidized Bed Co-gasification of Algae and Wood Pellets: Gas Yields and Bed Agglomeration Analysis. *Energy Fuels* **2016**, *30* (3), 1800−1809.

(46) Vassilev, S. V.; Baxter, D.; Vassileva, C. G. An overview of the behaviour of biomass during combustion: Part I. Phase-mineral transformations of organic and inorganic matter. *Fuel* **2013**, *112*, 391−449.

(47) Patnaik, P. *Handbook of Inorganic Chemicals*; McGraw-Hill: New York, 2003.

(48) Ruan, R.; Tan, H.; Wang, X.; Li, Y.; Li, s.; Hu, Z.; Wei, B.; Yang, T. Characteristics of fine particulate matter formation during combustion of lignite riched in AAEM (alkali and alkaline earth metals) and sulfur. *Fuel* **2018**, *211*, 206−213.

(49) Sevonius, C.; Yrjas, P.; Hupa, M. Defluidization of a quartz bed − Laboratory experiments with potassium salts. *Fuel* **2014**, *127*, 161−168.

(50) Ma, T.; Fan, C.; Hao, L.; Li, S.; Jensen, P. A.; Song, W.; Lin, W.; Dam-Johansen, K. Biomass ash induced agglomeration in fluidized bed. Part 2: Effect of potassium salts in different gas composition. *Fuel Process. Technol.* **2018**, *180*, 130−139.

(51) McKee, D. W. Gasification of graphite in carbon dioxide and water vapor—the catalytic effects of alkali metal salts. *Carbon* **1982**, *20* (1), 59−66.

(52) Lang, R. J. Anion effects in alkali-catalysed steam gasification. *Fuel* **1986**, *65* (10), 1324−1329.

(53) Wang, Y.; Wu, H.; Sárossy, Z.; Dong, C.; Glarborg, P. Release and transformation of chlorine and potassium during pyrolysis of KCl doped biomass. *Fuel* **2017**, *197*, 422−432.

(54) Brus, E.; Öhman, M.; Nordin, A. Mechanisms of Bed Agglomeration during Fluidized-Bed Combustion of Biomass Fuels. *Energy Fuels* **2005**, *19* (3), 825−832.

(55) Boström, D.; Skoglund, N.; Grimm, A.; Boman, C.; Öhman, M.; Broström, M.; Backman, R. Ash Transformation Chemistry during Combustion of Biomass. *Energy Fuels* **2012**, *26* (1), 85−93.

(56) Lin, W.; Dam-Johansen, K.; Frandsen, F. Agglomeration in bio-fuel fired fluidized bed combustors. *Chem. Eng. J.* **2003**, *96* (1), 171−185.

(57) Lin, C.-L.; Wey, M.-Y. The effect of mineral compositions of waste and operating conditions on particle agglomeration/defluidization during incineration. *Fuel* **2004**, *83* (17), 2335−2343.

(58) Khadilkar, A.; Rozelle, P. L.; Pisupati, S. V. Models of agglomerate growth in fluidized bed reactors: Critical review, status and applications. *Powder Technol.* **2014**, *264*, 216−228.

(59) Lin, C.-L.; Kuo, J.-H.; Wey, M.-Y.; Chang, S.-H.; Wang, K.-S. Inhibition and promotion: The effect of earth alkali metals and operating temperature on particle agglomeration/defluidization during incineration in fluidized bed. *Powder Technol.* **2009**, *189* (1), 57−63.

(60) Lindberg, D.; Backman, R.; Chartrand, P.; Hupa, M. Towards a comprehensive thermodynamic database for ash-forming elements in biomass and waste combustion — Current situation and future developments. *Fuel Process. Technol.* **2013**, *105*, 129−141.

(61) Wang, Z. J.; Shu, Q. F.; Sridhar, S.; Zhang, M.; Guo, M.; Zhang, Z. T. Effect of P2O5 and FetO on the Viscosity and Slag Structure in Steelmaking Slags. *Metall. Mater. Trans. B* **2015**, *46* (2), 758−765.

(62) Toplis, M. J.; Dingwell, D. B. The variable influence of P2O5 on the viscosity of melts of differing alkali/aluminium ratio: Implications for the structural role of phosphorus in silicate melts. *Geochim. Cosmochim. Acta* **1996**, *60* (21), 4107−4121.

Chapter 5

Paper III

Ash-Bed Material Interaction during the Combustion and Steam Gasification of Australian Agricultural Residues

Zimeng He*†‡, Daniel J. Lane†‡, Woei L. Saw†‡, Philip J. van Eyk†‡, Graham J. Nathan†§, Peter J. Ashman†‡

†*Centre for Energy Technology, The University of Adelaide, Adelaide, South Australia 5005, Australia*
‡*School of Chemical Engineering, The University of Adelaide, Adelaide, South Australia 5005, Australia*
§*School of Mechanical Engineering, The University of Adelaide, Adelaide, South Australia 5005, Australia*

Statement of Authorship

Title of Paper	Ash–Bed Material Interaction during the Combustion and Steam Gasification of Australian Agricultural Residues
Publication Status	☑ Published ☐ Accepted for Publication ☐ Submitted for Publication ☐ Unpublished and Unsubmitted work written in manuscript style
Publication Details	Z. He, D.J. Lane, W.L. Saw, P.J. van Eyk, G.J. Nathan, P.J. Ashman, Ash–Bed Material Interaction during the Combustion and Steam Gasification of Australian Agricultural Residues, Energy & Fuels, (2018)

Principal Author

Name of Principal Author (Candidate)	Zimeng He
Contribution to the Paper	Performed analysis on all samples, interpreted data, wrote manuscript and acted as corresponding author.
Overall percentage (%)	60
Certification:	This paper reports on original research I conducted during the period of my Higher Degree by Research candidature and is not subject to any obligations or contractual agreements with a third party that would constrain its inclusion in this thesis. I am the primary author of this paper.
Signature	Date 22.10.2019

Co-Author Contributions

By signing the Statement of Authorship, each author certifies that:

i. the candidate's stated contribution to the publication is accurate (as detailed above);

ii. permission is granted for the candidate in include the publication in the thesis; and

iii. the sum of all co-author contributions is equal to 100% less the candidate's stated contribution.

Name of Co-Author	Daniel J. Lane
Contribution to the Paper	Supervised development of work, helped in data interpretation, reactor construction and manuscript evaluation and edition
Signature	Date 8.8.2019

Name of Co-Author	Woei L.Saw
Contribution to the Paper	Supervised development of work, helped in data interpretation, reactor construction and manuscript evaluation and edition
Signature	Date 21/10/2019.

53

Name of Co-Author	Philip J. van Eyk			
Contribution to the Paper	Supervised development of work, helped in data interpretation and manuscript evaluation			
Signature			Date	21/10/2019

Name of Co-Author	Graham J. Nathan			
Contribution to the Paper	Supervised development of work, helped in data interpretation and manuscript evaluation and edition			
Signature			Date	17/10/19.

Name of Co-Author	Peter J. Ashman			
Contribution to the Paper	Supervised development of work, helped in data interpretation and manuscript evaluation			
Signature			Date	17-10-19

Ash−Bed Material Interaction during the Combustion and Steam Gasification of Australian Agricultural Residues

Zimeng He,[*,†,‡] Daniel J. Lane,[†,‡] Woei L. Saw,[†,‡] Philip J. van Eyk,[†,‡] Graham J. Nathan,[†,§] and Peter J. Ashman[†,‡]

†Centre for Energy Technology, ‡School of Chemical Engineering, and §School of Mechanical Engineering, The University of Adelaide, South Australia 5005, Australia

ABSTRACT: The time-dependent layer-formation process of the agglomerates for three common agricultural residues in Australia with different ash-forming elements, together with quartz sand as the bed material, were investigated in a lab-scale, fixed-bed reactor under combustion (5% v/v O_2) and steam-gasification (50% v/v steam) atmospheres at 900 °C. The impact of the atmosphere on the ash−bed material interaction was studied from the elemental composition and the morphology of the agglomerates, which were characterized with scanning electron microscopy in combination with energy-dispersive X-ray spectroscopy. The ash−bed material interaction mechanisms for the three feedstock were identified as part of the alkali metals react to form ash particles, which, for wheat straw and cotton stalks, consist of Na, Mg, Si, P, K, and Ca and, for grape marc, is composed mostly of $KCaPO_4$; the remaining alkali metals react with either Si from the quartz sand (for grape marc and cotton stalk) or reactive Si from the fuel (for wheat straw) to form a low-melting-point alkali silicate coating layer; Ca dissolves or diffuses into the coating layer (for wheat straw and cotton stalk); and the ash particles formed in the first step then deposit on, and progressively embed in, the coating layer. The elemental composition of the coating layer is relatively independent of both the reaction time and the gas atmosphere. The coating layer increases in thickness with an increase in the reaction time. The addition of steam results in the production of more liquid alkali silicates, which augment the agglomeration. Any residual S may form sulfate particles with K, Ca, or Na in a combustion atmosphere, while in a steam-gasification atmosphere, the S is released to the gas phase so that more alkali metal may remain to form the low-melting-point alkali silicate.

1. INTRODUCTION

Growing concern about the environmental impact of fossil fuel utilization has motivated research into renewable energy technologies such as the sustainable use of biomass resources.[1,2]

Gasification and combustion are common techniques used to convert biomass to energy.[3,4] Low-cost agricultural residues, the byproduct of agricultural industry, are often under-utilized compared to forestry biomass.[4] Fluidized bed reactors have been proven to offer advantages over other types of reactor for accommodating the variability and complexity of agricultural residues in combustion and gasification processes.[5,6] Agricultural residues generally contain high concentrations of alkali metal, which can form low-melting-point silicates with Si from the bed material to induce agglomeration in fluidized bed reactors.[7] Agglomeration can cause defluidization and may result in an unscheduled shutdown in fluidized bed reactors.[8] However, the process of agglomeration is not well-understood, so it remains a major challenge and limits the use of agricultural residues in a fluidized bed. Therefore, the agglomeration mechanism of agricultural residues in fluidized-bed combustion and gasification processes needs to be better understood before appropriate countermeasures can be proposed.

Australia is a country with extensive bioenergy resources. Several common agricultural residues in Australia, such as wheat straw, grape marc, and cotton stalk are anticipated to play an important role as a future source of bioenergy. Wheat straw and grape marc are the residues from wheat production and the wine industry, respectively. Wheat can produce approximately 2.5−5 t/ha of straw, while 10−15% of the grape material ends up as grape marc during winery process. Australia is also one of the largest cotton exporters in the world. Between 5.2 and 5.6 t/ha of the cotton stalk are left in the ground after the cotton harvest.[9] This has the potential to be utilized as an energy feedstock because the material has a similar structure to wood and appropriate chemical properties.[9] During 2015−2016 in Australia, approximately 22 Mt wheat for grain and 1.6 Mt grape for wine were produced, while approximately 0.3 M ha cotton was planted. In summary, grape marc, wheat straw, and cotton stalk can be considered as three promising sources of low-cost biomass feedstock. Moreover, the elemental composition of the ash-forming elements of the three feedstock is different, which implies that the agglomeration mechanism of each feedstock is also likely to be different. There is therefore a need for greater understanding of the differences in the agglomeration mechanism for each feedstock during both the combustion and gasification regimes before these agricultural residues can be effectively utilized in industrial-scale fluidized-bed installations.

The mechanism of bed agglomeration during the fluidized-bed conversion of biomass has been studied by many researchers over the past few decades.[10−15] Ohman et al.[13] have proposed the following chemical subprocess of bed

agglomeration. First, the ash particles deposit onto the bed materials through one or more of three different processes: (a) small ash particles adhere to the sand particles, (b) gaseous alkali metals condense onto the sand particles, and (c) gaseous alkali metals react with the sand particles. The homogeneity and strength of the coating layer of the bed particles can be increased by sintering. Bed agglomeration can then be induced by the melting of the coating layer at sufficiently high temperatures. Grimm et al.[14] and Brus et al.[15] have reported the following agglomeration mechanisms in fluidized bed combustors: (1) low-melting-temperature potassium silicates are formed first, accompanied by diffusion or dissolving of Ca into the coating layer, followed with subsequent viscous-flow sintering and agglomeration (typical for wood fuels); (2) K in the gas or aerosol phases reacts with the surface of bed particles to form low-melting-point potassium silicates with subsequent viscous-flow sintering and agglomeration (for fuels with high alkali content and low Si content); and (3) bed particles directly adhere to the molten ash-derived potassium silicate particles (for fuels with high concentration of alkalis and reactive Si). Alternatively, for fuels rich in P, partially molten phosphate particles react with, and adhere to, the bed particles to form a coating layer of silicate and phosphate. Although many studies have been conducted to identify the agglomeration mechanisms in fluidized bed reactors, the complexity of biomass, means that more work is needed to further explore the various agglomeration mechanisms of biomass fuels.

Most studies of agglomeration have been carried out in fluidized bed reactors, while other studies also used fixed-bed reactors to simulate the ash−bed material interaction in fluidized bed reactors.[16−19] Both the ash chemistry and the particle physics influence agglomeration in the fluidized bed reactor.[20] The ash chemistry influences the formation of chemical bonding between particles, while the effect of particle physics may include particle size, particle velocity, and collision frequency.[20] Fixed-bed tests typically used to assess the ash chemistry effect on the agglomeration mechanism (that is, the interaction between ash and bed material). This method was therefore chosen for the present investigation.

Most of the previous studies have investigated agglomerates that have been removed from the reactor after defluidization. Relatively few investigations have examined the agglomerates through the various stages of agglomeration to access how the composition and morphology of the coating layers on bed particles develop with time. However, this understanding is important, particularly for the early stages of agglomeration, to understand how the layer formed on bed particles.[15,21] He et al.[22] traced the evolution of bed particles by sampling at different reaction times during combustion of bark in a lab-scale fluidized bed reactor and wood-based fuels in a full-scale fluidized bed combustor. They deduced that agglomeration is initiated by K reacting with silica sand to form low-melting-point silicates.[22] The Ca-rich fly ash particles then adhere to the sticky bed particles and dissolve gradually into the initial inner coating layer. However, very few studies have focused on the time-dependent layer formation process of the agglomerates for agricultural residues under both combustion and gasification atmospheres. The present investigation therefore aims to meet this need.

The reaction atmosphere also influences the release of ash-forming elements and the melting behavior of inorganic matter, thus changing the interaction between the ash and the bed materials.[23−26] Therefore, the mechanism of agglomeration for

a given set of materials may differ for the gasification and combustion processes. The agglomeration mechanism under combustion atmosphere has been extensively investigated previously.[10,13−15,18] However, the understanding of the agglomeration mechanism under steam gasification is limited. The understanding of the difference between agglomeration mechanism under both combustion and steam gasification atmospheres is particularly important for a dual-fluidized-bed gasifier, which has both combustion and steam gasification processes. Some studies have compared the agglomeration mechanism during gasification and combustion.[16,17,27,28] Ohman et al.[27] found for Lucerne that, under combustion atmosphere, the layer formed on the bed particles is thin and consists of a salt matrix. On the basis of equilibrium calculations, the composition of the salt matrix formed under combustion atmosphere was found to consist of K, S, Cl, and solid K_2SO_4. In contrast, for the same feedstock under steam gasification atmosphere, a thicker and more homogeneous layer is formed on the bed particles. The equilibrium calculations show that under gasification atmosphere, more alkali metals release to the gas phase resulting a fast interaction with the surface of the bed particles. This may explain the formation of the thick coating layer. Kaknics et al. studied the agglomeration mechanism of Miscanthus under both combustion and gasification atmospheres.[16,17] They found that, for Miscanthus, S forms K_2SO_4 particles under combustion atmosphere, while, S releases to the gas phase and more potassium silicate layers are formed under gasification atmosphere.[17] Although several studies have focused on the effect of oxidizing (to simulate combustion) and reducing (to simulate gasification) atmospheres on the agglomeration mechanisms of biomass, to our knowledge, few of them have compared the agglomeration mechanisms with the two different atmospheres for the case in which steam is used as a gasification agent.[28] Moreover, instead of applying raw fuel to investigate the agglomeration mechanism, most researchers chose to use ash,[16,17,28] which will affect the result because the composition and structure of ash differ significantly from those of the raw fuel. Therefore, more work is still needed to better understand the effect of combustion and gasification atmospheres on the agglomeration mechanism based on measurements with the raw fuel.

For the reasons discussed above, the first aim of the present paper is to assess the time-dependent layer formation process during ash−bed material interaction for three agricultural residues with different ash-forming elements under both combustion and steam-gasification atmospheres. The second aim of the present paper is to compare the ash−bed material interactions under both combustion and steam-gasification atmospheres.

2. EXPERIMENTAL SECTION

2.1. Feedstock and Bed Material. A total of three common agricultural residues in Australia, which were grape marc, wheat straw, and cotton stalk, were selected as the feedstock. The raw grape marc samples were dried in an oven at 105 °C for 24 h. For the present investigation, each feedstock was ground with a centrifugal knife mill and sieved to the result size range of 200−500 μm. The proximate analysis was performed with a thermogravimetric analyzer (TGA) in an alumina crucible. Each sample was first heated to 105 °C at a heating rate of 10 °C/min and then held for 1 h to remove the moisture in a nitrogen atmosphere at 80 mL/min. The sample was then heated from 105 to 550 °C at a heating rate of 10 °C/min and held at that temperature for 1 h to measure the volatile matter. After that, the sample was combusted in air (80 mL/min) at 550 °C for 1 h

to burn any residual carbon in the sample and to determine the ash content. As for the content of Cl and Si, they were measured with ion chromatography (IC) and X-ray fluorescence (XRF), respectively. Other ash-forming elements, including K, Ca, Na, Mg, Al, Fe, P, and S were measured by digesting samples with HF (48% v/v)/HNO$_3$ (63% v/v)/H$_2$O$_2$ (30% v/v) and then analyzing the diluted solutions with inductively coupled plasma optical emission spectrometry (ICP-OES).

Table 1 presents the proximate and the ultimate analyses of the three feedstock. The volatile matter for those feedstock content is

Table 1. Proximate and Ultimate Analyses of the Feedstock

	grape marc	wheat straw	cotton stalk
moisture, %	2.49	7.29	3.58
proximate analysis (wt % db^a)			
volatile matter	68.74	68.78	67.52
fixed carbon	22.73	17.03	25.77
ash	8.53	14.19	6.70
ultimate analysis (wt % db^a)			
C	50.44	42.41	43.50
H	7.22	6.66	6.57
N	2.44	0.59	0.72
O, by difference	39.71	50.21	49.02
S	0.19	0.13	0.19

^{a}db: dry basis.

similar, while the ash content for wheat straw is the highest (14.19%), followed by grape marc (8.53%) and cotton stalk (6.70%). Table 2

Table 2. Ash-Forming Elementals Analysis of the Feedstock

g/kg of dry fuel	grape marc	wheat straw	cotton stalk
K	32.28	21.12	11.94
Ca	5.86	4.64	8.58
Na	0.17	6.91	2.56
Mg	1.21	1.12	2.80
Al	0.17	0.53	0.46
Fe	0.09	0.47	0.28
P	3.65	1.10	2.22
Cl	0.16	22.30	5.82
Si	0.72	17.64	0.26
K+Na	32.45	28.03	14.50

presents the elemental composition of the ash-forming elements of the three feedstock. The alkali metal content (K and Na) for grape marc and wheat straw is similar and nearly twice that of the cotton stalk, which suggests that they will have a greater tendency to agglomerate.[27] Grape marc has the greatest K content among the three feedstock but almost no Na. The content of K is nearly three times higher than that of Na in wheat straw and nearly five times higher than that of Na for the cotton stalk. The Si content in both grape marc and cotton stalk is negligible, but it is high in wheat straw. The content of Cl is high in wheat straw and cotton stalk but it is negligible in grape marc. Grape marc has a higher P content than in cotton stalk and wheat straw. Quartz sand was selected as the bed material and was obtained from the Coonarr Creek mine in Bundaberg, Australia with a particle size range of 75−212 μm. The composition of the quartz sand is given in Table 3.

2.2. Reactor. The experiments were carried out in a lab-scale, fixed-bed reactor, as shown in Figure 1. The reactor is composed of a 1.4 m stainless steel pipe with an inner diameter of 40.9 mm that was heated in a 3-zone horizontal tube furnace. Both ends of the reactor were sealed with flanges and gaskets. One end of the reactor houses a water-cooled "cooling jacket", which was used both to maintain the sample temperature below 50 °C before the test and to cool the sample after the test. Each feedstock sample was loaded into an alumina crucible. This was placed on an insertion probe to facilitate loading and

Table 3. Composition of the Bed Material

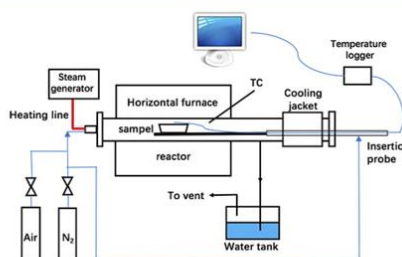| wt, %	quartz sand
SiO$_2$	99.84
Al$_2$O$_3$	0.038
Fe$_2$O$_3$	0.12
TiO$_2$	0.045
MgO	<0.01
K$_2$O	<0.01
Na$_2$O	<0.01
CaO	<0.01
Cr$_2$O$_3$	0.0001

Figure 1. Schematic diagram of the lab scale, fixed-bed reactor employed for the ash−bed material interaction tests and the ash and char preparation tests.

unloading, while a thermocouple inside the insertion probe was used to monitor the temperature of the sample. Steam was generated from a controlled evaporator mixer (CEM, Bronkhorst) and was introduced into the reactor with nitrogen as the carrier gas. These or other reaction gases were fed from the other end of the reactor to the "cooling jacket". All of the steam feeding lines were maintained at approximately 200 °C with a trace heater. Another nitrogen feeding line connecting to the insertion probe was used to cool the sample after each test. High-purity N$_2$ and industrial-grade air were used as reaction gases during the test, while their flow rate and that of water were controlled with mass flow controllers.

2.3. Ash−Bed Material Interaction Tests. The ash−bed material interaction tests were performed at 900 °C in the fixed-bed reactor under either combustion or steam-gasification atmospheres using air/N$_2$ (5% v/v O$_2$) or steam/N$_2$ (50% v/v steam) mixtures, respectively. The flow rate of the gas mixtures was held at 4 SLPM (standard liters per minute) for both the combustion and steam gasification atmospheres. Approximately 1.5 g of feedstock was mixed uniformly with quartz sand at a mass ratio of 3:1 (feedstock/quartz sand) in the alumina crucible before the test. Once the furnace had reached the target temperature, the crucible was placed in the cooling jacket while the reactor was purged for 10 min with the combustion or gasification mixtures. The crucible was then inserted into the middle of the tube furnace with the insertion probe for a reaction time of either 10 min, 30 min, 1 h, or 6 h to assess the evolution of the coating layer with time. At the end of each test, the insertion probe was used to retract the sample into the cooling jacket, and the gas was switched to 10 SLPM of N$_2$ to cool the sample to below 50 °C. The crucible was then removed from the cooling jacket and the mass of the crucible with the sample was recorded immediately. Following this, all samples were stored in a desiccator for further analyses.

2.4. Ash and Char Preparation Test. The procedure was the same as the ash−bed material interaction tests. However, the reaction time were 5 and 30 min for both the combustion and steam gasification atmospheres.

2.5. SEM−EDS and XRD Analyses. Both the morphology and composition of the agglomerates were analyzed with a scanning electron microscopy (Philips model XL30) in combination with
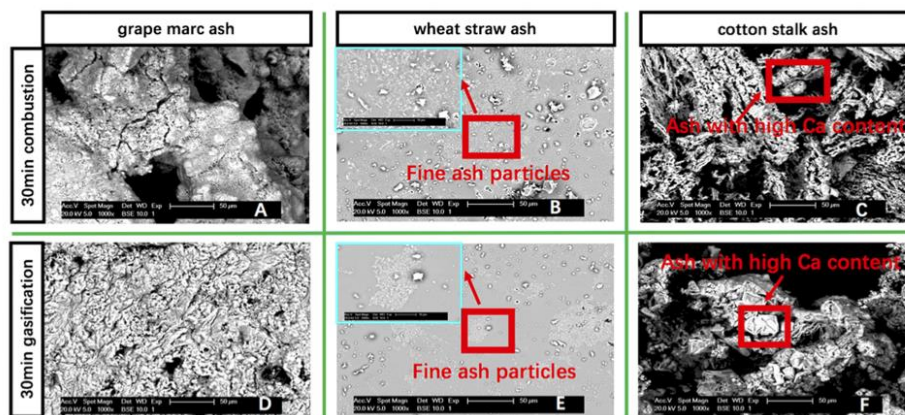
Figure 2. Typical images of the surface obtained with scanning electron microscopy for the three feedstock ash under either combustion or steam-gasification atmospheres for a reaction time of 30 min.
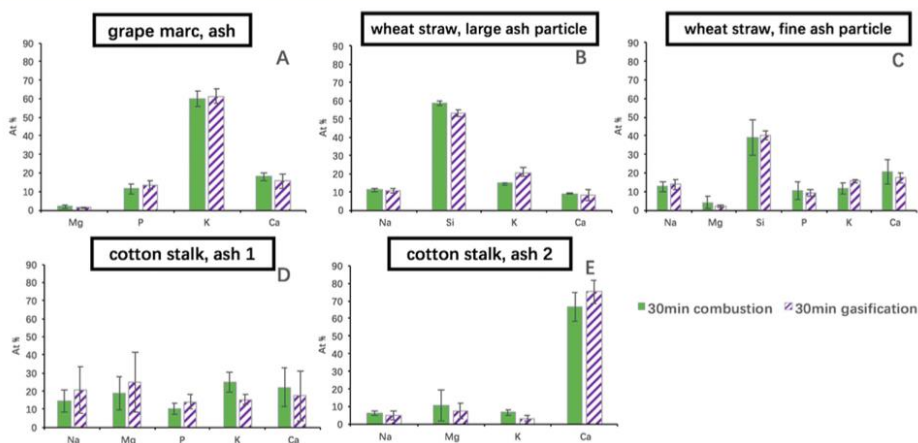

Figure 3. Elemental composition on a C-and O-free basis of the ash formed under the combustion and steam gasification atmospheres with a reaction time of 30 min for (a) ash particles from grape marc, (b) large ash particles from wheat straw, (c) fine ash particles deposited on the large ash particles for wheat straw, (d) type 1 ash particles for cotton stalk, and (e) type 2 ash particles for cotton stalk.

energy dispersive X-ray (SEM−EDX) at both the surface and a cross-section. Samples were mounted to a carbon tape for the surface analysis, or embedded in epoxy resin and polished for the cross-sectional analysis. Furthermore, samples were carbon-coated to reduce charging of the sample. The backscattering electron mode was employed to investigate the composition and the character of different parts within the agglomerates. For each agglomerate, five or six regions were measured with EDS for the composition, with two to four spots analyzed for each region. Both the morphology and composition of the samples from the 30 min ash preparation tests were analyzed with SEM−EDS at the surface with the same procedure as for the agglomerates. The crystalline phase of the agglomerates and the samples from the ash and char preparation tests was determined from an X-ray diffraction (XRD) measurement (Rigaku MiniFlex 600) with Cu Kα radiation.

3. RESULTS

3.1. Ash Elemental Composition under Combustion and Steam Gasification Atmospheres.
Figure 2 presents the images of the morphology of the ash at the SEM surface view for grape marc, wheat straw, and cotton stalk under combustion and steam gasification atmospheres for 30 min reaction time. Grape marc ash forms large ash particles under a steam-gasification atmosphere, while it forms small ash particles under a combustion atmosphere. For wheat straw ash, some very fine ash particles have deposited on the large ash particles for both atmospheres, while the color of the large ash particles was gray for steam gasification and black for combustion. Atmosphere has no obvious effect on the cotton stalk ash.

Figure 3 presents the elemental composition of the ash for grape marc, wheat straw, and cotton stalk obtained from the ash preparation tests under both the combustion and steam

Article

Table 4. Crystalline Phase of the Samples from the Ash and Char Preparation Tests Identified Using XRD

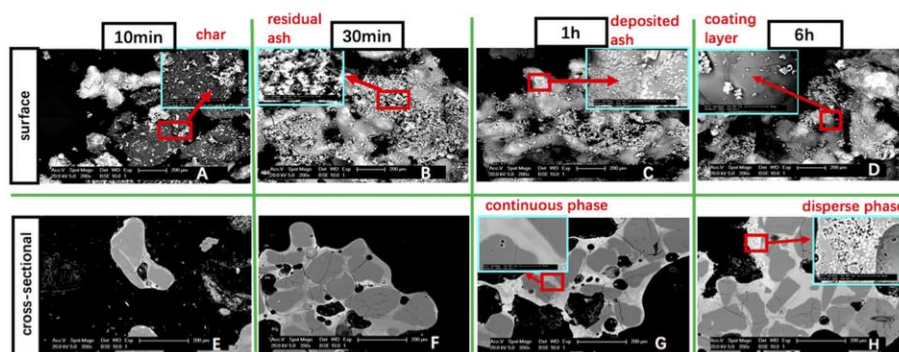|	reaction time	steam gasification	combustion
grape marc	5 min	CaO, K_2CO_3 $(H_2O)_{1.5}$, $KCaPO_4$	CaO, K_2CO_3 $(H_2O)_{1.5}$, $KCaPO_4$
	30 min	CaO, MgO, $KCaPO_4$, K_2CO_3	CaO, MgO, $KCaPO_4$, K_2CO_3
wheat straw	5 min	KCl, $NaCl$	KCl, $NaCl$
	30 min	$NaCaPO_4$, Ca_2SiO_4	$NaCaPO_4$, Ca_2SiO_4, $KCaPO_4$
cotton stalk	5 min	CaO, MgO, KCl, K_2CO_3	CaO, MgO, KCl, K_2CO_3
	30 min	CaO, MgO, K_2CO_3	CaO, MgO, K_2CO_3

Figure 4. Typical images of the surface (panels A−D) and cross-sections (panels E−H) obtained with SEM for the agglomerates of grape marc under the combustion atmosphere for reaction times of 10 min (panels A and E), 30 min (panels B and F), 1 h (panels C and G), and 6 h (panels D and H).

gasification atmospheres for a reaction time of 30 min. The elemental composition of the three feedstock ash is not significantly different for combustion and steam gasification atmospheres. This implies that the ash composition is not influenced by the gas atmosphere. Figure 3A shows that the grape marc ash under both combustion and gasification is dominated by P, K, and Ca with minor amounts of Mg. Ash-forming elements can be divided into two categories, basic compounds (KOH (l,g), $NaOH$ (l,g), CaO (s), and MgO (s)) and acidic compounds (P_2O_5 (g), SO_2 (g)/SO_3 (g), $SiO_2(s)$, HCl (g) (Cl_2), CO_2 (g) and H_2O (g)).[29] Basic compounds can react with acidic compounds. Among acidic compounds, P_2O_5 (g) reacts first with basic compounds, followed by other acidic compounds (SO_2 (g)/SO_3 (g), SiO_2 (s), HCl (g) (Cl_2), CO_2 (g), and H_2O (g)) successively.[14,29] Usually, potassium phosphate will be the first compound to form when both K and P are present, which then reacts with Ca, Mg or Si to form the K-Ca/Mg-phosphates/-silicates.[14,29,30] For the grape marc ash, the SEM−EDS results show that P may react with K first to form the K-phosphate, which then reacts with Ca to form the K-Ca phosphate. The much greater content of K than P in the grape marc ash, which has negligible Si and Cl content and relatively low S implies that the excess K may exist as potassium carbonate in the grape marc ash or char.[31]

For wheat straw, the elemental composition of the large ash particles and the very fine ash particles (smaller than 4 μm) in Figure 2 are shown in panels B and C of Figure 3, respectively. The very fine ash particle is rich in Na, Mg, Si, P, K, and Ca, while the large ash particle mostly consists of Na, Si, K, and Ca. The content of Si in both the fine and the large ash particles of wheat straw is much higher than that of other elements. The alkali metal (K and Na) in the wheat straw ash may react with P first to form alkali phosphate and then with Ca, Mg, or Si to

form the very fine and deposited ash particles consisting of alkali-Ca/Mg-phosphate/-silicate. Wheat straw has a much higher Cl and Si content than the other two feedstocks. The excess alkali metal in the wheat straw ash then reacts with Si and Cl to form the alkali silicate (may followed by further reactions with Ca to form alkali-Ca silicate) that generates the large ash particles of wheat straw and the alkali chloride that releases to the gas phase, respectively.[31]

Figure 3D,E presents the elemental composition of the cotton stalk ash. Some parts of the ash, labeled "ash 2", are dominated by Ca, as shown in Figure 2, and are formed under both atmospheres. The other part of the cotton stalk ash, which is dominated by Na, Mg, P, K, and Ca, is labeled "ash 1". Similar to the ash from grape marc and wheat straw, the alkali phosphate may form first and then react further with Ca or Mg to form the alkali-Ca/Mg-phosphate ash.

Table 4 presents the crystalline phase for the samples from the ash and char preparation tests under both combustion and steam-gasification atmospheres as identified with XRD. The crystalline phase for all the samples, except for the wheat straw sample under combustion atmosphere at 30 min, are almost the same under steam gasification and combustion atmospheres. It can be seen that $KCaPO_4$ is found in the grape marc ash and char samples under both atmospheres, which further confirms that the formation of K−Ca phosphate. Similarly, CaO and K_2CO_3 are detected in both the grape marc char and ash samples. However, MgO is only detected in the 30 min grape marc ash sample. For wheat straw, KCl and $NaCl$ can be detected for the 5 min char, which confirms the existence of alkali chloride in the wheat straw ash and char. For the 30 min wheat straw ash experiment, $NaCaPO_4$ and Ca_2SiO_4 can also be detected under both atmospheres, while $KCaPO_4$ is only found under the combustion atmosphere. The presence of $KCaPO_4$
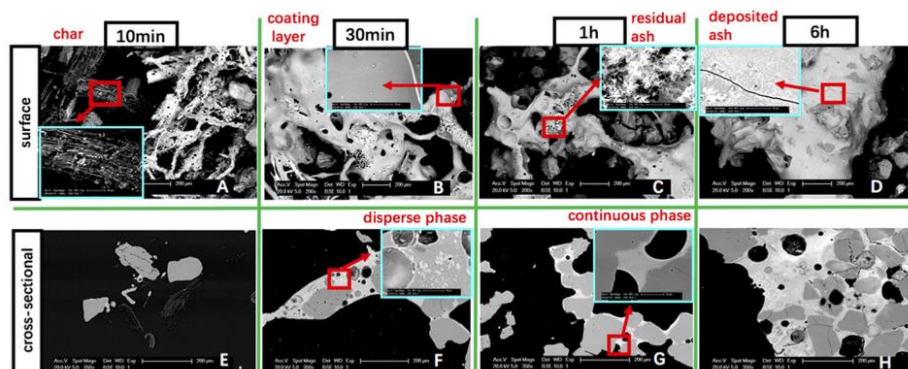
4282

Figure 5. Typical images of the surface (panels A−D) and cross-sections (panels E−H) obtained with SEM for the agglomerates of wheat straw under the combustion atmosphere for reaction times of 10 min (panels A and E), 30 min (panels B and F), 1 h (panels C and G), and 6 h (panels D and H).

Figure 6. Typical images of the surface (panels A−D) and cross-sections (panels E−H) obtained with SEM for the agglomerates of cotton stalk under the combustion atmosphere for reaction times of 10 min (panels A and E), 30 min (panels B and F), 1 h (panels C and G), and 6 h (panels D and H).
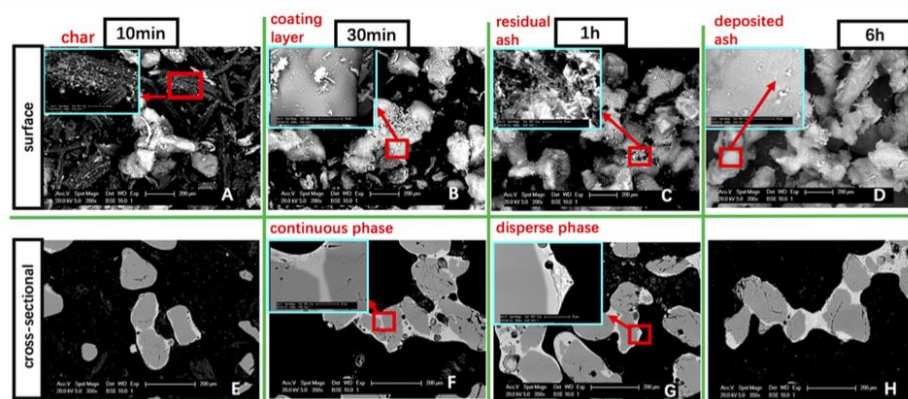
and $NaCaPO_4$ agrees with the SEM−EDS result; that is, alkali-Ca/Mg-phosphate/-silicate may form in the wheat straw ash. For the case of cotton stalk, CaO, MgO, and K_2CO_3 are found in both the char and ash samples, while the KCl is found only for the 5 min cotton stalk char sample. This implies that the KCl releases to the gas phase when the reaction time is sufficient. No phosphate phase can be detected with XRD in the cotton stalk char or ash, which may result from the low content of P in the cotton stalk samples. Therefore, the presence or absence of alkali phosphate or alkali-Ca/Mg-phosphate in the cotton stalk ash cannot be confirmed with XRD.

3.2. Morphology of the Agglomerates. *3.2.1. Morphology of the Agglomerates under Combustion.* Figures 4−6 present images of the morphology of the agglomerates at the surface and in the cross-sectional views for grape marc, wheat straw, and cotton stalk for a series of reaction times (10 min, 30 min, 1 h, and 6 h) under the combustion atmosphere. For the grape marc sample at a reaction time of 10 min, Figure 4A

shows that some dark residual char particles can be observed within the agglomerates. In addition, the sand particles are already coated with a thin and light coating layer, as shown in Figure 4E. Figure 4B shows the case for 30 min that many small ash particles, called the "residual ash", are found within the agglomerates. As shown in Figure 4B,F, the agglomerated particles have grown to incorporate more sand particles, while the coating layer is much thicker than that of the case for 10 min. For reaction times of 1 and 6 h, the number of the residual ash particles within the agglomerates has decreased as shown in Figure 4C,D, while the size of the agglomerates and the thickness of the coating layer have not changed significantly compared to the case of 30 min. As can be observed in the images of the agglomerates for different reaction times, large numbers of very fine and light ash particles (<4 μm), which is called the "deposited ash", have deposited on, and embedded in, the coating layer, as shown in Figure 4C. Figure 4D shows the enlarged image of the morphology of the coating layer with some small white residual ash particles distribute on it. Figure
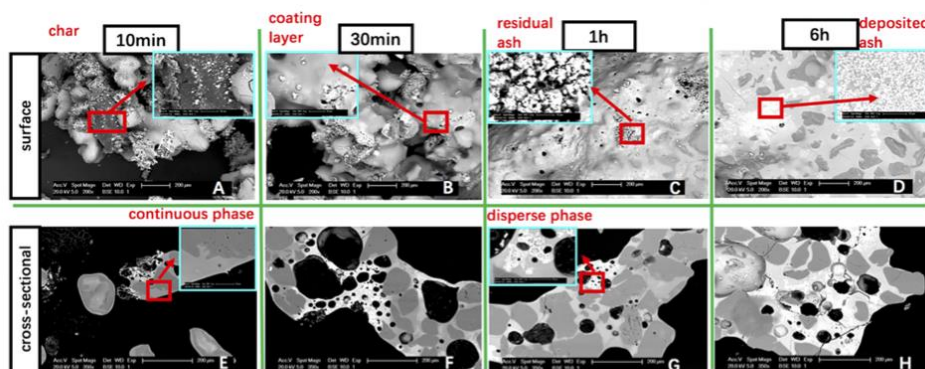
60

Figure 7. Typical images of the surface (panels A−D) and cross-sections (panels E−H) obtained with SEM for the agglomerates of grape marc under the steam-gasification atmosphere for reaction times of 10 min (panels A and E), 30 min (panels B and F), 1 h (panels C and G), and 6 h (panels D and H).
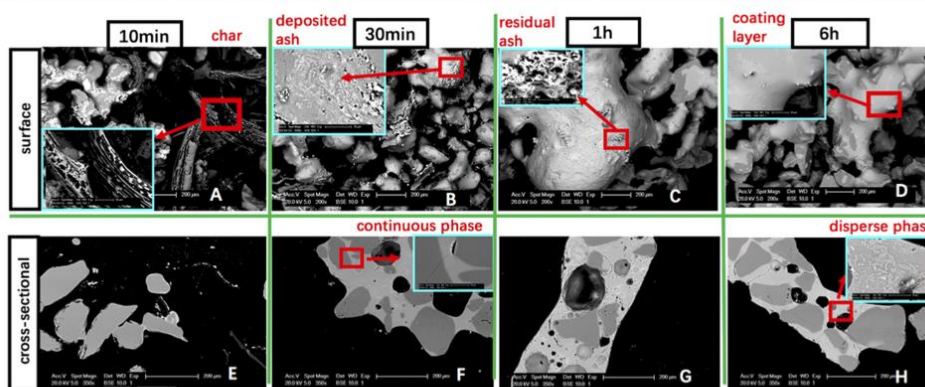
Figure 8. Typical images of the surface (panels A−D) and cross-sections (panels E−H) obtained with SEM for the agglomerates of wheat straw under the steam-gasification atmosphere for reaction times of 10 min (panels A and E), 30 min (panels B and F), 1 h (panels C and G), and 6 h (panels D and H).

4G shows the cross-sectional analysis of the sample for the 1 h test and the enlarged image of the cross-sectional of part of the coating layer, which is termed the "continuous phase", because that the color of the layer is homogeneous. Figure 4H shows the enlarged image of some heterogeneous coating layer. Many small lighter phases, which are called "disperse phases", are distributed within the darker continuous phase, and the presence of the disperse phase is greater for the 1 and 6 h tests than for the 30 min test. Residual ash, deposited ash, continuous phases, and disperse phases are found within the agglomerates for all reaction times (except for the 10 min reaction time because no deposited ash is detected).

Figure 5 shows that the morphology of the agglomerates of wheat straw is different from that of grape marc. The coating layer of wheat straw is not homogeneous, with some sand particles having little or no coating layer, while others are adhered together to form larger agglomerates with a much-thicker coating layer, even for a reaction time of 1 h. This suggests that the sand particles may be adhered together by big molten ash particles. Similar to grape marc, residual char particles still can be found within the agglomerates for the 10

min case, as shown in Figure 5A, while the coating layer on the sand particles is still very thin, which can be seen from the cross-sectional view in Figure 5E. Figure 5B,F shows that both the size of the agglomerates and the thickness of the coating layer have increased for a reaction time of 30 min, with some residual ash particles distributed within the agglomerates. The morphology of the coating layer, residual ash, and continuous phase are shown in panels B, C, and G in Figure 5, respectively. Large numbers of very fine and light ash particles can be seen from Figure 5D to have deposited on, and embedded in, the coating layers, while a lighter disperse phase, as shown in Figure 5F, is distributed within the darker continuous phase from the surface and the cross-sectional analyses, respectively. Residual char is found for the 10 min reaction time, while the residual ash, deposited ash, continuous phase, and disperse phase exist for all reaction times (except for the 6 h reaction time, during which no residual ash is detected).

The morphology of the agglomerates for cotton stalk, as shown in Figure 6, is similar to that of grape marc for a given reaction time. Similar to grape marc, the coating layer of the agglomerates from cotton stalk is relatively homogeneous. The

61

Figure 9. Typical images of the surface (panels A−D) and cross-sections (panels E−H) obtained with SEM for the agglomerates of cotton stalks under the steam-gasification atmosphere for reaction times of 10 min (panels A and E), 30 min (panels B and F), 1 h (panels C and G), and 6 h (panels D and H).
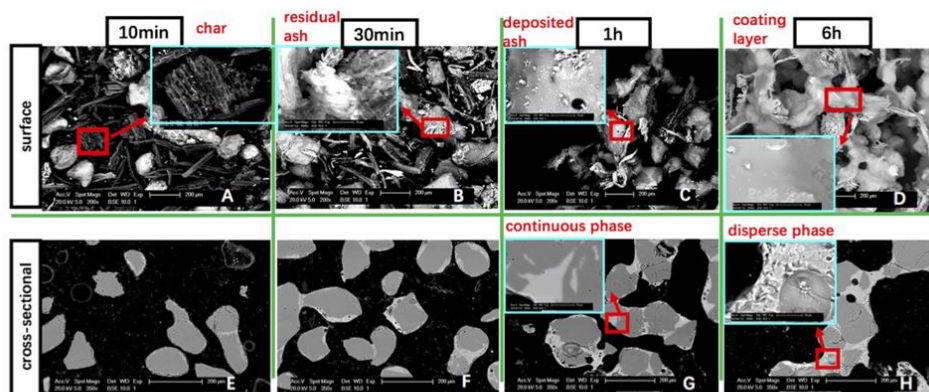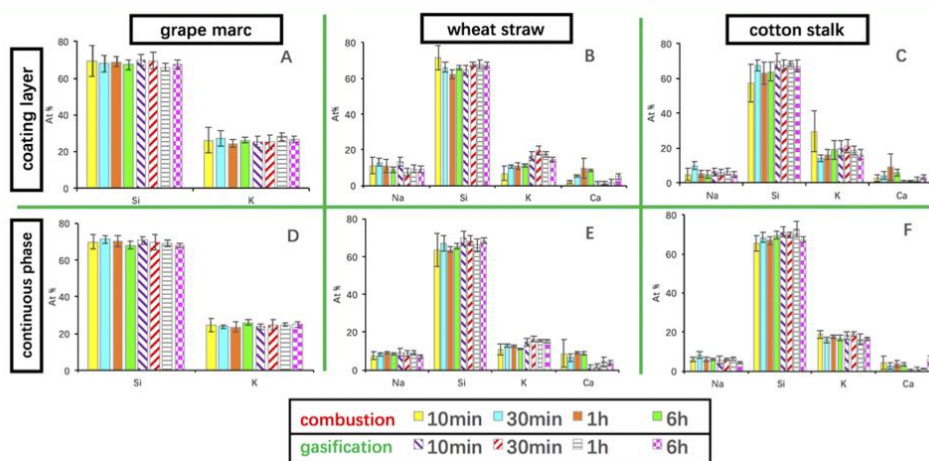

Figure 10. Elemental composition of some major ash-forming elements on a C-and O-free basis for the coating layer (panels A−C) in SEM−EDS surface analysis and for the continuous phase (D−F) in SEM−EDS cross-sectional analysis of the agglomerates for different reaction times (10 min, 30 min, 1 h, and 6 h) under combustion and steam-gasification atmospheres (panels A and D: grape marc; panels B and E: wheat straw; panels C and F: cotton stalk.).

residual char is detected for the 10 min reaction time, as shown in Figure 6A. The agglomerates grow slightly larger, and the coating layer becomes thicker as the reaction time increases to 30 min, as shown in Figure 6B,F. The residual ash, deposited ash, continuous phase, and disperse phase are detected for all reaction times (except for the 10 min reaction time, for which no deposited ash is detected). Interestingly, the coating layer of the agglomerates of cotton stalk does not grow as thick as that of the grape marc sample.

3.2.2. Morphology of the Agglomerates under Steam Gasification. Figures 7−9 present images of the morphology of the agglomerates at the surface and in the cross-sectional views for grape marc, wheat straw, and cotton stalk for a series of reaction times (10 min, 30 min, 1 h, and 6 h) under the steam gasification atmosphere. Figure 7 shows that the morphology of the agglomerates for grape marc for any given reaction time has

many similarities with the equivalent case in the combustion atmosphere as shown in Figure 4. The residual char is detected and the coating layer is relatively thin for the 10 min reaction time, as shown in Figure 7A,E. It can be seen from Figure 7B,F that both the size of the agglomerates and thickness of the coating layer increase with the reaction time to 30 min. The presence of residual ash, deposited ash, continuous phase, and disperse phase are detected for the steam gasification atmosphere for all reaction times (except for the 10 min and 6 h reaction times, for which no deposited ash and residual ash are detected, respectively). However, the size of the agglomerates is greater under the steam gasification atmosphere than that under the combustion atmosphere, and the number of fine ash particles (<4 μm) that are deposited onto the surface of the agglomerates is greater under the steam gasification
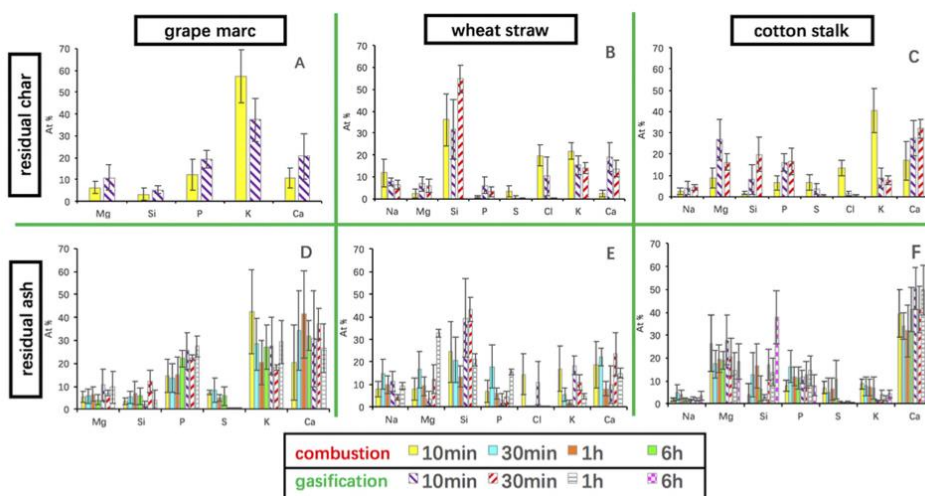
Article

Figure 11. Elemental composition of some major ash-forming elements on a C-and O-free basis for the residual char particles (panels A−C) and for the residual ash particles (panels D−F) within the agglomerates in the SEM−EDS surface analysis for different reaction times (10 min, 30 min, 1 h, and 6 h) under combustion and steam gasification atmospheres (panels A and D: grape marc; panels B and E: wheat straw; panels C and F: cotton stalk.).

atmosphere than under the combustion atmosphere (note the cases for reaction times of 1 and 6 h).

Figure 8 shows that the atmosphere has no significant influence on the morphology of the agglomerates for wheat straw. Similar to the case with combustion, the coating layer is not homogeneous. Some residual char is found, while the coating layer is thin for the 10 min reaction time, as shown in Figure 8A,E. Figure 8B,F shows that both the size of the agglomerates and the thickness of the coating layer have increased for a reaction time of 30 min. The residual ash, deposited ash, continuous phase, and disperse phase are generated under the steam gasification atmosphere for all reaction times (except for the 10 min and 6 h reaction times, for which no disperse phase and residual ash are detected, respectively). For both cases of combustion and steam gasification, it can be deduced that the coating layer melts and causes the sand particles to adhere together. The effect of the atmosphere on wheat straw is not as obvious as on grape marc, which has similar alkali metal content to wheat straw.

Figure 9 presents the equivalent case for cotton stalk under the steam gasification atmosphere. It can be seen that the morphology does depend on the atmosphere for this sample. Many residual char particles can be found within the agglomerates for the steam gasification atmosphere, while the size of the agglomerates is relatively small and the thickness of the coating layer is relatively small and thin (Figure 9A,B,E,F) compared to the combustion case even for a reaction time of 30 min. The size of the agglomerates is larger and the coating layer is thicker when the reaction time is increased to 1 h. The residual ash, deposited ash, continuous phase, and disperse phase are all found for the steam-gasification cases for all reaction times (except for the 10 and 30 min reaction times, for which no deposited ash is detected; no disperse phase is detected for the 10 min reaction time).

3.3. Composition of the Agglomerates from the Ash−Bed Material Interaction Tests. *3.3.1. Composition of the*

Coating Layer. Figure 10 presents the elemental composition of both the coating layer at the SEM−EDS surface analyses and the continuous phase in the SEM−EDS cross-sectionals analyses of the agglomerates for grape marc, wheat straw, and cotton stalk for a series of reaction times and for both combustion and steam-gasification atmospheres. It can be seen that the elemental composition of the coating layer and the continuous phase is similar for each feedstock. The main elements for the coating layer and the continuous phase of grape marc are Si and K, while for wheat straw and cotton stalk, they are Na, Si, K, and Ca. The elemental composition of the coating layer is independent of the atmosphere or the reaction time. This suggests that the reactions between alkali metal and Si are not affected significantly by the reaction time or the atmosphere, so that an increase in reaction time predominantly acts to increase the thickness of the coating layer.

3.3.2. Composition of the Residual Char and the Residual Ash Particles. Figure 11 presents the elemental composition of the residual ash and residual char particles within the agglomerates for the three feedstock processed for a series of reaction times both for the conditions of combustion and steam gasification. Figure 11A,D shows that both the residual char and ash particles for grape marc are rich in P, K, and Ca with minor amounts of Mg and Si. This is similar to the elemental composition of the grape marc ash in Figure 3A from the ash-preparation tests. It can also be seen that the atmosphere influences the S content, which is present only under the combustion atmosphere. During the SEM−EDS analysis of grape marc, under the combustion atmosphere, approximately half of the analyzed sections consist of S content, while no S content was detected under the steam gasification atmosphere. Figure 11D presents only the average composition for the sections with S content under the combustion atmosphere. The composition of other sections that without S content under the combustion atmosphere, which had the similar composition to that of the steam gasification atmosphere, is not reported.
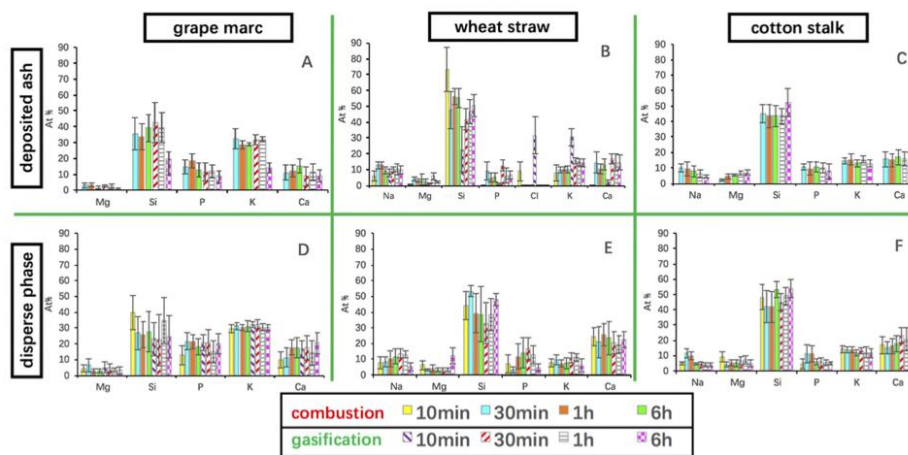
Figure 12. Elemental composition of some major ash-forming elements on a C-and O-free basis for the very fine deposited ash particles (A to C) in SEM−EDS surface analysis and for the disperse phase (panels D−F) in SEM−EDS cross-section analysis of the agglomerates for different reaction times (10 min, 30 min, 1 h, and 6 h) under combustion and steam gasification atmospheres (panels A and D: grape marc; panels B and E: wheat straw; panels C and F: cotton stalk.).

Figure 11B,E shows the elemental composition of the residual char and the residual ash particles of wheat straw sample, which are dominated by Na, Mg, Si, P, K, and Ca, is similar to that of the composition of the fine ash particles that have deposited on the large ash particles from the ash preparation tests, as shown in Figure 3C. A high Cl content is also detected in the residual ash and char particles of wheat straw for a reaction time of 10 min under both combustion and steam gasification atmospheres. This implies that some alkali metal may form alkali chloride. The residual ash and char particles have a lower Cl content under the steam gasification atmosphere than that under the combustion atmosphere, which can be explained by promoting the release of Cl by steam.[28] No S has been detected in the residual ash under both combustion and steam gasification atmospheres.

Figure 11C,F presents the elemental composition of the residual char and the residual ash particles of cotton stalk sample, which mainly consist of Na, Mg, Si, P, K, and Ca. This elemental composition is similar to that of the "ash1" in Figure 3D from the ash-preparation tests, except for the Si content, which is from the quartz sand. A high Cl content is detected in the residual char particles under the combustion atmosphere, while no Cl is detected under the steam-gasification atmosphere. Again, this provides further evidence that steam promotes the release of Cl.[28] Similar to the grape marc, S is found in the residual ash particles of cotton stalk under the combustion atmosphere but not under the steam-gasification atmosphere.

3.3.3. Composition of the Disperse Phase and Deposited Ash. Figure 12 presents the elemental composition of the fine ash particles (deposited ash) that deposited onto the coating layer and the disperse phase that was distributed inside the continuous phase for a series reaction time and under both atmospheres for all the three feedstock. It can be seen that the elemental composition of the deposited ash and the disperse phase is similar to its counterpart for all the three feedstock, which is consistent with Figure 11 (that is, the residual ash

particles within the agglomerates except for the S and Cl contents). For the deposited ash particles on the surface of the wheat-straw agglomerates, some Cl content can be detected for a 10 min reaction time under both atmospheres. It suggested that alkali chloride may exist in the deposited ash particles for a short reaction time, and then the Cl releases to the gas phase when reaction time is long enough. In addition, the crystalline phase of K−Ca phosphate can be detected with an XRD only for the agglomerates of grape marc, but no phase other than quartz sand is detected for wheat straw and cotton stalk. This may result from the lower P content for these two fuels than that for grape marc. The XRD results for grape marc agree with the results for the elemental composition of the residual ash, the deposited ash, and the disperse phase of grape marc.

3.4. Discussion of Ash−Bed Material Interaction Mechanism. In section 3.1, the elemental composition of the ash from the ash preparation tests of the three feedstock has been discussed. The elemental composition of the large ash particles for wheat straw in Figure 3B from the ash preparation is similar to that of the coating layer in Figure 10B and that of the continuous phase in Figure 10E. This further provides evidence that the ash−bed material interaction of wheat straw is a melting-induced mechanism.[8,15,32] The quartz sand particles are adhered together by the fuel-derived molten ash particles from wheat straw to form the agglomerate.[15,32] The elemental composition of the coating layer for grape marc and cotton stalk in Figure 10 is different from that of the P-dominated ash particles in Figure 3. This suggests that the ash−bed material interaction for grape marc and cotton stalk is a coating-induced mechanism; that is, alkali metal from the fuel interacts with Si from the quartz sand to form the alkali silicate coating layer.[15] The formation of the coating layer also accompanied by Ca dissolves or diffuses into the coating layer for wheat straw and cotton stalk.[22] For grape marc, however, no Ca can be found in the coating layer may because it could be reacted with the P.

Four possible ash−bed material interaction mechanisms can explain how alkali metal interacts with Si from the quartz sand

Figure 13. Pictures of the agglomerates of grape marc, wheat straw, and cotton stalk for a reaction time of 6 h under both combustion and steam-gasification atmospheres.

or from the feedstock: (1) the ash particles generate from the char particles deposit onto the surface of the coating layer and gradually embed in the coating layer. The alkali metal (K and Na) from the deposited ash particles and then transfers to the coating layer;[33] (2) gaseous alkali metal reacts with the surface of the quartz sand to form the coating layer of low-melting-point alkali silicate;[15] (3) reactions of potassium carbonate or sodium carbonate with the quartz sand to form the coating layer of low-melting-point alkali silicate;[26,34,35] and (4) bed particles are adhered together by the fuel-derived molten ash particles to form the agglomerates.[15,32]

The elemental composition of the residual ash particles distributed within the agglomerates in Figure 11, the fine ash particles (deposited ash) that deposited on the coating layer and the disperse phase in Figure 12 are similar for all the three feedstock. They are all dominated by alkali metals, Mg, Si, P, and Ca. This gives evidence of the ash–bed material interaction mechanism 1, as discussed above. For grape marc, K reacts with P first and then with Ca to form $KCaPO_4$. For wheat straw and cotton stalk, the residual ash particles are dominated by Na, Mg, Si, P, K, and Ca. Parts of the alkali metals in wheat straw and cotton stalk could potentially form phosphate first and then react with Ca, Mg, or Si to form the alkali- Ca/Mg-phosphate/-silicate ash particles. However, the composition of the residual ash particles of wheat straw and cotton stalk has yet to be confirmed. These residual ash particles for the three feedstock then deposit on, or adhere to, the coating layer to form the very fine ash particles (deposited ash) that deposit on the coating layer and may also gradually embed inside the coating layer to form the light disperse phase that distributed inside the coating layer.[18,36] It has been reported the bed particles are at risk of agglomeration, in which the P content in a fuel is sufficiently high, by the molten alkali phosphate ash particles via a melting-induced agglomeration mechanism.[37]

For the K, it exists as water-soluble inorganic salts or organically bound K ions in biomass[38] and the organically associated K releases at temperatures lower than 500 °C under both gasification and combustion.[39,40] At higher temperatures, K releases with Cl and S or releases after the decomposition of K_2CO_3.[40] Na has similar behavior to K.[38] Either the alkali metal that released to the gas phase or that in the form of K_2CO_3 or Na_2CO_3 can react with the quartz sand to form the coating layer.[15,26,34,35] For mechanism 2, compared with the reactions of the quartz sand with alkali carbonate in mechanism 3, the reactions with alkali chloride take place at a significantly slow rate and only to a very limited extent.[26,35] In Figures 11E and 12B, the residual ash particles distributed within the agglomerates and the fine ash particles that deposited on the coating layer for wheat straw both have a high Cl content for a

reaction time of 10 min under both combustion and steam gasification atmospheres. This gives further evidence that for the fuels with a relatively high Cl content, such as the wheat straw used in the present study, alkali chloride can interact with the surface of the sand particles. Mechanisms 1 and 3 may play a major role for grape marc and cotton stalk, while mechanism 4, a melting-induced mechanism, plays a dominant role for wheat straw.

3.5. Discussion of the Differences for Ash–Bed Material Interaction under Combustion and Steam Gasification Atmospheres. Both the morphology and the elemental composition of the agglomerates from the ash–bed material interaction test are different for combustion and steam gasification atmospheres. For the morphology of the agglomerates of grape marc, the agglomerates are larger under a steam-gasification atmosphere than that under combustion atmosphere for a given reaction time, as shown in Figures 4 and 7. Figure 7 shows that the coating layer on the agglomerates could be in the molten phase so that the sand particles adhere together to form large agglomerates for these atmospheres (reaction times of 1 and 6 h). Steam can reduce the melting point of potassium carbonate and sodium carbonate.[41,42] For a $H_2O–N_2$ atmosphere, the melting point of potassium carbonate and sodium carbonate can be as low as 700 and 725 °C, respectively.[41] Kosminski et al.[25,26] suggested that a liquid–solid phase reaction takes place between liquid sodium carbonate and silica under steam atmosphere compared to the solid–solid phase reaction under carbon dioxide and nitrogen atmospheres. K has similar behavior to Na.[38] Therefore, more liquid silicates are generated from the reactions between liquid alkali carbonate and quartz sand under the steam atmosphere. As discussed in section 3.1, potassium carbonate presents in the grape marc char and ash. The potassium carbonate generates more liquid potassium silicates and that explains why larger agglomerates can be observed for the steam gasification atmosphere than that for the combustion atmosphere.

For the case of wheat straw, the difference for the morphology of the agglomerates under the two atmospheres is not that significant. It is generally considered that the agglomeration mechanism for fuels with a highly reactive Si content, for example, wheat straw, is induced by the molten, fuel-derived ash particles, while no reactions take place between the molten ash particles and the sand particles.[15,32] The coating layer for wheat straw that consists of the fuel-derived alkali silicates had been molten for both modes.[7] This explains why there is no obvious difference for the two atmospheres.

For cotton stalk, the influence of the atmosphere on the morphology of the agglomerates is not significant. Cotton stalk has much lower alkali metal content and higher Cl and S

65

content than those of grape marc. Alkali metal reacts with P_2O_5 (g), SO_2(g)/SO_3(g), SiO_2(s), and HCl(g)(Cl_2) before reacting with CO_2(g).[29] Therefore, much less alkali carbonate may form for cotton stalk than for grape marc (as shown in section 3.1, K_2CO_3 can be detected in the char and ash of cotton stalk). This explains why the effect of steam on the agglomeration for cotton stalk is much slighter than on grape marc.

Figure 13 presents the pictures of the agglomerates for grape marc, wheat straw, and cotton stalk for a 6 h reaction time and for both cases of combustion and steam gasification. It can be seen that the size of the agglomerates is greater for the steam gasification atmosphere than that for the combustion atmosphere for all the three feedstock, especially for the grape marc. For the grape marc under a steam-gasification atmosphere, the surface of the coating layer has melted to form one large agglomerate, while the increase in size is less significant for the wheat straw and the cotton stalk. This further proves that steam generates more liquid silicates than the combustion atmosphere.

The elemental composition of the agglomerates for grape marc and cotton stalk is different for combustion and steam gasification atmospheres, while for wheat straw, no significant difference is detected under both the atmospheres. For grape marc and cotton stalk samples, S is detected in the residual ash under combustion atmosphere, while no S is detected under steam gasification atmosphere, as shown in Figure 11. Some studies have reported that, under the combustion atmosphere, some of the S reacts with K to form K_2SO_4 particles.[17,27] Other sulfates, such as $CaSO_4$ or Na_2SO_4, may also form; however, the presence of either one of the phases cannot be detected with XRD, which could be due the concentration was below the detection limit. However, under the steam gasification atmosphere, most of the S releases to the gas phase, leaving the residual K to form potassium silicate.[17,27] If S forms K_2SO_4 or Na_2SO_4 in the combustion agglomerates and release to the gas phase under the steam gasification atmosphere, the increased in the presence of alkali silicates in the coating layer under the steam-gasification atmosphere implies that, agglomeration will be more serious under a steam-gasification atmosphere than that under combustion atmosphere, as shown in Figure 13. For wheat straw, the absence of S in the residual ash particles within the agglomerates under either atmosphere, as shown in Figure 11, suggests that the content of S in wheat straw, which has the lowest S content among the three feedstock, is sufficiently low for most of the S to release to the gas phase under both atmospheres.

4. CONCLUSIONS

The coating layer of the agglomerates formed in fluidized beds for both combustion and gasification atmospheres with grape marc as the feedstock is dominated by Si and K, while for wheat straw and cotton stalk, it is dominated by Na, Si, K, and Ca. The elemental composition of the coating layer for the three feedstock is found to be independent of both the reaction time and the gas atmosphere. However, the thickness of the coating layer increase with reaction time, while the size of the agglomerates is greater under the steam gasification atmosphere than under the combustion atmosphere.

The ash−bed material interaction mechanisms deduced for the three feedstock are as follows. For grape marc, K reacts with P first to form the K phosphate and then with Ca to form the KCaPO$_4$ ash particles. For wheat straw and cotton stalk, the residual ash particles within the agglomerates are dominated by

Na, Mg, Si, P, K, and Ca. For grape marc and cotton stalk, alkali metals react with the quartz sand to form a low-melting-point alkali silicate coating layer on the surface of the sand particles. This generates a coating-induced mechanism. For wheat straw, alkali metals react with the reactive Si in the fuel to form the low-melting-point, fuel-derived ash particles. Sand particles adhere to these molten ash particles to form the agglomerates by a melting-induced mechanism. For wheat straw and cotton stalk, which have a high Cl content, alkali chloride in the gas phase can react with the surface of the quartz sand to form a coating layer but at a much lower rate and only to a limited extent. The formation of a coating layer for the cotton stalk and wheat straw is also accompanied by Ca diffusion or dissolution into the alkali silicate coating layer.

Any residual ash particles from the first stage can also deposit on, or adhere to, the coating layer of the sand particles to become embedded into the coating layer.

The difference between the ash−bed material interaction under combustion and steam gasification atmospheres is as follows. For a steam-gasification atmosphere, steam lowers the melting point of alkali carbonates to generate more liquid alkali silicates to form larger agglomerates. This effect is the most evident for grape marc owing to the high alkali carbonate content in the grape marc. For grape marc and cotton stalk, which both have a relatively high S content, the S stays in the agglomerates and may form sulfates with K, Ca, or Na under a combustion atmosphere. Under a steam-gasification atmosphere, the S releases to the gas phase to free up more K or Na to form silicate. These atmospheres imply a more-serious risk of agglomeration.

■ AUTHOR INFORMATION

Corresponding Author
*E-mail: zimeng.he@adelaide.edu.au.
ORCID ●
Zimeng He: 0000-0001-5420-3661
Daniel J. Lane: 0000-0002-8052-4175
Philip J. van Eyk: 0000-0003-3768-2044
Notes
The authors declare no competing financial interest.

■ REFERENCES

(1) Saidur, R.; Abdelaziz, E. A.; Demirbas, A.; Hossain, M. S.; Mekhilef, S. A review on biomass as a fuel for boilers. *Renewable Sustainable Energy Rev.* **2011**, *15*, 2262−2289.
(2) Chen, W.-H.; Peng, J.; Bi, X. T. A state-of-the-art review of biomass torrefaction, densification and applications. *Renewable Sustainable Energy Rev.* **2015**, *44*, 847−866.

(3) Demirbas, A. Combustion characteristics of different biomass fuels. *Prog. Energy Combust. Sci.* **2004**, *30*, 219−230.

(4) Ahmad, A. A.; Zawawi, N. A.; Kasim, F. H.; Inayat, A.; Khasri, A. Assessing the gasification performance of biomass: A review on biomass gasification process conditions, optimization and economic evaluation. *Renewable Sustainable Energy Rev.* **2016**, *53*, 1333−1347.

(5) Warnecke, R. Gasification of biomass: comparison of fixed bed and fluidized bed gasifier. *Biomass Bioenergy* **2000**, *18*, 489−497.

(6) Khan, A. A.; de Jong, W.; Jansens, P. J.; Spliethoff, H. Biomass combustion in fluidized bed boilers: Potential problems and remedies. *Fuel Process. Technol.* **2009**, *90*, 21−50.

(7) Werther, J.; Saenger, M.; Hartge, E. U.; Ogada, T.; Siagi, Z. Combustion of agricultural residues. *Prog. Energy Combust. Sci.* **2000**, *26*, 1−27.

(8) Bartels, M.; Lin, W.; Nijenhuis, J.; Kapteijn, F.; van Ommen, J. R. Agglomeration in fluidized beds at high temperatures: Mechanisms, detection and prevention. *Prog. Energy Combust. Sci.* **2008**, *34*, 633−666.

(9) Hamawand, I.; Sandell, G.; Pittaway, P.; Chakrabarty, S.; Yusaf, T.; Chen, G.; Seneweera, S.; Al-Lwayzy, S.; Bennett, J.; Hopf, J. Bioenergy from Cotton Industry Wastes: A review and potential. *Renewable Sustainable Energy Rev.* **2016**, *66*, 435−448.

(10) Lin, W.; Dam-Johansen, K.; Frandsen, F. Agglomeration in bio-fuel fired fluidized bed combustors. *Chem. Eng. J.* **2003**, *96*, 171−185.

(11) Chaivatamaset, P.; Tia, S. The characteristics of bed agglomeration during fluidized bed combustion of eucalyptus bark. *Appl. Therm. Eng.* **2015**, *75*, 1134−1146.

(12) Chaivatamaset, P.; Sricharoon, P.; Tia, S.; Bilitewski, B. The characteristics of bed agglomeration/defluidization in fluidized bed firing palm fruit bunch and rice straw. *Appl. Therm. Eng.* **2014**, *70*, 737−747.

(13) Öhman, M.; Nordin, A.; Skrifvars, B.-J.; Backman, R.; Hupa, M. Bed Agglomeration Characteristics during Fluidized Bed Combustion of Biomass Fuels. *Energy Fuels* **2000**, *14*, 169−178.

(14) Grimm, A.; Skoglund, N.; Boström, D.; Öhman, M. Bed Agglomeration Characteristics in Fluidized Quartz Bed Combustion of Phosphorus-Rich Biomass Fuels. *Energy Fuels* **2011**, *25*, 937−947.

(15) Brus, E.; Öhman, M.; Nordin, A. Mechanisms of Bed Agglomeration during Fluidized-Bed Combustion of Biomass Fuels. *Energy Fuels* **2005**, *19*, 825−832.

(16) Kaknics, J.; Michel, R.; Richard, A.; Poirier, J. High-Temperature Interactions between Molten Miscanthus Ashes and Bed Materials in a Fluidized-Bed Gasifier. *Energy Fuels* **2015**, *29*, 1785−1792.

(17) Kaknics, J.; Michel, R.; Poirier, J. Miscanthus ash transformation and interaction with bed materials at high temperature. *Fuel Process. Technol.* **2016**, *141*, 178−184.

(18) Lane, D. J.; Zevenhoven, M.; Ashman, P. J.; van Eyk, P. J.; Hupa, M.; de Nys, R.; Lewis, D. M. Algal Biomass: Occurrence of the Main Inorganic Elements and Simulation of Ash Interactions with Bed Material. *Energy Fuels* **2014**, *28*, 4622−4632.

(19) Ergudenler, A.; Ghaly, A. E. Agglomeration of silica sand in a fluidized bed gasifier operating on wheat straw. *Biomass Bioenergy* **1993**, *4*, 135−147.

(20) Khadilkar, A. B.; Rozelle, P. L.; Pisupati, S. V. Review of Particle Physics and Chemistry in Fluidized Beds for Development of Comprehensive Ash Agglomeration Prediction Models. *Energy Fuels* **2016**, *30*, 3714−3734.

(21) Kuba, M.; He, H.; Kirnbauer, F.; Skoglund, N.; Boström, D.; Öhman, M.; Hofbauer, H. Mechanism of Layer Formation on Olivine Bed Particles in Industrial-Scale Dual Fluid Bed Gasification of Wood. *Energy Fuels* **2016**, *30*, 7410−7418.

(22) He, H.; Boström, D.; Öhman, M. Time Dependence of Bed Particle Layer Formation in Fluidized Quartz Bed Combustion of Wood-Derived Fuels. *Energy Fuels* **2014**, *28*, 3841−3848.

(23) Bläsing, M.; Müller, M. Mass spectrometric investigations on the release of inorganic species during gasification and combustion of German hard coals. *Combust. Flame* **2010**, *157*, 1374−1381.

(24) Song, G.; Song, W.; Qi, X.; Lu, Q. Transformation Characteristics of Sodium of Zhundong Coal Combustion/Gas-ification in Circulating Fluidized Bed. *Energy Fuels* **2016**, *30*, 3473−3478.

(25) Kosminski, A.; Ross, D. P.; Agnew, J. B. Influence of gas environment on reactions between sodium and silicon minerals during gasification of low-rank coal. *Fuel Process. Technol.* **2006**, *87*, 953−962.

(26) Kosminski, A.; Ross, D. P.; Agnew, J. B. Reactions between sodium and silica during gasification of a low-rank coal. *Fuel Process. Technol.* **2006**, *87*, 1037−1049.

(27) Öhman, M.; Pommer, L.; Nordin, A. Bed Agglomeration Characteristics and Mechanisms during Gasification and Combustion of Biomass Fuels. *Energy Fuels* **2005**, *19*, 1742−1748.

(28) Ma, T.; Fan, C.; Hao, L.; Li, S.; Song, W.; Lin, W. Biomass-Ash-Induced Agglomeration in a Fluidized Bed. Part 1: Experimental Study on the Effects of a Gas Atmosphere. *Energy Fuels* **2016**, *30*, 6395−6404.

(29) Boström, D.; Skoglund, N.; Grimm, A.; Boman, C.; Öhman, M.; Broström, M.; Backman, R. Ash Transformation Chemistry during Combustion of Biomass. *Energy Fuels* **2012**, *26*, 85−93.

(30) Boström, D.; Eriksson, G.; Boman, C.; Öhman, M. Ash Transformations in Fluidized-bed Combustion of Rapeseed Meal. *Energy Fuels* **2009**, *23*, 2700−2706.

(31) Knudsen, J. N.; Jensen, P. A.; Dam-Johansen, K. Transformation and Release to the Gas Phase of Cl, K, and S during Combustion of Annual Biomass. *Energy Fuels* **2004**, *18*, 1385−1399.

(32) Grimm, A.; Öhman, M.; Lindberg, T.; Fredriksson, A.; Boström, D. Bed Agglomeration Characteristics in Fluidized-Bed Combustion of Biomass Fuels Using Olivine as Bed Material. *Energy Fuels* **2012**, *26*, 4550−4559.

(33) Scala, F.; Chirone, R. An SEM/EDX study of bed agglomerates formed during fluidized bed combustion of three biomass fuels. *Biomass Bioenergy* **2008**, *32*, 252−266.

(34) Sevonius, C.; Yrjas, P.; Hupa, M. Defluidization of a quartz bed − Laboratory experiments with potassium salts. *Fuel* **2014**, *127*, 161−168.

(35) Narayan, V.; Jensen, P. A.; Henriksen, U. B.; Glarborg, P.; Lin, W.; Nielsen, R. G. Defluidization in fluidized bed gasifiers using high-alkali content fuels. *Biomass Bioenergy* **2016**, *91*, 160−174.

(36) Piotrowska, P.; Zevenhoven, M.; Davidsson, K.; Hupa, M.; Åmand, L.-E.; Barišić, V.; Coda Zabetta, E. Fate of Alkali Metals and Phosphorus of Rapeseed Cake in Circulating Fluidized Bed Boiler Part 1: Cocombustion with Wood. *Energy Fuels* **2010**, *24*, 333−345.

(37) Piotrowska, P.; Grimm, A.; Skoglund, N.; Boman, C.; Öhman, M.; Zevenhoven, M.; Boström, D.; Hupa, M. Fluidized-Bed Combustion of Mixtures of Rapeseed Cake and Bark: The Resulting Bed Agglomeration Characteristics. *Energy Fuels* **2012**, *26*, 2028−2037.

(38) Zevenhoven, M.; Yrjas, P.; Skrifvars, B.-J.; Hupa, M. Characterization of Ash-Forming Matter in Various Solid Fuels by Selective Leaching and Its Implications for Fluidized-Bed Combustion. *Energy Fuels* **2012**, *26*, 6366−6386.

(39) Johansen, J. M.; Jakobsen, J. G.; Frandsen, F. J.; Glarborg, P. Release of K, Cl, and S during Pyrolysis and Combustion of High-Chlorine Biomass. *Energy Fuels* **2011**, *25*, 4961−4971.

(40) van Lith, S. C.; Jensen, P. A.; Frandsen, F. J.; Glarborg, P. Release to the Gas Phase of Inorganic Elements during Wood Combustion. Part 2: Influence of Fuel Composition. *Energy Fuels* **2008**, *22*, 1598−1609.

(41) Song, B. H.; Kim, S. D. Catalytic activity of alkali and iron salt mixtures for steam-char gasification. *Fuel* **1993**, *72*, 797−803.

(42) Hüttinger, K. J.; Minges, R. Catalytic water vapour gasification of carbon. *Fuel* **1985**, *64*, 491−494.

Chapter 6

Paper IV

The ash-quartz sand interaction behaviours during steam gasification or combustion of a freshwater and a marine species of macroalgae

Zimeng He *[, a, b], Woei L. Saw [a, b], Daniel J. Lane [a, b], Philip J. van Eyk [a, b], Rocky de Nys [d], Graham J. Nathan [b, c], Peter J. Ashman [a, b]

[a] School of Chemical Engineering and Advanced Materials, The University of Adelaide, Adelaide, South Australia 5005, Australia
[b] Centre for Energy Technology, The University of Adelaide, Adelaide, South Australia 5005, Australia
[c] School of Mechanical Engineering, The University of Adelaide, Adelaide, South Australia 5005, Australia
[d] MACRO - Centre for Macroalgal Resources & Biotechnology, College of Science and Engineering, James Cook University, Townsville, Queensland, Australia

A link to this publication

https://doi.org/10.1016/j.fuel.2019.116621

Statement of Authorship

Title of Paper	The ash-bed material interaction behaviour during the steam gasification or combustion of a freshwater and a marine species of macroalgae
Publication Status	☐ Published ☐ Accepted for Publication ☑ Submitted for Publication ☐ Unpublished and Unsubmitted work written in manuscript style
Publication Details	A revised manuscript was resubmitted ~~to~~ to the journal of Fuel for review

Principal Author

Name of Principal Author (Candidate)	Zimeng He
Contribution to the Paper	Performed analysis on all samples, interpreted data, wrote manuscript and acted as corresponding author.
Overall percentage (%)	60
Certification:	This paper reports on original research I conducted during the period of my Higher Degree by Research candidature and is not subject to any obligations or contractual agreements with a third party that would constrain its inclusion in this thesis. I am the primary author of this paper.
Signature	Date 22.10.2019

Co-Author Contributions

By signing the Statement of Authorship, each author certifies that:

i.   the candidate's stated contribution to the publication is accurate (as detailed above);

ii. permission is granted for the candidate in include the publication in the thesis; and

iii. the sum of all co-author contributions is equal to 100% less the candidate's stated contribution.

Name of Co-Author	Woei L.Saw
Contribution to the Paper	Supervised development of work, helped in data interpretation, reactor construction and manuscript evaluation and edition
Signature	Date 21/10/2019.

Name of Co-Author	Daniel J. Lane
Contribution to the Paper	Supervised development of work, helped in data interpretation and reactor construction
Signature	Date 15/10/2019

Name of Co-Author	Philip J. van Eyk
Contribution to the Paper	Supervised development of work, helped in data interpretation, and manuscript evaluation
Signature	Date 21/10/2019

Name of Co-Author	Rocky de Nys
Contribution to the Paper	helped in data interpretation and manuscript evaluation and edition
Signature	Date 4Oct 2a9

Name of Co-Author	Graham J. Nathan
Contribution to the Paper	Supervised development of work, helped in data interpretation and manuscript evaluation and edition
Signature	Date 17/10/19.

Name of Co-Author	Peter J. Ashman
Contribution to the Paper	Supervised development of work, helped in data interpretation and manuscript evaluation
Signature	Date 17-10-19

Full Length Article

The ash-quartz sand interaction behaviours during steam gasification or combustion of a freshwater and a marine species of macroalgae

Zimeng He[a,b,*], Woei L. Saw[a,b], Daniel J. Lane[a,b,1], Philip J. van Eyk[a,b], Rocky de Nys[d], Graham J. Nathan[b,c], Peter J. Ashman[a,b]

[a] School of Chemical Engineering and Advanced Materials, The University of Adelaide, Adelaide, South Australia 5005, Australia
[b] Centre for Energy Technology, The University of Adelaide, Adelaide, South Australia 5005, Australia
[c] School of Mechanical Engineering, The University of Adelaide, Adelaide, South Australia 5005, Australia
[d] MACRO - Centre for Macroalgal Resources & Biotechnology, College of Science and Engineering, James Cook University, Townsville, Queensland, Australia

ABSTRACT

The interactions between ash and quartz sand as the bed material were studied for two species of macroalgae, *Oedogonium intermedium* (a freshwater species) and *Derbesia tenuissima* (a marine species). The interaction tests were performed in a lab-scale, fixed-bed reactor under a steam gasification (50% v/v steam) or a combustion (5% v/v O_2) atmosphere at 900 °C for different reaction times (10 min to 6 h). For both macroalgae, some of the Na and K are found to interact with other elements, such as Mg, Si, P, Ca and Fe to form ash particles. For ODN, these low melting-point phosphorus-rich ash particles are present in sufficient quantities to adhere to the quartz sand and form ash agglomerates via a melting-induced mechanism. In addition, some of the Na and K react with Si from the quartz sand to form a coating layer, which promotes a coating-induced mechanism. Both mechanisms contribute to a similar extent for ODN; while the coating-induced mechanism dominates for Deb, which includes the diffusion of some Ca into the coating layer. For Deb, the steam gasification atmosphere significantly affects the size of the agglomerates, the mass fractions of K and Na retained in the agglomerates and the formation of various types of silicates in the agglomerates, when compared with those under the combustion atmosphere. However, the influence of the steam gasification atmosphere on both the morphology and the elemental composition of the ODN agglomerates is less obvious. For Deb, a high content of S is detected for the individual separate ash particles within the agglomerates during combustion, whereas negligible S is found during steam gasification.

1. Introduction

Macroalgae have been proposed as the feedstock for third-generation biofuels because of their high growth rate and productivity and the capacity to be cultivated on non-arable land or in the sea [1,2]. The food industry accounts for 83–90% of the total seaweed industry [1]. However, the utilization of macroalgae as biofuels is quite limited due to the current low cost of fossil fuel. Macroalgae are commonly rich in carbohydrates (3% to 40% dry weight (DW)), which makes them suitable biofuels [1–4]. Macroalgae can be converted by a range of biochemical and thermochemical processes to produce biogas, biocrude, methane, ethanol or hydrogen, which has been the motivation for considerable research on the conversion of macroalgae to energy [4–6]. Thermochemical conversion processes (direct combustion, pyrolysis or gasification) are more efficient and flexible than biochemical conversions (anaerobic digestion, alcoholic fermentation or transesterification) [7–10]. Macroalgae are easier to harvest than microalgae, which reduces the labour cost significantly [2,11]. Nevertheless, compared with microalgae, which have been investigated intensively, macroalgae are still untapped resource for energy [12]. The performance of combustion or gasification of several species of macroalgae has been assessed previously [10,13–16]. The catalytic effect of inorganic metals in macroalgae that is beneficial to gasification processes has been reported [10,17]. However, the ash-related issues of macroalgae have been suggested as the major obstacles in the literature, which limit the utilization of macroalgae as a feedstock for combustion or gasification [14].

The ash-forming elements of macroalgae have many differences

---

from those of terrestrial biomass, which can have considerable impacts on combustion or gasification process. The ash content for algae is in the range of 13.1–42.8% (with a mean of 26.6%), while for terrestrial biomass it is in the range of 0.1–46.3% (with a mean of 6.8%) [17]. The content of several major ash-forming elements, including K, Na, Ca, Mg, Si, Cl, P and S, is generally high in macroalgae [2,17]. The ash, alkali metal (K and Na) and halogens contents in macroalgae are usually higher than those in terrestrial biomass and sulfates (K_2SO_4) or chlorides (KCl or NaCl) are commonly present in macroalgae, when compared with terrestrial biomass [17]. These are the most technological and environmental challenges and are not practical for the utilization of macroalgae as feedstock for combustion or gasification process [1,2,4,12,17,18]. Nevertheless, the high content of Ca and Mg in macroalgae is an advantage for combustion or gasification process. Therefore, the ash-forming elemental composition of macroalgae can easily lead to ash-related issues of slagging, fouling and agglomeration during combustion or gasification process [19]. A clear understanding of the ash-related problems associated with the combustion or gasification process of macroalgae is therefore necessary.

Combustion or gasification of macroalgae in fluidized bed reactors to produce bio-products is beneficial because fluidized bed reactors can easily adapt to various types of feedstock [20,21]. However, agglomeration is a challenging ash-related issue in fluidized bed reactors during combustion or gasification process if macroalgae are considered as feedstock [17]. The agglomeration behaviour of macroalgae can be different from that of terrestrial biomass due to the difference in ash-forming elemental composition. The agglomeration behaviour of terrestrial biomass has been investigated extensively [22–35]. The agglomeration behaviour for terrestrial biomass with a high K and a low Si content, tends to be coating-induced and to result from the reaction of K and Si from the bed material [32]. This may be followed by the diffusion of Ca into the coating layer [32]. Zevenhoven-Onderwater et al. [35] have found that for wood-derived fuels, K, Ca and Si react to form the coating layer with up to 50% of K and 8–30% of Ca introduced from the fuels having participated in the layer's formation. Several layers are usually formed on the bed material, typically with an inner layer consisting of K, Ca and Si or Ca and Si and an outer layer having similar composition as the fuel ash [29]. For terrestrial biomass with a high K and Si/P content, the bed materials are likely to adhere to the partially molten, fuel-derived alkali silicates/phosphates ash to form agglomerates through a melting-induced mechanism [27,32]. The co-existence of a coating-induced (formation of K-Ca silicates) and a melting-induced (formation of alkali phosphates ash) mechanism has been found by Piotrowska et al. [28] when bark with a low P content was co-combusted with rapeseed cake rich in P. A possible pathway to form agglomerates is the collision between the bed materials with the high-temperature burning char particles which could be partially molten on the surface [22]. The bed material then be adhered together to form large particles [22]. Scala et al. [33] have concluded that the ash particles, which originate from the burning fuel particles, can be deposited onto and gradually embedded into the coating layer on the bed material. Then K and Na from the ash particles diffuse into the coating layer [33]. However, the agglomeration behaviour for algae has received much less attention than that for coal and terrestrial biomass [7,36–39]. More work is required for a clear understanding of the agglomeration behaviour of algal ash due to the complicated composition of ash-forming elements present within the ash resulting from the wide range of different compositions for different algae species.

Both ash chemistry (ash-bed material interactions) and particle physics in fluidized bed reactors affect the agglomeration [40]. Bed temperature does not affect the ash chemistry of agglomeration significantly, while it has a critical impact on the physical properties of bed particles, such as the melting behaviour of the coating layer [41]. The effects of fluidizing gas velocity, bed particle size, fluidizing gas velocity, static bed height and gas distribution uniformity in fluidized bed reactors on agglomeration have been evaluated [42]. The

agglomeration mechanisms tested in lab-scale or pilot-scale reactors are normally consistent with the initial stage of agglomeration in full-scale reactors [42]. The influence of particle physics in fluidized bed reactors on agglomeration can be studied by modelling work [40]. The macroalgae ash-quartz sand (the bed material) interaction behaviours in the present work was evaluated in a lab-scale, fixed-bed reactor independently by separating the possible influence of particle physics in fluidized bed reactors. This contributes to a better understanding of the impacts of both the ash-quartz sand interactions and particle physics in fluidized bed reactors on agglomeration.

The investigation of the time-dependent biomass ash-bed material interaction behaviours or layer formation contributes to a better understanding of agglomeration. The layer formation process for different bed materials including quartz sand, olivine, ilmenite, manganese ore, Na-Feldspar and K-Feldspar has been assessed with terrestrial biomass as the feedstock [30,31,34,43–48]. The agglomeration tendency of quartz sand is significantly higher than that of olivine and K-feldspar with woody biomass as the feedstock in a dual fluidized bed gasifier [49]. The thermodynamic equilibrium modelling results have also showed that the driving force for K to be retained by olivine is much lower than that of quartz sand with woody biomass as the feedstock in a dual fluidized bed gasifier [50]. Both the experimental and the thermodynamic equilibrium modelling work in terms of the time-dependent layer formation in fluidized bed combustion of wood-derived fuels have been conducted by He et al. [31,34]. They have proposed that at an initial stage of agglomeration, only one layer is formed by reactions between K and the quartz sand. The Ca-rich ash particles then attach onto the coating layer to form the outer coating layer and Ca gradually diffuses into the inner coating layer. The K/Ca ratio decreases while the Ca/Si ratio increases in the inner layer. The change of these ratios and the growth rate of the coating layer decrease over time when an inner layer dominated by Ca-silicates have been formed. This layer protects the quartz sand from further reacting with K. The layer formation rate is affected by both the chemical reaction and the Ca diffusion at the initial stage. When the Ca content is high in the inner layer, the layer growth rate is diffusion controlled and becomes much slower at a later stage. The agglomeration behaviour of the two macroalgae used in the present paper has been studied previously [7,38,39]. However, the information on the time-dependent layer formation of macroalgae is not available. Therefore, this paper aims to provide this understanding for the two selected macroalgae.

The influence of the reaction atmosphere on the agglomeration behaviour should also be assessed for macroalgae since this is known to be critical for coal and terrestrial biomass [26,51–60]. For the cases of coal, Kosminski et al. [55,56] have concluded that steam lowers the melting point of sodium carbonate, causing the reaction of liquid sodium carbonate with silica to generate more liquid sodium silicate, when compared with that under either a CO_2 or N_2 atmosphere. This, in turn, has a potential to lead to more serious agglomeration. Manzoori et al. [57] and van Eyk et al. [59] have identified that, for low-rank coals with a high Na and S content under a combustion atmosphere, that agglomeration is formed by the deposition of an ash-derived, low melting-point Na sulfate eutectic onto the bed material. This is a physical process without any chemical reaction. In contrast, McCullough et al. [58] have reported that for a similar low-rank coal during steam/air gasification, the coating layer is formed by the reaction between sodium and silica. For the cases of terrestrial biomass, He et al. [51] have showed that steam augments the ash-bed material interactions for grape marc more strongly than for wheat straw and cotton stalk. However, no similar investigations have yet been performed for macroalgae as the feedstock, generating a need to understand the difference in the agglomeration behaviour between steam gasification and combustion atmospheres. The agglomeration behaviour of the two macroalgae utilized in the present paper under a combustion atmosphere has been investigated by Lane et al. [38]. The agglomeration behaviour of the two macroalgae during co-gasification with wood or coal have been

studied by Zhu et al. [7,39]. Nevertheless, no work has been done to evaluate the impact of the reaction atmosphere (steam gasification vs combustion) on the agglomeration behaviour of the two selected macroalgae and the present paper aims to meet this need.

To address these gaps in understanding, the present paper aims to evaluate the ash-quartz sand interaction behaviour for two species of macroalgae by investigating the time-dependent layer formation process. We further aim to compare the macroalgae ash-quartz sand interaction behaviour under both the steam gasification and combustion atmospheres for the two species of macroalgae.

2. Experimental methods

2.1. Feedstock and bed material

Two species of macroalgae, a freshwater species, *Oedogonium intermedium* (denoted as ODN) and a marine species, *Derbesia tenuissima* (denoted as Deb) were selected as the feedstock in the present study. Compared with other species of freshwater macroalgae, ODN is a competitive and the most widely investigated species, which has a high productivity, a low ash content and a wide distribution under various environments [61–64]. Usually, in many respects, ODN is a model for the broader development of freshwater macroalgae as a resource for the bioremediation of waste waters [62,63,65]. The ODN cultivated in waste waters can then be used to produce bio-products including bio-fuels during thermochemical processes [3]. The growth of Deb is adapted to a wide range of temperature [66]. Deb can be cultivated in marine waters and is specifically targeted for cultivation in water released from land-based aquaculture [67]. The growth rate and productivity of Deb are high and it also has a high bioenergy potential (a higher heating value of 20.5 MJ/kg) [7,66]. In contrast to most macroalgae, Deb has a unique biochemical profile as it has a comparatively high lipid content of up to 12% DW [66–68]. In addition, Deb has a relatively consistent biochemical profile across cultivation conditions, which is important for commercialization [66–68]. Therefore, Deb has the potential to be a valuable source for bio-oil production as the costs for harvest and drying are lower than those of microalgae [67]. The residues of Deb left after the production of biodiesel or bioethanol can still be utilized as feedstock for thermochemical conversions such as combustion or gasification [12]. As the investment of labour and equipment for macroalgae cultivation and conversion is high, it is not economically practicable to explore macroalgae only for energy [3,12,18]. The biorefinery process, where high-value products are extracted and the resultant biomass is used as a bioenergy resource, can provide an option for the production of bioenergy. Both ODN and Deb have been considered as the bioresource for the biorefinery concept.

Both species have been investigated for their bioenergy potential and cultivation and harvesting methods for each species have been discussed elsewhere [7,38,62,63,69]. For the present work they were cultivated with no limiting nutrients including nitrogen [7,38]. The two macroalgae were dried and ground with a centrifugal knife mill and sieved to the particle size range of 200–500 μm. The proximate analysis was performed with a thermogravimetric analyser (TGA) in an alumina crucible. The methods for the proximate analysis and the ash-forming elements (K, Ca, Na, Mg, Al, Fe, S, P, Cl and Si) composition analysis can be found elsewhere [51]. The ultimate analysis was conducted using a LECO CHNS analyser.

The proximate and the ultimate analyses of the two macroalgae are presented in Table 1. The two macroalgae have a similar volatile matter and fixed carbon content, while Deb has a much higher ash content than does ODN. Deb also has a six-fold higher S content than does ODN. The volatile matter content is much higher while the ash content is much lower for the two macroalgae than the mean values of different species [17]. The fixed carbon, C, H, O and N content of the two macroalgae is close to the mean values of different species [17]. The S content of the two macroalgae is lower than the mean value of different

Table 1
Proximate and ultimate analyses of the two macroalgae.

	ODN	Deb	Mean values of different species [17]
Moisture, %	7.8	8.3	
Proximate analysis (wt.% db^a)			
Volatile matter	72.6	69.5	52.4
Fixed carbon	19.6	18.4	21.0
Ash	7.8	12.1	26.6
Ultimate analysis (wt.% db^a)			
C	44.0	44.4	45.1
H	7.2	7.6	7.3
N	4.4	6.2	5.6
S	0.17	1.1	1.6
O, by difference	44.2	40.7	40.4
db = dry basis			

Table 2
Composition of ash-forming elementals in the two macroalgae.

Element	ODN (g/kg of dry fuel)	Deb (g/kg of dry fuel)	Mean values of different species (g/kg of dry fuel) [17]
K	14.7	7.0	36.6
Ca	2.4	17.1	12.4
Na	7.6	13.8	35.1
Mg	3.5	4.6	7.2
Al	0.21	0.25	1.25
Fe	1.7	1.6	1.57
P	6.6	4.3	8.2
Cl	3.4	15.2	31.1
Si	3.7	4.8	23.0
K + Na	22.3	20.8	

species, especially for ODN [17]. Table 2 presents the ash-forming elemental composition of the two macroalgae. It can be seen that ODN has a higher K content while Deb has a higher Na content. However, the total content of alkali metals (K + Na) is quite similar for the two macroalgae. Another difference is that Deb has a high Ca and Cl content, while ODN has a high P content. The contents of K, Na, Mg, Al, Cl and Si of the two macroalgae is much lower than the mean values of different species [17]. The low contents of K, Na, Cl and Si of the two macroalgae is an advantage for the gasification or combustion process. The Ca content of ODN is much lower while it of Deb is much higher than the mean value of different species [17]. A high Ca content is beneficial to the gasification or combustion process, which suggests that Deb may have less ash-related issues than ODN [17]. The P content of the two macroalgae is a bit lower than the mean value of different species, which is also beneficial to the gasification or combustion process [17]. The elemental composition of the quartz sand that was used as the bed material is reported elsewhere [51]. This comes from the Coonarr Creek mine in Bundaberg, Australia, and was used with a particle size range of 75–212 μm.

2.2. Ash-quartz sand interaction test and ash/char preparation test

All the tests were carried out in a lab-scale, fixed-bed reactor shown in Fig. 1, as described previously by He et al. [51]. Approximately 1 g feedstock was mixed uniformly with quartz sand at a mass ratio of 3:1 (feedstock:quartz-sand) in an alumina crucible for each ash-quartz sand interaction test. The ash-quartz sand interaction test was conducted at 900 °C for a range of reaction times, namely 10 min, 30 min, 1 h and 6 h under either a steam gasification or a combustion atmosphere using steam/N_2 (50% v/v steam) or air/N_2 (5% v/v O_2) mixtures, respectively. The reaction time for each interaction test was started when the crucible was inserted into the reactor and was ended when the crucible was retracted from the reactor, with an insertion probe. The procedure of the ash-quartz sand tests has been described previously [51]. The
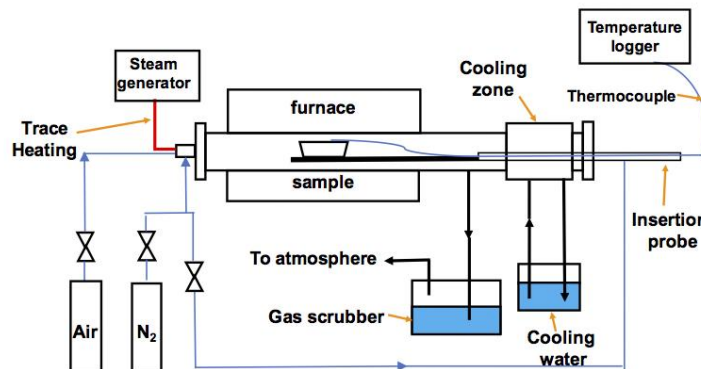
3

Fig. 1. Schematic diagram of the lab-scale, fixed-bed reactor employed for the ash-quartz sand interaction tests and the ash/char preparation tests.

char/ash preparation test (without quartz sand) was performed at 900 °C for reaction times of 5 min and 30 min under either a steam gasification or a combustion atmosphere following the same procedure as for the ash-quartz sand interaction test. Samples from the above tests were further analysed using a range of techniques as described in Sections 2.3 and 2.4.

2.3. SEM/EDS and XRD analyses

The morphology and the elemental compositions of the samples from the ash-quartz sand interaction tests were analysed with a scanning electron microscopy (Philips model XL30) in combination with energy dispersive spectroscopy (SEM-EDS) at both the surface and the cross-sections. Each sample was either loaded on a carbon tape for the surface analysis, or mounted into a resin and then polished for the cross-sectional analysis. Following this, the samples were carbon coated to reduce charging. The SEM/EDS instrument was operated under a backscattering electron mode (BSE). For each sample, several areas were identified, from which several spots in each were selected for analysis. The elemental composition present in this study is the average of all the selected spots for each sample. The samples from the 30 min ash preparation tests were also analysed at the surface with SEM/EDS for the elemental composition employing the same procedure as described above. The crystalline phase for selected samples from both tests were analysed using an X-ray diffraction (XRD) measurement (Rigaku MiniFlex 600), with the Cu Kα radiation applied.

2.4. Elemental analysis of K and Na in the agglomerates

The 30 min agglomerates obtained under the steam gasification or the combustion atmosphere for both macroalgae were digested with high concentration nitric acid (70%) and hydrofluoric acid (48%) for a week at 140 °C. Each sample was then diluted with 0.1 M HCl and analysed with a Schimadzu Atomic Absorption Spectrophotometer (AAS, AA-6300) for the elemental compositions of K and Na.

Three individual samples prepared separately from the 30 min interaction test under the steam gasification or combustion atmosphere for the two macroalgae were leached with both cold water (15–25 °C) and hot water (90–100 °C) to determine the mass fractions of K and Na retained in the silicates. Alkali silicates that can be dissolved in cold water (15–25 °C), have a lower silica content, while those that can be dissolved in hot water (90–100 °C, nearly boiling water) have a higher silica content [56]. A silicate with a silica to alkali ratio less than 2 is soluble in cold and hot water, while one with a ratio greater than 2.5 is generally considered insoluble even in boiling water [70,71]. Cold water and hot water leaching tests were conducted by stirring for 4 h. The cold and hot water leachates were diluted with 0.1 M HCl and further analysed with AAS for the concentration of K and Na. The elemental content of K and Na in the cold/hot water leaching fractions is the average value of the three repeated tests.
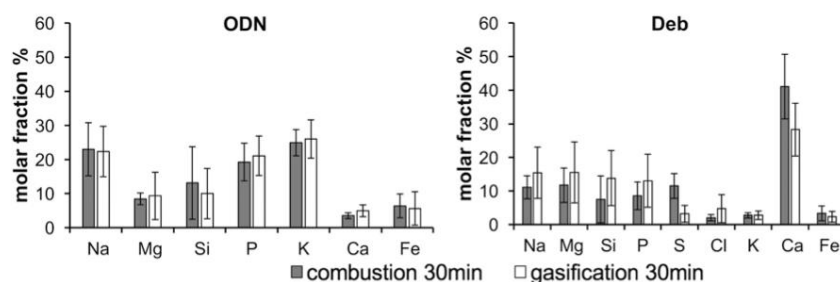

Fig. 2. Elemental composition on a C-and O-free basis of the ash formed under the steam gasification or combustion atmosphere with a reaction time of 30 min at 900 °C for ODN and Deb.

Table 3
Crystalline phase of the samples from the ash/char preparation tests identified using XRD.

	Reaction time	Steam gasification/combustion atmosphere
ODN	5 min	Na_3PO_4, KCl, CaO
	30 min	Na_3PO_4, Fe_3O_4, CaO
DEB	5 min	CaS, CaO, KCl, NaCl
	30 min	$Ca_5(PO_4)_3(OH)$, CaO, MgO, Ca_2SiO_4, $CaMgSiO_4$, Fe_2O_3, $Ca_2Mg(Si_2O_7)$

3. Results

3.1. Ash particles prepared during steam gasification or combustion

Fig. 2 presents the elemental composition for the ash particles prepared at 900 °C under both the steam gasification and combustion atmospheres for 30 min. This shows that the elemental composition for the ash of the two macroalgae is similar under both atmospheres, specifically for the ash of ODN, which is dominated by Na, Mg, Si, P and K, with small amounts of Ca and Fe. The Deb ash particles under both atmospheres consist mostly of Na, Mg, Si, P, S and Ca, with small amounts of Cl, K and Fe. The Deb ash has a much higher content of Ca and S than does the ODN ash, consistent with the high Ca and S content of raw Deb. The ODN ash has a much higher K content than does the Deb ash under both atmospheres.

Table 3 presents the crystalline phase of the samples from the char/ash preparation tests of the two macroalgae as identified with XRD under both the steam gasification and combustion atmospheres. The crystalline phase identified from the char/ash particles for the two macroalgae is the same for both atmospheres. The crystalline phases of the ODN sample comprise Na_3PO_4 and CaO for both the 5 min and the 30 min reaction times. In addition, KCl is found for the 5 min case, while Fe_3O_4 is found for the 30 min case. This implies that Na is mostly present as phosphate with P, while K is mostly found as KCl in the 5 min ODN sample, but is released when the reaction time is increased to 30 min. For the Deb sample, CaO is detected for both reaction times, together with CaS, KCl and NaCl for the 5 min case. For the 30 min Deb sample, $Ca_5(PO_4)_3(OH)$, MgO, Ca_2SiO_4, $CaMgSiO_4$, Fe_2O_3 and $Ca_2Mg(Si_2O_7)$ are also detected. Similar phases of Ca phosphates, Ca silicates and Ca-Mg silicates have been identified when 10 wt% Deb was gasified with wood in a fluidized bed reactor [7]. Hence, Ca in Deb tends to form Ca phosphates or Ca silicates during thermochemical conversions. As Deb has a high Cl content, so that both K and Na are presented as chlorides in the 5 min Deb sample but have been released when the reaction time is increased to 30 min.

3.2. Morphology of the agglomerates

3.2.1. Morphology of the agglomerates under the combustion atmosphere
Figs. 3 and 4 present the morphology of the agglomerates based on the surface and the cross-sectional views for the ODN and Deb samples, respectively, for a series of reaction times (10 min, 30 min, 1 h and 6 h) under the combustion atmosphere at 900 °C. For the 10 min agglomerates of ODN, as seen from Fig. 3(A) and 3(E), the size of most agglomerates is approximately less than 5 mm. The coating layer of the agglomerates is relatively thin, or even non-existent. However, the size of the agglomerates is increased progressively to several millimetres or even larger than 1 cm as the reaction time is increased to 30 min, 1 h and 6 h. For the 1 h and 6 h reaction times, the sand particles have adhered together to form one large agglomerate. The size of some of the agglomerates can reach to several centimetres (commonly less than 4 cm). Large quantity of partially molten coating layer adheres the bed particles together to form the agglomerates for the reaction times of 30 min, 1 h and 6 h. Separate individual ash particles are distributed within the agglomerates, while some of these ash particles have already

been deposited onto or embedded into the surface of the coating layer for different reaction times, as observed from the enlarged images from the SEM surface analysis (Fig. 3A–D). Ash particles that have already been deposited onto or embedded into the surface of the coating layer are denoted as the "deposited ash", while other separate individual ash particles are denoted as the "residual ash". Two types of coating layer are found within the enlarged images of the agglomerates from the SEM cross-sectional analysis for different reaction times (Fig. 3E–H). The first type of coating layer, is termed the "continuous coating layer" due to its homogenous colour; the second type of coating layer, termed the "discontinuous coating layer", is heterogeneous in colour, with some small lighter particles and some small black holes being distributed within the darker continuous coating layer.

For the Deb agglomerates under the combustion atmosphere, as shown in Fig. 4, the size of the agglomerates is small and the coating layer is much thinner than the equivalent cases of ODN for all the reaction times. No agglomerates are found, and only a few sand particles with the size of approximately 100–200 μm are coated with a relatively thin or even non-existent coating layer for the 10 min reaction time. As the reaction time is increased from 10 min to 6 h, the coating layer is still relatively thin, but the size of most agglomerates reaches to approximately less than 5 mm. As for the case of ODN, the residual ash and deposited ash particles are detected within the Deb agglomerates (Fig. 4A–D). In addition, the continuous coating layer is dominant for the Deb agglomerates (Fig. 4E–H).

3.2.2. Morphology of the agglomerates under the steam gasification atmosphere
Figs. 5 and 6 present the morphology of the agglomerates obtained under the steam gasification atmosphere based on the surface and the cross-sectional views for ODN and Deb samples, respectively, also for a series of reaction times (10 min, 30 min, 1 h and 6 h) at 900 °C. The morphology of these ODN agglomerates (Fig. 5) is similar to those formed under the combustion atmosphere (Fig. 3). In addition, the size of the agglomerates is approximately less than 5 mm and their coating layer is relatively thin for the reaction time of 10 min. However, the size of the agglomerates is increased to several millimetres or even to larger than 1 cm as the reaction time is increased progressively, first to 30 min, and then to 6 h for which many sand particles have adhered together to form large agglomerates. The size of some of the agglomerates can reach to several centimetres (commonly less than 4 cm). Large quantity of partially molten coating layer adheres the bed particles together to form the agglomerates for the reaction times of 30 min, 1 h and 6 h. As for the combustion case, the residual ash and the deposited ash particles were detected within the agglomerates (Fig. 5A–D). More deposited ash can be found within the 6 h agglomerates than for the other reaction times. Similar to the cases with a combustion atmosphere, two types of coating layer, the continuous coating layer and the discontinuous coating layer, are present within the ODN agglomerates under the steam gasification atmosphere (Fig. 5E–H).

Fig. 6 shows that the size of the Deb agglomerates obtained under the steam gasification atmosphere is much larger than the equivalent cases of the combustion tests (Fig. 4) for any given reaction time. For the 10 min reaction time, small agglomerates have already formed with the size of several millimetres, even though the coating layer is relatively thin. The size of the agglomerates is increased to approximately several centimetres (commonly less than 5 cm) as the reaction time is increased. Large quantity of partially molten coating layer is present in the agglomerates. However, these agglomerates are very fragile and may be broken easily in fluidized bed reactors. Therefore, the Deb agglomerates formed in fluidized reactors may not reach the same size in fixed-bed reactors under the steam gasification atmosphere. As for the combustion case, the residual ash and the deposited ash particles are detected within the agglomerates (Fig. 6A–D). Similar to the cases with a combustion atmosphere, both the continuous coating layer and the
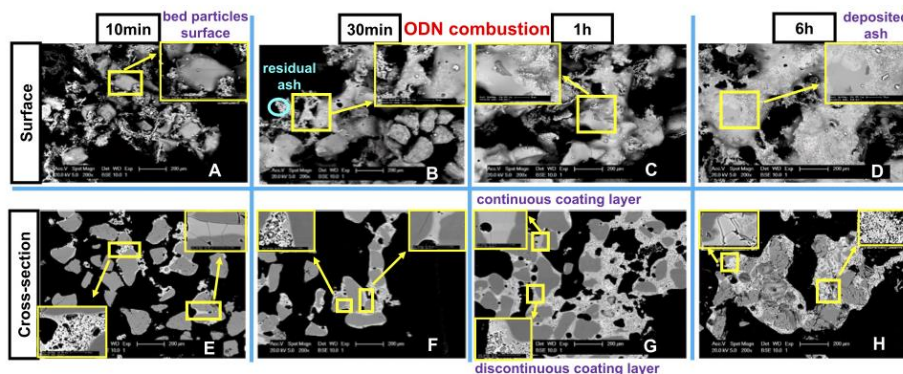
5

Fig. 3. Typical images of the surface (A to D) and cross-sections (E to H) based on the Scanning Electron Microscopy (SEM) analysis for the agglomerates of ODN under the combustion atmosphere at 900 °C for reaction times of 10 min (A and E), 30 min (B and F), 1 h (C and G) and 6 h (D and H).

discontinuous coating layer can be found (Fig. 6E–H). However, the continuous coating layer is dominant.

3.3. Composition of the agglomerates

3.3.1. Composition of the coating layer

Fig. 7 presents the elemental composition of both the surface of bed particles, based on the SEM/EDS surface analysis, and the continuous coating layer, based on the SEM/EDS cross-sectional analysis of the agglomerates for ODN and Deb samples for a series of reaction times under both the steam gasification and combustion atmospheres at 900 °C. The surface of bed particles and the continuous coating layer are taken from the same part of the agglomerates. The continuous coating layer of ODN for most reaction times is rich in Na, Si and K under the two atmospheres, while for the cases of the 1 h and 6 h reaction times the continuous coating layer is dominated by Na, Mg, Si, P and K with small contributions of Ca and Fe. The main elemental composition of the continuous coating layer for Deb is Na, Si, K and Ca with small amounts of Mg and Fe. For the 10 min reaction time, some Cl is also detected under both the two atmospheres for Deb. This indicates that NaCl or KCl are deposited onto the surface of bed particles, releasing Cl to the gas phase and leaving Na or K in the surface of bed particles when

the reaction time is increased. The reaction atmosphere has no significant influence on the elemental composition of the continuous coating layer for either type of the macroalgae.

3.3.2. Composition of the ash particles within the agglomerates

Fig. 8 presents the elemental composition of the residual ash and the deposited ash particles within the agglomerates based on the SEM/EDS surface analysis of the agglomerates for ODN and Deb, for a series of reaction times under both the steam gasification and combustion atmospheres at 900 °C. For ODN, the elemental composition for the two types of ash particles are rich in Na, Mg, Si, P, K, Ca and Fe under the two atmospheres. For Deb, they are dominated by Na, Mg, Si, P and Ca, with small content of Cl, K and Fe for most reaction times under the two atmospheres. The residual ash for ODN also has a high content of S under the combustion atmosphere, however, no S is detected under the steam gasification atmosphere. For Deb, the deposited ash for a 10 min reaction time under the steam gasification atmosphere mostly consists of Na, Si, K, which is different from that for the other reaction times. In contrast, no deposited ash is found for the equivalent case of combustion. This suggests that ash deposited onto the surface of bed particles during steam gasification for Deb is rich in NaCl and KCl, but the Cl then is released to the gas phase to leave the K and Na in the

Fig. 4. Typical images of the surface (A to D) and cross-sections (E to H) based on the Scanning Electron Microscopy (SEM) analysis for the agglomerates of Deb under the combustion atmosphere at 900 °C for reaction times of 10 min (A and E), 30 min (B and F), 1 h (C and G) and 6 h (D and H).
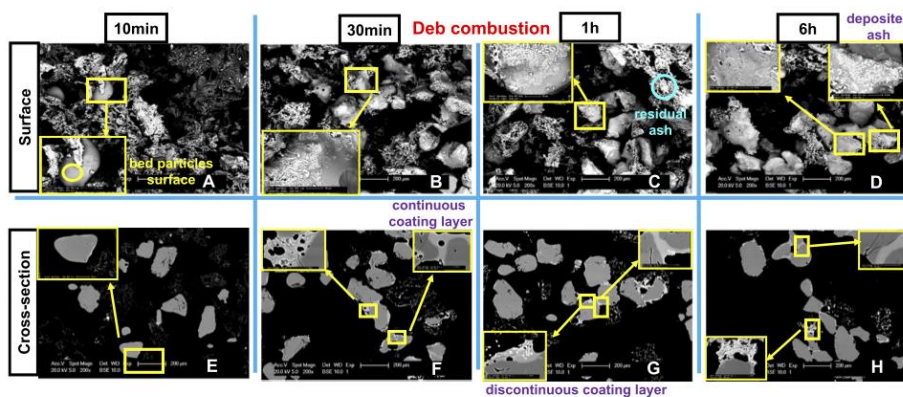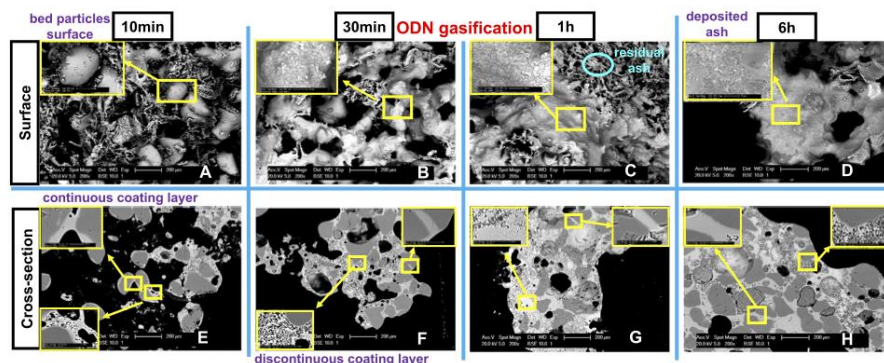
6

Fig. 5. Typical images of the surface (A to D) and cross-sections (E to H) based on the Scanning Electron Microscopy (SEM) analysis for the agglomerates of ODN under the steam gasification atmosphere at 900 °C for reaction times of 10 min (A and E), 30 min (B and F), 1 h (C and G) and 6 h (D and H).

surface of bed particles. This finding is consistent with that from Section 3.3.1.

3.3.3. Composition of the discontinuous coating layer

The discontinuous coating layer based on the SEM/EDS cross-sectional analysis of both ODN and Deb is rich in Na, Mg, Si, P, K and Ca, while ODN also contains a small amount of Fe under both atmospheres, as is shown in Fig. 9. The elemental composition of the discontinuous coating layer for the two macroalgae is similar to that of the residual and the deposited ash, except for the S and Cl content for the Deb case. The formation process of these ash particles is that the individual separate ash particles originated from the fuel are retained within the agglomerates. Then some of these ash particles have been deposited onto or embedded into the surface of the coating layer to form the deposited ash (observed from SEM/EDS surface analysis) and the discontinuous coating layer (observed from SEM/EDS cross-sectional analysis). However, the XRD patterns of the agglomerates for ODN and Deb are all dominated by quartz sand, whose strong peaks mask the identification of other phases.

3.4. Ash-quartz sand interaction behaviour

Both macroalgae used in the present study have a relatively high Si content. However, this is not reactive based on the chemical fractionation analysis because the Si is mostly present in the leached residual fraction, as have been indicated by other studies [38,72]. This implies that the Si in the two macroalgae is unlikely to react with the alkali metals in the macroalgae so that the low melting-point alkali silicates is more likely to be formed by a reaction between the alkali metals and the Si from the quartz sand.

Two interaction behaviour are identified for the case of ODN. In most cases, Bostrom et al. have indicated that K and Na will react with P first before reacting with Si [73]. Therefore, part of the K and Na from the ODN form the individual separate ash particles within the agglomerates by associating with P and then with other elements, such as Mg, Si, Ca and Fe. Some of these partially molten ash particles then adhere to the quartz sand to form the agglomerates, via a melting-induced mechanism (the formation of the discontinuous coating layer). In addition, some other fractions of the K and Na from the ODN react with Si from the quartz sand to form a continuous coating layer, via a coating-induced mechanism. Similar observations have been reported in the study of co-combustion rapeseed cake with bark by Piotrowska
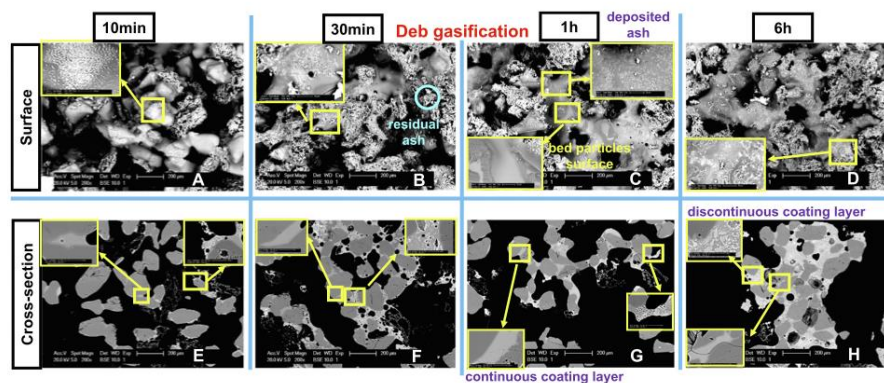

Fig. 6. Typical images of the surface (A to D) and cross-sections (E to H) based on the Scanning Electron Microscopy (SEM) analysis for the agglomerates of Deb under the steam gasification atmosphere at 900 °C for reaction times of 10 min (A and E), 30 min (B and F), 1 h (C and G) and 6 h (D and H).

7

Fig. 7. Elemental composition of some major ash-forming elements on a C-and O-free basis for the surface of bed particles based on the SEM/EDS surface analysis and for the continuous coating layer based on the SEM/EDS cross-sectional analysis of the ODN and Deb agglomerates for different reaction times (10 min, 30 min, 1 h and 6 h) under the steam gasification or combustion atmosphere at 900 °C.

Fig. 8. Elemental composition of some major ash-forming elements on a C-and O-free basis for the residual ash particles and for the deposited ash particles within the ODN and Deb agglomerates based on the SEM/EDS surface analysis for different reaction times (10 min, 30 min, 1 h and 6 h) under the steam gasification or combustion atmosphere at 900 °C.
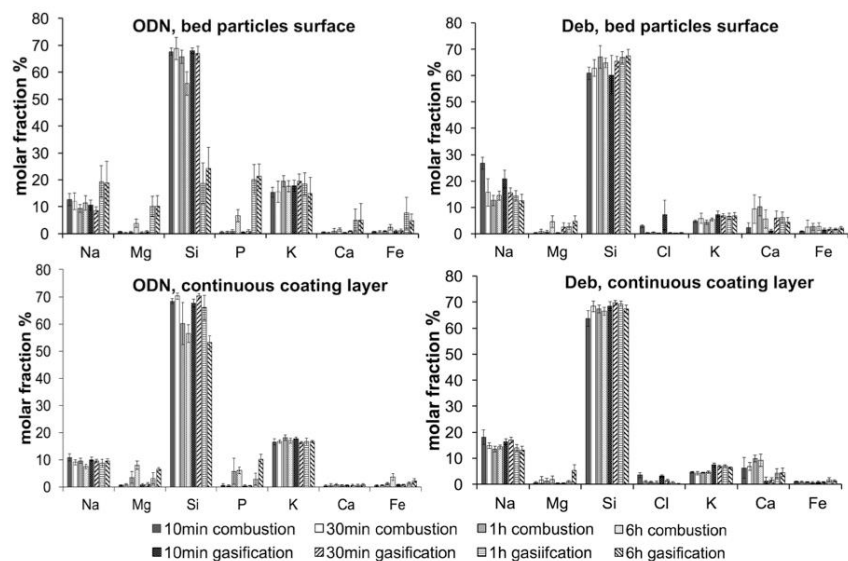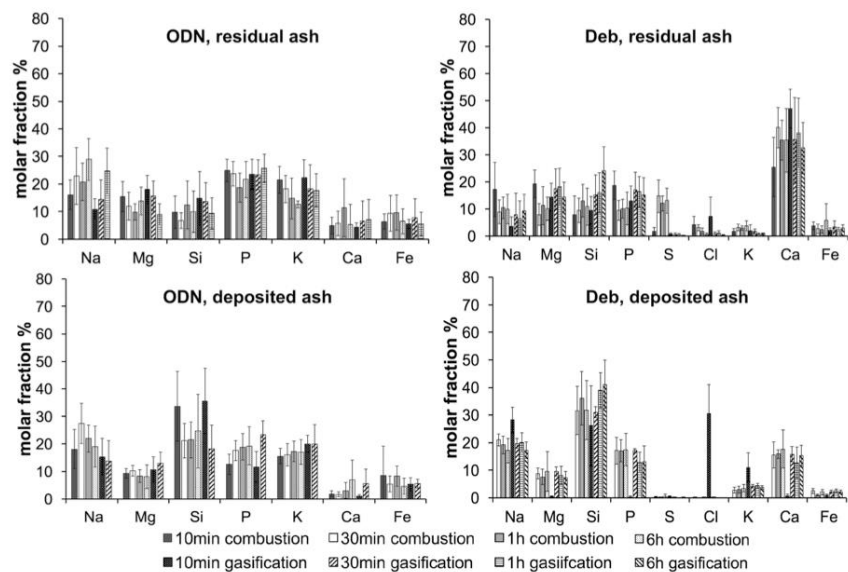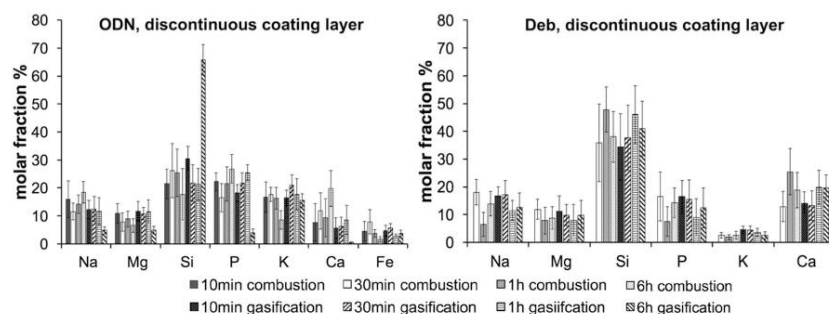
8

Fig. 9. Elemental composition of some major ash-forming elements on a C-and O-free basis for the discontinuous coating layer based on the SEM/EDS cross-sectional analysis for different reaction times (10 min, 30 min, 1 h and 6 h) under the steam gasification or combustion atmosphere at 900 °C.

et al. [28]. They have identified that both the melting-induced mechanism for the phosphate ash and the coating-induced mechanism for the reaction of K with the Si from the sand occur conjunctionly [28]. The study of Grimm et al. have reported that the fraction of K that reacts with Si from the bed material is decreased by adding P additives or P-rich biomass fuel to wood during combustion [27]. Furthermore, Piotrowaska et al. have found that when the P content in the fuel is high enough, the agglomeration mechanism is switched from a coating-induced mechanism to another mechanism, in which the bed material adheres to the partially molten phosphate-rich ash to form the agglomerates [28].

For Deb, the P-rich ash particles found in the ODN agglomerates are also formed, however, the fraction of these ash particles is not sufficient to cause the quartz sand to adhere together. Therefore, most of the quartz sand is coated with the continuous coating layer formed by the reaction of Na and K with Si from the quartz sand (a coating-induced mechanism), following by the diffusion of some Ca into the coating layer. This is consistent with the results of other studies [32]. The P-rich ash particles are then deposited onto or embedded into the continuous coating layer.

Table 2 shows that the raw Deb and ODN have similar total alkali metals content, while the major difference in the ash-forming elemental composition for the two macroalgae is that Deb contains a much higher Ca and Cl content while a slightly lower P content than ODN. Most alkali metals in the raw Deb can be in the form of alkali chlorides, while most alkali metals in the raw ODN can be in the form of alkali phosphates, as have been suggested by Lane et al. [38]. Generally, alkali chlorides are stable and favours to evaporate than to react with Si and form silicates [74]. Therefore, the agglomeration tendency of Deb can be low as small amount of alkali silicates are formed for Deb. In addition, Ca can be found in the continuous coating layer of Deb, while almost no Ca can be detected in that of ODN as shown in Fig. 7. The increase of the Ca content in the continuous coating layer can increase the melting point of the layer, which mitigates the agglomeration for Deb, as have been suggested by Ohman et al. [75]. The high Ca content in Deb also has a significant effect on the behaviour of P during agglomeration. Several studies have indicated that Ca favours to form Ca phosphates in the presence of P [7,76,77]. Therefore, most of the P in Deb can be in the form of Ca phosphates. The rest of Ca in Deb can form Ca silicates with Si, as have been suggested by Zhu et al. [7]. Zhu et al. have detected both Ca phosphates and Ca silicates in the bed ash and fly ash when Deb was co-combusted with wood in a fluidized bed reactor [7]. In addition, Ca phosphates and Ca silicates phases were found in the Deb ash in the present work, as shown in Table 3. Consequently, these phases could be formed in the Deb agglomerates in this study. These phases generally have high melting-points [78]. Therefore, they increase the melting temperature of Deb agglomerates significantly. In

contrast, as the Ca content in ODN is low, the P in ODN tends to form amorphous alkali phosphates, which generally have low melting-points, as have been indicated by other studies [7,78,79]. To sum up, the Deb agglomerates contain more high melting-point compounds than the ODN agglomerates, which reduces the agglomeration tendency of Deb, when compared with that of ODN.

The size of the ODN agglomerates under both atmospheres and the size of the Deb agglomerates under the steam gasification atmosphere are increased from only approximately several millimetres to several centimetres with the increase of the reaction time. In addition, large quantity of partially molten coating layer forms in these agglomerates to adhere the bed particles together as the reaction time is increased. In contrast, for Deb under the combustion atmosphere, the size of the agglomerates is only increased to approximately less than 5 mm when the reaction time is increased. Very small quantity of partially molten coating layer can be observed in the Deb agglomerates under the combustion atmosphere. The chemical reaction mechanisms of the ash-quartz sand interactions are independent of the reaction time for Deb. In contrast, for ODN, the melting-induced discontinuous coating layer progressively diffuses further into the coating-induced continuous coating layer with an increase in the reaction time. Therefore, the continuous coating layer of ODN for the reaction times of 1 h and 6 h are dominated by Na, Mg, Si, P, K, Ca and Fe, which is different from the cases with a shorter reaction time, as described in Section 3.3.1.

3.5. Effect of the reaction atmosphere (steam gasification vs combustion) on the ash-quartz sand interactions

The morphology of the ODN and Deb agglomerates is affected by the reaction atmosphere. Fig. 10 presents images of the agglomerates obtained after a 6 h of reaction under both the steam gasification and combustion atmospheres at 900 °C for the ODN and Deb samples. The agglomerates formed under the steam gasification atmosphere are larger than those under the combustion atmosphere, especially for the case of Deb. The mass fractions (%) of K and Na dissolved in the acid, cold water and hot water can be used to quantify the retention of K and Na and the formation of alkali silicates with different silica content in the agglomerates. These contribute to the understanding of the difference in the morphology of the agglomerates observed from the SEM/EDS analysis under the two atmospheres.

Fig. 11 presents mass fractions (%) of K and Na dissolved in the acid, cold water and hot water for the 30 min steam gasification and combustion agglomerates relative to the fuel input for Deb and ODN at 900 °C. The acid digestion fraction (the total mass fractions of K and Na retained in the agglomerates) of both K and Na is between 71–90% for ODN and 23–73% for Deb. The effect of the reaction atmosphere on the retention of K and Na in the agglomerates and the formation of silicates
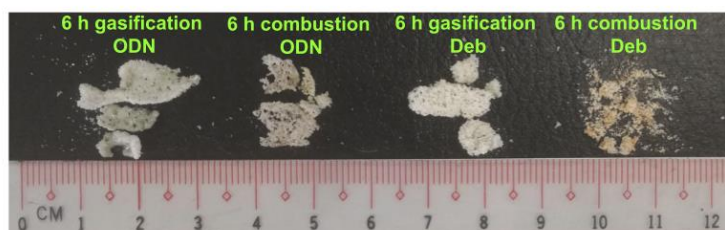
9

Fig. 10. Images of the agglomerates of ODN and Deb from the 6 h ash-quartz sand interaction tests under both the steam gasification and combustion atmospheres at 900 °C.

with different silica content is significant for Deb, while the influence of the reaction atmosphere on those is insignificant for ODN, which is consistent with the SEM/EDS results. The presence of steam increases the reaction between quartz sand and the alkali chlorides from Deb, which results in a higher retention of K and Na in the agglomerates, as have been suggested by Kosminski et al. [56]. The mass fractions of cold water leaching of both K and Na for Deb during the steam gasification is lower than that during the combustion, while the opposite trend is found for the mass fractions of hot water leaching. These results suggest that the Deb agglomerates contain more silicates with a lower silica content under the combustion atmosphere, while they contain more silicates with a higher silica content under the steam gasification atmosphere. Potassium tetrasilicate and sodium disilicate with a higher silica content and a lower melting-point (770 °C and 874 °C, respectively) are suggested to be the alkali silicates which are soluble in hot water [70,71]. In contrast, potassium metasilicate or disilicate with a lower silica content and a higher melting-point (976 °C for metasilicate and 1045 °C for disilicate) are suggested to be the K silicates which are soluble in cold water; Sodium metasilicate with a lower silica content and a higher melting-point (1086 °C) is suggested to be the Na silicate which is soluble in cold water [70,71]. Therefore, the steam gasification atmosphere favours the formation of more K or Na silicates with a lower melting-point, when compared with the combustion atmosphere. This aggravates agglomeration under the steam gasification atmosphere. The reaction atmosphere has an insignificant effect on the ODN agglomerates and the mass fractions of acid digestion and water leaching for ODN are much higher, when compared with those of Deb. These can be attributed to the presence of water-soluble alkali phosphates, such as Na_3PO_4 (Table 3), in the ODN agglomerates, which may also lead to the higher retention of Na than K in the ODN agglomerates. Further work is required to differentiate the concentration of silicates and phosphates.

The above results suggest that the steam gasification atmosphere has an insignificant impact on the ash-quartz sand interaction behaviour of ODN, as the formation of the ODN agglomerates is via a combination of the coating-induced and melting-induced mechanisms. This is consistent with the morphology of the ODN agglomerates observed from the SEM images in Sections 3.2.1 and 3.2.2, as insignificant difference has been observed between the two atmospheres. On the other hand, the above results indicate that the steam gasification atmosphere has considerable effect on the ash-quartz sand interaction behaviour of Deb. Much more K and Na are retained in the Deb agglomerates and more alkali silicates with lower melting-points are formed under the steam gasification atmosphere than those under the combustion atmosphere. Consequently, the tendency towards the formation of agglomerates for Deb under the steam gasification atmosphere is much higher than that under the combustion atmosphere. This is consistent with the morphology of the Deb agglomerates from the SEM images in Sections 3.2.1 and 3.2.2, as insignificant agglomerates are observed for Deb under the combustion atmosphere, while much larger agglomerates are formed under the steam gasification atmosphere.

The individual separate ash particles that have been distributed within the agglomerates for Deb during combustion have a high S content. In contrast, no S is detected in these ash particles during steam gasification. Previous studies of low-rank coals with a high Na and S content reveals that, the agglomeration is induced by the formation of sulfate-dominated ash particles during combustion, but by the formation of alkali silicates during steam/air gasification [57–59]. However, the coating layer of Deb is formed by the alkali silicates under both the steam gasification and combustion atmospheres. Therefore, the ash particles with a high S content for Deb does not influence the ash-quartz sand interaction behaviour.
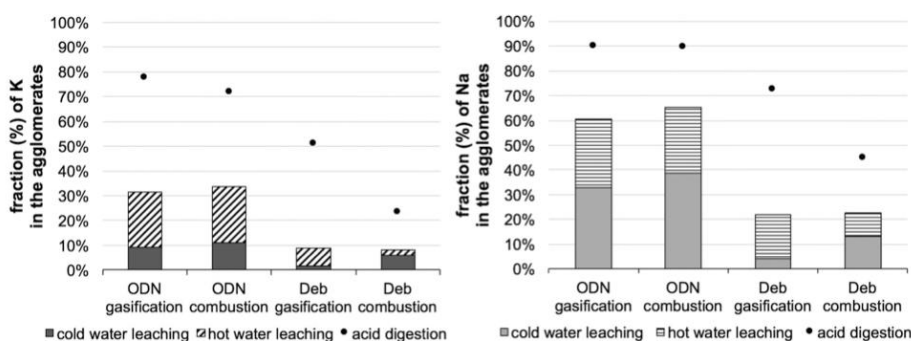

Fig. 11. The mass fractions (%) of K and Na dissolved in acid, cold water and hot water in the 30 min steam gasification and combustion (900 °C) agglomerates relative to the fuel input for ODN and Deb.

10

80

4. Conclusion

The interaction between the ash and quartz sand for ODN occurs by a combination of a melting-induced mechanism, resulting from the partially molten fuel-derived P-dominated ash particles, and a coating-induced mechanism, induced by the formation of alkali silicates. In contrast, the interaction for Deb is dominated by the coating-induced mechanism to form alkali-Ca silicates. The high Ca and Cl content of Deb mitigates the tendency towards the formation of agglomerates, when compared with that of ODN. Alkali chlorides in Deb tends to be released to the gas phase than to form silicates. The formation of high melting-point Ca phosphates, Ca silicates or alkali-Ca silicates increases the melting temperature of the Deb agglomerates. In contrast, low melting-point alkali phosphates or alkali silicates dominate the ODN agglomerates. An increase in the reaction time leads to an increase both in the size of the agglomerates from millimetres to centimetres and in the quantity of the partially molten coating layer formed in the agglomerates for ODN under both atmospheres and Deb under the steam gasification atmosphere. For the combustion atmosphere, both the size of the Deb agglomerates and the quantity of the partially molten coating layer formed are small and have no significant changes with the increase of the reaction time. The chemical interaction is independent of the reaction time for Deb, while for ODN, the melting-induced coating layer gradually diffuses further into the coating-induced coating layer with an increase in the reaction time.

For Deb, the size of the agglomerates formed is much greater during steam gasification (several centimetres) than that during combustion (approximately 1 mm) and the total mass fractions of K and Na remained in the agglomerates is also higher. However, for ODN, the influence of the reaction atmosphere is insignificant. Furthermore, for Deb, more silicates with lower melting-points are generated in the agglomerates under the steam gasification atmosphere than that under the combustion atmosphere. For ODN, the amount of the various types of silicates generated under the two atmospheres cannot be easily compared in the present study due to the co-existence of alkali phosphates. The presence of steam augments the release of S from the individual separate ash particles that are distributed within the agglomerates for Deb. However, a high amount of S is retained in these ash particles during combustion. The ash-quartz sand interaction behaviour of Deb is influenced more by the reaction atmosphere than that of ODN.

The potential of the utilization of Deb as a feedstock in industrial-scale fluidized bed reactors is higher than that of ODN, especially for combustion processes, as insignificant agglomerates can be formed for Deb under a combustion atmosphere. These agglomerates are fragile and can be broken easily by the fluidization conditions in fluidized bed reactors. In contrast, ODN is not an ideal feedstock for industrial-scale fluidized bed reactors as large agglomerates can be formed at an initial stage under either a steam gasification or a combustion atmosphere. Co-combustion or co-gasification ODN with other feedstock, such as wood, that contains high Ca and low other ash-forming elements may mitigate the agglomeration. The addition of Ca additives, such as calcite, may also be beneficial to the utilization of ODN in industrial-scale fluidized bed reactors.

Acknowledgements

Appendix A. Supplementary data

Supplementary data to this article can be found online at https://doi.org/10.1016/j.fuel.2019.116621.

References

[1] Jung KA, Lim S-R, Kim Y, Park JM. Potentials of macroalgae as feedstocks for biorefinery. Bioresour Technol 2013;135:182–90.
[2] Chen H, Zhou D, Luo G, Zhang S, Chen J. Macroalgae for biofuels production: progress and perspectives. Renew Sustain Energy Rev 2015;47:427–37.
[3] Montingelli ME, Tedesco S, Olabi AG. Biogas production from algal biomass: a review. Renew Sustain Energy Rev 2015;43:961–72.
[4] Sudhakar K, Mamat R, Samykano M, Azmi WH, Ishak WFW, Yusaf T. An overview of marine macroalgae as bioresource. Renew Sustain Energy Rev 2018;91:165–79.
[5] Bharathiraja B, Chakravarthy M, Ranjith Kumar R, Yogendran D, Yuvaraj D, Jayamuthunagai J, et al. Aquatic biomass (algae) as a future feed stock for bio-refineries: a review on cultivation, processing and products. Renew Sustain Energy Rev 2015;47:634–53.
[6] Suganya T, Varman M, Masjuki HH, Renganathan S. Macroalgae and microalgae as a potential source for commercial applications along with biofuels production: a biorefinery approach. Renew Sustain Energy Rev 2016;55:909–41.
[7] Zhu Y, Piotrowska P, van Eyk PJ, Boström D, Wu X, Boman C, et al. Fluidized bed co-gasification of algae and wood pellets: gas yields and bed agglomeration analysis. Energy Fuels 2016;30:1800–9.
[8] Aziz M, Oda T, Kashiwagi T. Advanced energy harvesting from macro-algae—innovative integration of drying, gasification and combined cycle. Energies 2014;7:8217–35.
[9] Elliott DC. Review of recent reports on process technology for thermochemical conversion of whole algae to liquid fuels. Algal Res 2016;13:255–63.
[10] Rowbotham JS, Dyer PW, Greenwell HC, Theodorou MK. Thermochemical processing of macroalgae: a late bloomer in the development of third-generation biofuels? Biofuels 2012;3:441–61.
[11] Jiang R, Ingle KN, Golberg A. Macroalgae (seaweed) for liquid transportation biofuel production: what is next? Algal Res 2016;14:48–57.
[12] Michalak I. Experimental processing of seaweeds for biofuels, Wiley Interdisciplinary Reviews. Energy Environ 2018;7. e288.
[13] Skoglund N, Werner K, Nylund GM, Pavia H, Albers E, Boström M. Combustion of seaweed — a fuel design strategy. Fuel Process Technol 2017;165:155–61.
[14] Ross AB, Jones JM, Kubacki ML, Bridgeman T. Classification of macroalgae as fuel and its thermochemical behaviour. Bioresour Technol 2008;99:6494–504.
[15] Lane DJ, Truong E, Larizza F, Chiew P, de Nys R, van Eyk PJ. Effect of hydrothermal carbonization on the combustion and gasification behavior of agricultural residues and macroalgae: devolatilization characteristics and char reactivity. Energy Fuels 2018;32:4149–59.
[16] Zhu Y, van Eyk PJ, Boman C, Broström M, Kirtania K, Piotrowska P, et al. Preliminary understanding on the ash behavior of algae during co-gasification in an entrained flow reactor. Fuel Process Technol 2018;175:26–34.
[17] Vassilev SV, Vassileva CG. Composition, properties and challenges of algae biomass for biofuel application: an overview. Fuel 2016;181:1–33.
[18] Ghadiryanfar M, Rosentrater KA, Keyhani A, Omid M. A review of macroalgae production, with potential applications in biofuels and bioenergy. Renew Sustain Energy Rev 2016;54:473–81.
[19] Asomaning J, Omidghane M, Chae M, Bressler DC. Thermal processing of algal biomass for biofuel production. Curr Opin Green Sustainable Chem 2016;2:1–5.
[20] Warnecke R. Gasification of biomass: comparison of fixed bed and fluidized bed gasifier. Biomass Bioenergy 2000;18:489–97.
[21] Khan AA, de Jong W, Jansens PJ, Spliethoff H. Biomass combustion in fluidized bed boilers: Potential problems and remedies. Fuel Process Technol 2009;90:21–50.
[22] Lin W, Dam-Johansen K, Frandsen F. Agglomeration in bio-fuel fired fluidized bed combustors. Chem Eng J 2003;96:171–85.
[23] Bartels M, Lin W, Nijenhuis J, Kapteijn F, van Ommen JR. Agglomeration in fluidized beds at high temperatures: mechanisms, detection and prevention. Prog Energy Combust Sci 2008;34:633–66.
[24] Anicic B, Lin W, Dam-Johansen K, Wu H. Agglomeration mechanism in biomass fluidized bed combustion – reaction between potassium carbonate and silica sand. Fuel Process Technol 2018;173:182–90.
[25] Niu Y, Tan H, Hui S. Ash-related issues during biomass combustion: Alkali-induced slagging, silicate melt-induced slagging (ash fusion), agglomeration, corrosion, ash utilization, and related countermeasures. Prog Energy Combust Sci 2016;52:1–61.
[26] Öhman M, Pommer L, Nordin A. Bed agglomeration characteristics and mechanisms during gasification and combustion of biomass fuels. Energy Fuels 2005;19:1742–8.
[27] Grimm A, Skoglund N, Boström D, Öhman M. Bed agglomeration characteristics in fluidized quartz bed combustion of phosphorus-rich biomass fuels. Energy Fuels 2011;25:937–47.
[28] Piotrowska P, Grimm A, Skoglund N, Boman C, Öhman M, Zevenhoven M, et al. Fluidized-bed combustion of mixtures of rapeseed cake and bark: the resulting bed agglomeration characteristics. Energy Fuels 2012;26:2028–37.
[29] Gatternig B, Karl J. Investigations on the mechanisms of ash-induced agglomeration in fluidized-bed combustion of biomass. Energy Fuels 2015;29:931–41.
[30] Kuba M, He H, Kirnbauer F, Skoglund N, Boström D, Öhman M, et al. Mechanism of layer formation on olivine bed particles in industrial-scale dual fluid bed gasification of wood. Energy Fuels 2016;30:7410–8.
[31] He H, Ji X, Boström D, Backman R, Öhman M. Mechanism of quartz bed particle

layer formation in fluidized bed combustion of wood-derived fuels. Energy Fuels 2016;30:2227–32.

[32] Brus E, Öhman M, Nordin A. Mechanisms of bed agglomeration during fluidized-bed combustion of biomass fuels. Energy Fuels 2005;19:825–32.

[33] Scala F, Chirone R. An SEM/EDX study of bed agglomerates formed during fluidized bed combustion of three biomass fuels. Biomass Bioenergy 2008;32:252–66.

[34] He H, Boström D, Öhman M. Time dependence of bed particle layer formation in fluidized quartz bed combustion of wood-derived fuels. Energy Fuels 2014;28:3841–8.

[35] Zevenhoven-Onderwater M, Öhman M, Skrifvars B-J, Backman R, Nordin A, Hupa M. Bed agglomeration characteristics of wood-derived fuels in FBC. Energy Fuels 2006;20:818–24.

[36] Alghurabie IK, Hasan BO, Jackson B, Kosminski A, Ashman PJ. Fluidized bed gasification of Kingston coal and marine microalgae in a spouted bed reactor. Chem Eng Res Des 2013;91:1614–24.

[37] Yang K-C, Wu K-T, Hsieh M-H, Hsu H-T, Chen C-S, Chen H-W. Co-gasification of woody biomass and microalgae in a fluidized bed. J Taiwan Inst Chem Eng 2013;44:1027–33.

[38] Lane DJ, Zevenhoven M, Ashman PJ, van Eyk PJ, Hupa M, de Nys R, et al. Algal biomass: occurrence of the main inorganic elements and simulation of ash interactions with bed material. Energy Fuels 2014;28:4622–32.

[39] Zhu Y, Piotrowska P, van Eyk PJ, Boström D, Kwong CW, Wang D, et al. Cogasification of Australian brown coal with algae in a fluidized bed reactor. Energy Fuels 2015;29:1686–700.

[40] Khadilkar AB, Rozelle PL, Pisupati SV. Review of particle physics and chemistry in fluidized beds for development of comprehensive ash agglomeration prediction models. Energy Fuels 2016;30:3714–34.

[41] Scala F. Particle agglomeration during fluidized bed combustion: Mechanisms, early detection and possible countermeasures. Fuel Process Technol 2018;171:31–8.

[42] Morris JD, Daood SS, Chilton S, Nimmo W. Mechanisms and mitigation of agglomeration during fluidized bed combustion of biomass: a review. Fuel 2018;230:452–73.

[43] He H, Skoglund N, Öhman M. Time-dependent layer formation on K-Feldspar bed particles during fluidized bed combustion of woody fuels. Energy Fuels 2017;31:12848–56.

[44] Corcoran A, Knutsson P, Lind F, Thunman H. Mechanism for migration and layer growth of biomass ash on ilmenite used for oxygen carrier aided combustion. Energy Fuels 2018;32:8845–56.

[45] Wagner K, Häggström G, Mauerhofer AM, Kuba M, Skoglund N, Öhman M, et al. Layer formation on K-feldspar in fluidized bed combustion and gasification of bark and chicken manure. Biomass Bioenergy 2019;127. 105251.

[46] Hanning M, Corcoran A, Lind F, Rydén M. Biomass ash interactions with a manganese ore used as oxygen-carrying bed material in a 12 MWth CFB boiler. Biomass Bioenergy 2018;119:179–90.

[47] Faust R, Hannl TK, Vilches TB, Kuba M, Öhman M, Seemann M, et al. Layer formation on feldspar bed particles during indirect gasification of wood. 1. K-feldspar. Energy Fuels 2019;33:7321–32.

[48] Hannl TK, Faust R, Kuba M, Knutsson P, Berdugo Vilches T, Seemann M, et al. Layer formation on feldspar bed particles during indirect gasification of Wood. 2. Na-feldspar. Energy Fuels 2019;33:7333–44.

[49] Kuba M, He H, Kirnbauer F, Skoglund N, Boström D, Öhman M, et al. Thermal stability of bed particle layers on naturally occurring minerals from dual fluid bed gasification of woody biomass. Energy Fuels 2016;30:8277–85.

[50] Moradian F, Tchoffor PA, Davidsson KO, Pettersson A, Backman R. Thermodynamic equilibrium prediction of bed agglomeration tendency in dual fluidized-bed gasification of forest residues. Fuel Process Technol 2016;154:82–90.

[51] He Z, Lane DJ, Saw WL, van Eyk PJ, Nathan GJ, Ashman PJ. Ash-bed material interaction during the combustion and steam gasification of Australian agricultural residues. Energy Fuels 2018;32:4278–90.

[52] Kaknics J, Michel R, Richard A, Poirier J. High-temperature interactions between molten miscanthus ashes and bed materials in a fluidized-bed gasifier. Energy Fuels 2015;29:1785–92.

[53] Kaknics J, Michel R, Poirier J. Miscanthus ash transformation and interaction with bed materials at high temperature. Fuel Process Technol 2016;141:178–84.

[54] Ma T, Fan C, Hao L, Li S, Song W, Lin W. Biomass-ash-induced agglomeration in a fluidized bed. Part 1: experimental study on the effects of a gas atmosphere. Energy

Fuels 2016;30:6395–404.

[55] Kosminski A, Ross DP, Agnew JB. Influence of gas environment on reactions between sodium and silicon minerals during gasification of low-rank coal. Fuel Process Technol 2006;87:953–62.

[56] Kosminski A, Ross DP, Agnew JB. Reactions between sodium and silica during gasification of a low-rank coal. Fuel Process Technol 2006;87:1037–49.

[57] Manzoori AR, Agarwal PK. The role of inorganic matter in coal in the formation of agglomerates in circulating fluid bed combustors. Fuel 1993;72:1069–75.

[58] McCullough DP, van Eyk PJ, Ashman PJ, Mullinger PJ. Impact of sodium and sulfur species on agglomeration and defluidization during spouted bed gasification of south Australian lignite. Energy Fuels 2015;29:3922–32.

[59] van Eyk PJ, Kosminski A, Ashman PJ. Control of agglomeration and defluidization during fluidized-bed gasification of south Australian low-rank coals. Energy Fuels 2012;26:118–29.

[60] Ma T, Fan C, Hao L, Li S, Jensen PA, Song W, et al. Biomass ash induced agglomeration in fluidized bed. Part 2: effect of potassium salts in different gas composition. Fuel Process Technol 2018;180:130–9.

[61] Lawton RJ, de Nys R, Paul NA. Selecting reliable and robust freshwater macroalgae for biomass applications. PLoS ONE 2013;8. e64168.

[62] Neveux N, Magnusson M, Mata L, Whelan A, de Nys R, Paul NA. The treatment of municipal wastewater by the macroalga Oedogonium sp. and its potential for the production of biocrude. Algal Res 2016;13:284–92.

[63] Cole A, Dinburg Y, Haynes BS, He Y, Herskowitz M, Jazrawi C, et al. From macroalgae to liquid fuel via waste-water remediation, hydrothermal upgrading, carbon dioxide hydrogenation and hydrotreating. Energy Environ Sci 2016;9:1828–40.

[64] Lawton RJ, de Nys R, Skinner S, Paul NA. Isolation and identification of oedogonium species and strains for biomass applications. PLoS ONE 2014;9. e90223.

[65] Lawton RJ, Cole AJ, Roberts DA, Paul NA, de Nys R. The industrial ecology of freshwater macroalgae for biomass applications. Algal Res 2017;24:486–91.

[66] Mata L, Magnusson M, Paul NA, de Nys R. The intensive land-based production of the green seaweeds Derbesia tenuissima and Ulva ohnoi: biomass and bioproducts. J Appl Phycol 2016;28:365–75.

[67] Magnusson M, Mata L, de Nys R, Paul NA. Biomass, lipid and fatty acid production in large-scale cultures of the marine macroalga derbesia tenuissima (Chlorophyta). Mar Biotechnol 2014;16:456–64.

[68] Gosch BJ, Lawton RJ, Paul NA, de Nys R, Magnusson M. Environmental effects on growth and fatty acids in three isolates of Derbesia tenuissima (Bryopsidales, Chlorophyta). Algal Res 2015;9:82–93.

[69] Neveux N, Yuen AKL, Jazrawi C, Magnusson M, Haynes BS, Masters AF, et al. Biocrude yield and productivity from the hydrothermal liquefaction of marine and freshwater green macroalgae. Bioresour Technol 2014;155:334–41.

[70] Merrill RC. Chemistry of the soluble silicates. J Chem Educ 1947;24:262.

[71] Weldes HH, Lange KR. Properties of soluble silicates. Ind Eng Chem 1969;61:29–44.

[72] Zevenhoven M, Yrjas P, Skrifvars B-J, Hupa M. Characterization of ash-forming matter in various solid fuels by selective leaching and its implications for fluidized-bed combustion. Energy Fuels 2012;26:6366–86.

[73] Boström D, Skoglund N, Grimm A, Boman C, Öhman M, Brostrom M, et al. Ash Transformation chemistry during combustion of biomass. Energy Fuels 2012;26:85–93.

[74] Knudsen JN, Jensen PA, Dam-Johansen K. Transformation and release to the gas phase of Cl, K, and S during combustion of annual biomass. Energy Fuels 2004;18:1385–99.

[75] Öhman M, Nordin A, Skrifvars B-J, Backman R, Hupa M. Bed agglomeration characteristics during fluidized bed combustion of biomass fuels. Energy Fuels 2000;14:169–78.

[76] Billen P, Van Caneghem J, Vandecasteele C. Predicting melt formation and agglomeration in fluidized bed combustors by equilibrium calculations. Waste Biomass Valorization 2014;5:879–92.

[77] Billen P, Creemers B, Costa J, Van Caneghem J, Vandecasteele C. Coating and melt induced agglomeration in a poultry litter fired fluidized bed combustor. Biomass Bioenergy 2014;69:71–9.

[78] Vassilev SV, Baxter D, Vassileva CG. An overview of the behaviour of biomass during combustion: part I. Phase-mineral transformations of organic and inorganic matter. Fuel 2013;112:391–449.

[79] Lindström E, Sandström M, Boström D, Öhman M. Slagging characteristics during combustion of cereal grains rich in phosphorus. Energy Fuels 2007;21:710–7.

12

Chapter 7. Conclusions and Recommendations

7.1 Conclusions

7.1.1 Interaction behaviours between quartz sand and alkali salt-doped wood

Interactions between quartz sand and alkali carbonate, acetate, sulfate or chloride salt-doped wood were a coating-induced mechanism, by formation of alkali silicate that resulted from reactions between alkali metals and Si from the quartz sand. Apart from reactions between these pure alkali salts and the quartz sand, interactions between alkali carbonates, chlorides or sulfates and the organic components of wood generated some intermediates that reacted with the quartz sand to form agglomerates. The gas-solid phase reactions between the quartz sand and gaseous alkali metals were also an important reaction pathway, especially for K salts in biomass.

Large agglomerates were formed for alkali carbonate or acetate salt-doped wood, while relatively small agglomerates were formed for alkali chloride-doped wood. Alkali sulfate-doped wood formed agglomerates with a moderate size. Greater mass fractions of K or Na (70-100%) were retained in the agglomerates for alkali carbonate, acetate or sulfate salt-doped wood than those for alkali chloride-doped wood. This suggested that for biomass with a high content of alkali chloride, more alkali metals are released to cause other ash-related problems, such as ash deposition or fouling, while the tendency towards bed agglomeration is low. In contrast, for biomass rich in other alkali salts or organic-associated alkali metals, less alkali metals are released to induce other ash-related problems, while bed agglomeration is more serious.

Steam significantly aggravated bed agglomeration. For alkali carbonate, acetate or sulfate salt-doped wood, similar amounts of alkali silicates were generated under both atmospheres. However, the steam favoured formation of more alkali silicates with lower melting points, when compared with that under a combustion atmosphere. This contributed to larger agglomerates during steam gasification. For alkali chloride-doped wood, the steam favoured generation of more alkali silicates, while insignificant agglomerates were formed under a combustion atmosphere. This could result from the hydrolysis of alkali chloride by steam. The gas-solid

84

phase reactions between the quartz sand and gaseous alkali metals were also facilitated by the steam through a hydrolysis step, especially for alkali sulfate-doped wood.

7.1.2 Effects of Ca and P on interaction behaviours of individual K salt-doped wood

The presence of Ca mitigated interactions between quartz sand and K salt-doped wood due to formation of Ca compounds in coating layer, which decreased formation of K silicate. Therefore, the size of agglomerates was reduced with the addition of Ca. The effect of Ca on agglomerates varied with species of K salts in biomass, which was more significant for K_2SO_4 or KCl salt-doped wood than for K_2CO_3-doped wood.

The presence of P, especially with Ca together, had a significant influence on interactions between alkali salt-doped wood and the quartz sand. For K salt-doped wood with a high P content, its interactions with the quartz sand was dominated by a melting-induced mechanism, which resulted from the adhesion of quartz sand particles to partially molten phosphate ash particles, or the co-existence of both coating-induced and melting-induced mechanisms. When both P and Ca were present, Ca phosphate might form first, as a very stable compound in biomass ash. Individual K salts in wood samples reacted with both P and Ca, or with Ca phosphates. These reactions formed partially molten ash particles of alkali-Ca phosphates. These alkali-Ca phosphates could adhere the quartz sand to form agglomerates, when the amounts of them were great. The other fractions of individual K salts in wood samples reacted with the quartz sand to form K silicate coating layer. It could be concluded that, the presence of both Ca and P, or Ca phosphate, had two effects, it increased K retention by increasing formation of K-Ca phosphates, while decreased K retention by reducing formation of K silicate. The domination of the two opposite effects on K retention and formation of agglomerates depended on the amounts of Ca and P present and species of K salts in wood samples. Furthermore, steam had insignificant effects on agglomerates formed by a melting-induced mechanism or on behaviours of both Ca and P during bed agglomeration.

7.1.3 Interactions between quartz sand and several agricultural residues or macroalgae

The interaction behaviours between the quartz sand and several agricultural residues (grape marc, wheat straw or cotton stalk) or macroalgae (ODN or Deb) were consistent with those between the quartz sand and alkali salt-doped wood.

Alkali metals from these agricultural residues or macroalgae either reacted with Si from the quartz sand to form alkali silicate coating layer, via a coating-induced mechanism (a reactive mechanism), or reacted with P or Si from the biomass to form partially molten ash of alkali silicate or alkali phosphate and formed agglomerates via a melting-induced mechanism (a non-reactive mechanism). A coating-induced mechanism (formation of alkali silicates) dominated for Deb, grape marc and cotton stalk; A melting-induced mechanism (formation of fuel-derived partially molten alkali-silicate ash) dominated for wheat straw; Both coating-induced (formation of alkali silicates) and melting-induced (formation of fuel-derived partially molten phosphate ash) mechanisms co-existed for ODN. For wheat straw, cotton stalk and Deb, the formation of the coating layer was followed with the diffusion of Ca into the coating layer.

The effect of the steam on interactions between quartz sand and the agricultural residues or macroalgae was consistent with those between quartz sand and alkali salt-doped wood. Grape marc was dominated by K_2CO_3 or organic-associated K, while Deb was rich in alkali chloride. Grape marc formed much larger agglomerates during steam gasification, while Deb formed insignificant agglomerates during combustion. Much larger agglomerates were formed during steam gasification than that during combustion for grape marc and Deb. For wheat straw and ODN, the steam had insignificant impacts on agglomerates formed wholly or partially through a melting-induced mechanism. For cotton stalk, alkali metals were present as a mixture of various types of alkali salts. Therefore, the influence of the steam on cotton stalk agglomerates was also insignificant, which resulted from its complex inorganic composition.

7.1.4 Time-dependent layer formation process of agglomerates

Time-dependent layer formation of agglomerates was affected significantly by both the species of alkali salts in wood samples and the reaction atmosphere. For alkali carbonate or acetate salt-doped wood, large agglomerates were developed at an initial stage (a 7 min reaction time), especially during steam gasification. In contrast, for alkali sulfate or alkali chloride salt-doped wood, insignificant agglomerates were developed at an initial stage. Steam facilitated reactions between these alkali salts and the organic components of wood. Therefore, steam increased formation of agglomerates at an initial stage significantly. On the contrary, the combustion atmosphere (5% O_2) slowed down the formation of agglomerates due to a low oxygen concentration, as it slowed down the consumption of the organic components. For biomass with a high P content, formation of agglomerates through a melting-induced mechanism was insignificant at an initial stage.

The size of agglomerates for all the raw biomass tested at an initial stage was insignificant, with a thin coating layer. The size of agglomerates and amounts of partially molten compounds in coating layer increased significantly with the increase of reaction time, except for the Deb case during combustion, as Deb was dominated by alkali chloride salts. Ash chemistry of biomass ash-quartz sand interactions for all the biomass tested, except for ODN, was independent of the reaction time, while the melting-induced coating layer gradually diffused into the coating-induced coating layer for ODN.

7.2. Recommendations for future work

Further work is still necessary to advance our understanding of agglomeration in fluidized bed reactors during thermochemical processes.

All the work that have been done in this thesis were performed in a lab-scale, fixed-bed reactor and have only focused on the ash chemistry of agglomeration. The influence of physical aspects and operational conditions in fluidized bed reactors, such as fluidization, gas velocity, collision frequency, particle size and the continuous feeding of feedstock, was not considered in this thesis. The fluidization

behaviour can influence formation of agglomerates. Continuous feeding of feedstock in fluidized bed reactors can also affect the ash chemistry of bed agglomeration, which was identified in the fixed-bed reactor in the present thesis. The interaction behaviours suggested in this thesis need to be further examined in fluidized bed reactors.

Interactions between alkali salts and the organic components in biomass affects bed agglomeration process. Therefore, it is necessary to study the effect of organic compositions of biomass on bed agglomeration. This can be performed by doping individual alkali salts with biomass of different organic compositions or with some macromolecules in biomass, such as cellulose, lignin, xylan and pectin.

The interaction behaviours identified in this thesis have suggested that biomass with certain inorganic compositions can increase or decrease release of alkali metals and tendency towards agglomeration. Future work is required to achieve a more comprehensive understanding on how to control the tendency towards agglomeration practically, either by adjusting configuration of reactors or by altering compositions of feedstock and bed materials, to achieve optimized conditions in fluidized bed reactors.

All the work in the present thesis were based on experimental work. Some future modelling work that are related to the experimental work in the present thesis are recommended. Such modelling work help to understand the interaction behaviours between quartz sand and raw biomass or alkali salts in wood samples, which have been suggested in this thesis.

References

[1] S.N. Naik, V.V. Goud, P.K. Rout, A.K. Dalai, Production of first and second generation biofuels: A comprehensive review, Renewable and Sustainable Energy Reviews, 14 (2010) 578-597.

[2] K. Ullah, M. Ahmad, Sofia, V.K. Sharma, P. Lu, A. Harvey, M. Zafar, S. Sultana, Assessing the potential of algal biomass opportunities for bioenergy industry: A review, Fuel, 143 (2015) 414-423.

[3] J. Werther, M. Saenger, E.U. Hartge, T. Ogada, Z. Siagi, Combustion of agricultural residues, Progress in Energy and Combustion Science, 26 (2000) 1-27.

[4] S.V. Vassilev, C.G. Vassileva, Composition, properties and challenges of algae biomass for biofuel application: An overview, Fuel, 181 (2016) 1-33.

[5] Y. Niu, H. Tan, S.e. Hui, Ash-related issues during biomass combustion: Alkali-induced slagging, silicate melt-induced slagging (ash fusion), agglomeration, corrosion, ash utilization, and related countermeasures, Prog. Energy Combust. Sci., 52 (2016) 1-61.

[6] M. Öhman, L. Pommer, A. Nordin, Bed Agglomeration Characteristics and Mechanisms during Gasification and Combustion of Biomass Fuels, Energy & Fuels, 19 (2005) 1742-1748.

[7] E. Brus, M. Öhman, A. Nordin, Mechanisms of Bed Agglomeration during Fluidized-Bed Combustion of Biomass Fuels, Energy & Fuels, 19 (2005) 825-832.

[8] A.B. Khadilkar, P.L. Rozelle, S.V. Pisupati, Review of Particle Physics and Chemistry in Fluidized Beds for Development of Comprehensive Ash Agglomeration Prediction Models, Energy & Fuels, 30 (2016) 3714-3734.

[9] F. Scala, Particle agglomeration during fluidized bed combustion: Mechanisms, early detection and possible countermeasures, Fuel Processing Technology, 171 (2018) 31-38.

[10] A. Kosminski, D.P. Ross, J.B. Agnew, Reactions between sodium and silica during gasification of a low-rank coal, Fuel Processing Technology, 87 (2006) 1037-1049.

[11] S. Octave, D. Thomas, Biorefinery: Toward an industrial metabolism, Biochimie, 91 (2009) 659-664.

[12] S.R. Paudel, S.P. Banjara, O.K. Choi, K.Y. Park, Y.M. Kim, J.W. Lee, Pretreatment of agricultural biomass for anaerobic digestion: Current state and

challenges, Bioresource Technology, 245 (2017) 1194-1205.

[13] N. Sarkar, S.K. Ghosh, S. Bannerjee, K. Aikat, Bioethanol production from agricultural wastes: An overview, Renewable Energy, 37 (2012) 19-27.

[14] J.K. Saini, R. Saini, L. Tewari, Lignocellulosic agriculture wastes as biomass feedstocks for second-generation bioethanol production: concepts and recent developments, 3 Biotech, 5 (2015) 337-353.

[15] F. Cherubini, S. Ulgiati, Crop residues as raw materials for biorefinery systems – A LCA case study, Applied Energy, 87 (2010) 47-57.

[16] I. Hamawand, G. Sandell, P. Pittaway, S. Chakrabarty, T. Yusaf, G. Chen, S. Seneweera, S. Al-Lwayzy, J. Bennett, J. Hopf, Bioenergy from Cotton Industry Wastes: A review and potential, Renewable and Sustainable Energy Reviews, 66 (2016) 435-448.

[17] A. Salihu, M.Z. Alam, M.I. AbdulKarim, H.M. Salleh, Lipase production: An insight in the utilization of renewable agricultural residues, Resources, Conservation and Recycling, 58 (2012) 36-44.

[18] D. Jiang, D. Zhuang, J. Fu, Y. Huang, K. Wen, Bioenergy potential from crop residues in China: Availability and distribution, Renewable and Sustainable Energy Reviews, 16 (2012) 1377-1382.

[19] O. Santana-Méridas, A. González-Coloma, R. Sánchez-Vioque, Agricultural residues as a source of bioactive natural products, Phytochemistry Reviews, 11 (2012) 447-466.

[20] A.B. Ross, J.M. Jones, M.L. Kubacki, T. Bridgeman, Classification of macroalgae as fuel and its thermochemical behaviour, Bioresource Technology, 99 (2008) 6494-6504.

[21] R. Rajkumar, Z. Yaakob, M.S. Takriff, Potential of Micro and Macro Algae for Biofuel Production: A Brief Review, BioResources; Vol 9, No 1 (2014), (2013).

[22] T. Suganya, M. Varman, H.H. Masjuki, S. Renganathan, Macroalgae and microalgae as a potential source for commercial applications along with biofuels production: A biorefinery approach, Renewable and Sustainable Energy Reviews, 55 (2016) 909-941.

[23] H. Chen, D. Zhou, G. Luo, S. Zhang, J. Chen, Macroalgae for biofuels production: Progress and perspectives, Renewable and Sustainable Energy Reviews,

47 (2015) 427-437.

[24] M. Aziz, T. Oda, T. Kashiwagi, Advanced Energy Harvesting from Macroalgae—Innovative Integration of Drying, Gasification and Combined Cycle, Energies, 7 (2014) 8217-8235.

[25] N. Wei, J. Quarterman, Y.-S. Jin, Marine macroalgae: an untapped resource for producing fuels and chemicals, Trends in Biotechnology, 31 (2013) 70-77.

[26] I. Michalak, Experimental processing of seaweeds for biofuels, Wiley Interdisciplinary Reviews: Energy and Environment, 7 (2018) e288.

[27] M. Ghadiryanfar, K.A. Rosentrater, A. Keyhani, M. Omid, A review of macroalgae production, with potential applications in biofuels and bioenergy, Renewable and Sustainable Energy Reviews, 54 (2016) 473-481.

[28] N. Neveux, M. Magnusson, L. Mata, A. Whelan, R. de Nys, N.A. Paul, The treatment of municipal wastewater by the macroalga Oedogonium sp. and its potential for the production of biocrude, Algal Research, 13 (2016) 284-292.

[29] B.J. Gosch, R.J. Lawton, N.A. Paul, R. de Nys, M. Magnusson, Environmental effects on growth and fatty acids in three isolates of Derbesia tenuissima (Bryopsidales, Chlorophyta), Algal Research, 9 (2015) 82-93.

[30] D.P. Ho, H.H. Ngo, W. Guo, A mini review on renewable sources for biofuel, Bioresource Technology, 169 (2014) 742-749.

[31] D.C. Elliott, Review of recent reports on process technology for thermochemical conversion of whole algae to liquid fuels, Algal Research, 13 (2016) 255-263.

[32] R. Warnecke, Gasification of biomass: comparison of fixed bed and fluidized bed gasifier, Biomass and Bioenergy, 18 (2000) 489-497.

[33] A.A. Khan, W. de Jong, P.J. Jansens, H. Spliethoff, Biomass combustion in fluidized bed boilers: Potential problems and remedies, Fuel Processing Technology, 90 (2009) 21-50.

[34] M. Bartels, W. Lin, J. Nijenhuis, F. Kapteijn, J.R. van Ommen, Agglomeration in fluidized beds at high temperatures: Mechanisms, detection and prevention, Prog. Energy Combust. Sci., 34 (2008) 633-666.

[35] J.D. Morris, S.S. Daood, S. Chilton, W. Nimmo, Mechanisms and mitigation of agglomeration during fluidized bed combustion of biomass: A review, Fuel, 230

(2018) 452-473.

[36] L.L. Baxter, T.R. Miles, T.R. Miles, B.M. Jenkins, T. Milne, D. Dayton, R.W. Bryers, L.L. Oden, The behavior of inorganic material in biomass-fired power boilers: field and laboratory experiences, Fuel Processing Technology, 54 (1998) 47-78.

[37] M. Öhman, A. Nordin, B.-J. Skrifvars, R. Backman, M. Hupa, Bed Agglomeration Characteristics during Fluidized Bed Combustion of Biomass Fuels, Energy & Fuels, 14 (2000) 169-178.

[38] W. Lin, K. Dam-Johansen, F. Frandsen, Agglomeration in bio-fuel fired fluidized bed combustors, Chemical Engineering Journal, 96 (2003) 171-185.

[39] B. Gatternig, J. Karl, Investigations on the Mechanisms of Ash-Induced Agglomeration in Fluidized-Bed Combustion of Biomass, Energy & Fuels, 29 (2015) 931-941.

[40] F. Scala, R. Chirone, An SEM/EDX study of bed agglomerates formed during fluidized bed combustion of three biomass fuels, Biomass and Bioenergy, 32 (2008) 252-266.

[41] D.J. Lane, M. Zevenhoven, P.J. Ashman, P.J. van Eyk, M. Hupa, R. de Nys, D.M. Lewis, Algal Biomass: Occurrence of the Main Inorganic Elements and Simulation of Ash Interactions with Bed Material, Energy & Fuels, 28 (2014) 4622-4632.

[42] Y. Zhu, P. Piotrowska, P.J. van Eyk, D. Boström, C.W. Kwong, D. Wang, A.J. Cole, R. de Nys, F.G. Gentili, P.J. Ashman, Cogasification of Australian Brown Coal with Algae in a Fluidized Bed Reactor, Energy & Fuels, 29 (2015) 1686-1700.

[43] Y. Zhu, P. Piotrowska, P.J. van Eyk, D. Boström, X. Wu, C. Boman, M. Broström, J. Zhang, C.W. Kwong, D. Wang, A.J. Cole, R. de Nys, F.G. Gentili, P.J. Ashman, Fluidized Bed Co-gasification of Algae and Wood Pellets: Gas Yields and Bed Agglomeration Analysis, Energy & Fuels, 30 (2016) 1800-1809.

[44] I.K. Alghurabie, B.O. Hasan, B. Jackson, A. Kosminski, P.J. Ashman, Fluidized bed gasification of Kingston coal and marine microalgae in a spouted bed reactor, Chemical Engineering Research and Design, 91 (2013) 1614-1624.

[45] K.-C. Yang, K.-T. Wu, M.-H. Hsieh, H.-T. Hsu, C.-S. Chen, H.-W. Chen, Co-gasification of woody biomass and microalgae in a fluidized bed, Journal of the

Taiwan Institute of Chemical Engineers, 44 (2013) 1027-1033.

[46] S.V. Vassilev, D. Baxter, L.K. Andersen, C.G. Vassileva, An overview of the chemical composition of biomass, Fuel, 89 (2010) 913-933.

[47] P. Piotrowska, A. Grimm, N. Skoglund, C. Boman, M. Öhman, M. Zevenhoven, D. Boström, M. Hupa, Fluidized-Bed Combustion of Mixtures of Rapeseed Cake and Bark: The Resulting Bed Agglomeration Characteristics, Energy & Fuels, 26 (2012) 2028-2037.

[48] H. He, X. Ji, D. Boström, R. Backman, M. Öhman, Mechanism of Quartz Bed Particle Layer Formation in Fluidized Bed Combustion of Wood-Derived Fuels, Energy & Fuels, 30 (2016) 2227-2232.

[49] H. He, D. Boström, M. Öhman, Time Dependence of Bed Particle Layer Formation in Fluidized Quartz Bed Combustion of Wood-Derived Fuels, Energy & Fuels, 28 (2014) 3841-3848.

[50] M. Kuba, H. He, F. Kirnbauer, N. Skoglund, D. Boström, M. Öhman, H. Hofbauer, Mechanism of Layer Formation on Olivine Bed Particles in Industrial-Scale Dual Fluid Bed Gasification of Wood, Energy & Fuels, 30 (2016) 7410-7418.

[51] A. Corcoran, P. Knutsson, F. Lind, H. Thunman, Mechanism for Migration and Layer Growth of Biomass Ash on Ilmenite Used for Oxygen Carrier Aided Combustion, Energy & Fuels, 32 (2018) 8845-8856.

[52] K. Wagner, G. Häggström, A.M. Mauerhofer, M. Kuba, N. Skoglund, M. Öhman, H. Hofbauer, Layer formation on K-feldspar in fluidized bed combustion and gasification of bark and chicken manure, Biomass and Bioenergy, 127 (2019) 105251.

[53] M. Hanning, A. Corcoran, F. Lind, M. Rydén, Biomass ash interactions with a manganese ore used as oxygen-carrying bed material in a 12 MWth CFB boiler, Biomass and Bioenergy, 119 (2018) 179-190.

[54] R. Faust, T.K. Hannl, T.B. Vilches, M. Kuba, M. Öhman, M. Seemann, P. Knutsson, Layer Formation on Feldspar Bed Particles during Indirect Gasification of Wood. 1. K-Feldspar, Energy & Fuels, 33 (2019) 7321-7332.

[55] T.K. Hannl, R. Faust, M. Kuba, P. Knutsson, T. Berdugo Vilches, M. Seemann, M. Öhman, Layer Formation on Feldspar Bed Particles during Indirect Gasification of Wood. 2. Na-Feldspar, Energy & Fuels, 33 (2019) 7333-7346.

[56] M. Zevenhoven, P. Yrjas, B.-J. Skrifvars, M. Hupa, Characterization of Ash-Forming Matter in Various Solid Fuels by Selective Leaching and Its Implications for Fluidized-Bed Combustion, Energy & Fuels, 26 (2012) 6366-6386.

[57] S.V. Vassilev, C.G. Vassileva, Y.-C. Song, W.-Y. Li, J. Feng, Ash contents and ash-forming elements of biomass and their significance for solid biofuel combustion, Fuel, 208 (2017) 377-409.

[58] I. Obernberger, T. Brunner, G. Bärnthaler, Chemical properties of solid biofuels—significance and impact, Biomass and Bioenergy, 30 (2006) 973-982.

[59] J.N. Knudsen, P.A. Jensen, K. Dam-Johansen, Transformation and Release to the Gas Phase of Cl, K, and S during Combustion of Annual Biomass, Energy & Fuels, 18 (2004) 1385-1399.

[60] S.C. van Lith, V. Alonso-Ramírez, P.A. Jensen, F.J. Frandsen, P. Glarborg, Release to the Gas Phase of Inorganic Elements during Wood Combustion. Part 1: Development and Evaluation of Quantification Methods, Energy & Fuels, 20 (2006) 964-978.

[61] B.M. Jenkins, L.L. Baxter, T.R. Miles, T.R. Miles, Combustion properties of biomass, Fuel Processing Technology, 54 (1998) 17-46.

[62] S.C. van Lith, P.A. Jensen, F.J. Frandsen, P. Glarborg, Release to the Gas Phase of Inorganic Elements during Wood Combustion. Part 2: Influence of Fuel Composition, Energy & Fuels, 22 (2008) 1598-1609.

[63] D.J. Lane, P.J. van Eyk, P.J. Ashman, C.W. Kwong, R. de Nys, D.A. Roberts, A.J. Cole, D.M. Lewis, Release of Cl, S, P, K, and Na during Thermal Conversion of Algal Biomass, Energy & Fuels, 29 (2015) 2542-2554.

[64] C. Sevonius, P. Yrjas, M. Hupa, Defluidization of a quartz bed – Laboratory experiments with potassium salts, Fuel, 127 (2014) 161-168.

[65] C. Sevonius, P. Yrjas, D. Lindberg, L. Hupa, Impact of sodium salts on agglomeration in a laboratory fluidized bed, Fuel, 245 (2019) 305-315.

[66] B. Anicic, W. Lin, K. Dam-Johansen, H. Wu, Agglomeration mechanism in biomass fluidized bed combustion – Reaction between potassium carbonate and silica sand, Fuel Processing Technology, 173 (2018) 182-190.

[67] T. Ma, C. Fan, L. Hao, S. Li, P.A. Jensen, W. Song, W. Lin, K. Dam-Johansen, Biomass ash induced agglomeration in fluidized bed. Part 2: Effect of potassium

salts in different gas composition, Fuel Processing Technology, 180 (2018) 130-139.

[68] V. Narayan, P.A. Jensen, U.B. Henriksen, P. Glarborg, W. Lin, R.G. Nielsen, Defluidization in fluidized bed gasifiers using high-alkali content fuels, Biomass and Bioenergy, 91 (2016) 160-174.

[69] R.J. Lang, Anion effects in alkali-catalysed steam gasification, Fuel, 65 (1986) 1324-1329.

[70] K. Hashimoto, K. Miura, J.-J. Xu, A. Watanabe, H. Masukami, Relation between the gasification rate of carbons supporting alkali metal salts and the amount of oxygen trapped by the metal, Fuel, 65 (1986) 489-494.

[71] K.J. Hüttinger, R. Minges, Influence of the catalyst precursor anion in catalysis of water vapour gasification of carbon by potassium: 1. Activation of the catalyst precursors, Fuel, 65 (1986) 1112-1121.

[72] D.W. McKee, Gasification of graphite in carbon dioxide and water vapor—the catalytic effects of alkali metal salts, Carbon, 20 (1982) 59-66.

[73] D.W. McKee, C.L. Spiro, P.G. Kosky, E.J. Lamby, Catalysis of coal char gasification by alkali metal salts, Fuel, 62 (1983) 217-220.

[74] M.J. Veraa, A.T. Bell, Effect of alkali metal catalysts on gasification of coal char, Fuel, 57 (1978) 194-200.

[75] L. Jiang, S. Hu, K. Xu, Y. Wang, S.S.A. Syed-Hassan, S. Su, C. Liu, J. Xiang, Formation, fates and roles of catalytic precursors generated from the K2CO3-carbon interactions in the K2CO3-catalyzed CO2 gasification of coal char, Journal of Analytical and Applied Pyrolysis, 124 (2017) 384-392.

[76] H. Zhu, X. Wang, F. Wang, G. Yu, In Situ Study on K2CO3-Catalyzed CO2 Gasification of Coal Char: Interactions and Char Structure Evolution, Energy & Fuels, 32 (2018) 1320-1327.

[77] J. Kopyscinski, M. Rahman, R. Gupta, C.A. Mims, J.M. Hill, K2CO3 catalyzed CO2 gasification of ash-free coal. Interactions of the catalyst with carbon in N2 and CO2 atmosphere, Fuel, 117 (2014) 1181-1189.

[78] P. Ehrburger, A. Addoun, F. Addoun, J.-B. Donnet, Carbonization of coals in the presence of alkaline hydroxides and carbonates: Formation of activated carbons, Fuel, 65 (1986) 1447-1449.

[79] D.W. McKee, Mechanisms of the alkali metal catalysed gasification of carbon,

Fuel, 62 (1983) 170-175.

[80] D.W. McKee, D. Chatterji, The catalytic behavior of alkali metal carbonates and oxides in graphite oxidation reactions, Carbon, 13 (1975) 381-390.

[81] Y. Wang, H. Wu, Z. Sárossy, C. Dong, P. Glarborg, Release and transformation of chlorine and potassium during pyrolysis of KCl doped biomass, Fuel, 197 (2017) 422-432.

[82] H. Chen, X. Chen, Z. Qiao, H. Liu, Release and transformation characteristics of K and Cl during straw torrefaction and mild pyrolysis, Fuel, 167 (2016) 31-39.

[83] D. Zhao, H. Liu, L. Jiang, J. Ge, L. Xu, Q. Cao, Investigation into the Relationship between Oxygen-Containing Groups and the Release of Na and Cl during Preoxidation and Pyrolysis of Na-Enriched Zhundong Coal, Energy & Fuels, 31 (2017) 11939-11946.

[84] P.J. van Eyk, P.J. Ashman, Z.T. Alwahabi, G.J. Nathan, The release of water-bound and organic sodium from Loy Yang coal during the combustion of single particles in a flat flame, Combustion and Flame, 158 (2011) 1181-1192.

[85] S. Guo, Y. Jiang, T. Liu, J. Zhao, J. Huang, Y. Fang, Investigations on interactions between sodium species and coal char by thermogravimetric analysis, Fuel, 214 (2018) 561-568.

[86] X. Qi, G. Song, W. Song, Q. Lu, Influence of sodium-based materials on the slagging characteristics of Zhundong coal, Journal of the Energy Institute, 90 (2017) 914-922.

[87] E.R. Lindner, T.F. Wall, Sodium ash reactions during combustion of pulverised coal, Symposium (International) on Combustion, 23 (1991) 1313-1321.

[88] D. Boström, N. Skoglund, A. Grimm, C. Boman, M. Öhman, M. Broström, R. Backman, Ash Transformation Chemistry during Combustion of Biomass, Energy & Fuels, 26 (2012) 85-93.

[89] K.L. Chin, P.S. H'ng, M. Maminski, W.Z. Go, C.L. Lee, R.A. Raja-Nazrin, P.S. Khoo, S.N. Ashikin, I. Halimatun, Additional additives to reduce ash related operation problems of solid biofuel from oil palm biomass upon combustion, Industrial Crops and Products, 123 (2018) 285-295.

[90] C. Gollmer, I. Höfer, M. Kaltschmitt, Additives as a fuel-oriented measure to mitigate inorganic particulate matter (PM) emissions during small-scale

combustion of solid biofuels, Biomass Conversion and Biorefinery, 9 (2019) 3-20.

[91] L. Wang, G. Skjevrak, J.E. Hustad, M. Grønli, Ø. Skreiberg, Effects of Additives on Barley Straw and Husk Ashes Sintering Characteristics, Energy Procedia, 20 (2012) 30-39.

[92] H. Chi, M.A. Pans, C. Sun, H. Liu, An investigation of lime addition to fuel as a countermeasure to bed agglomeration for the combustion of non-woody biomass fuels in a 20kWth bubbling fluidised bed combustor, Fuel, 240 (2019) 349-361.

[93] H. Risnes, J. Fjellerup, U. Henriksen, A. Moilanen, P. Norby, K. Papadakis, D. Posselt, L.H. Sørensen, Calcium addition in straw gasification☆, Fuel, 82 (2003) 641-651.

[94] C. Zhou, C. Rosén, K. Engvall, Biomass oxygen/steam gasification in a pressurized bubbling fluidized bed: Agglomeration behavior, Applied Energy, 172 (2016) 230-250.

[95] A. Grimm, N. Skoglund, D. Boström, M. Öhman, Bed Agglomeration Characteristics in Fluidized Quartz Bed Combustion of Phosphorus-Rich Biomass Fuels, Energy & Fuels, 25 (2011) 937-947.

[96] Q. Wang, K. Han, J. Wang, J. Gao, C. Lu, Influence of phosphorous based additives on ash melting characteristics during combustion of biomass briquette fuel, Renewable Energy, 113 (2017) 428-437.

[97] Q. Wang, K. Han, J. Qi, J. Zhang, H. Li, C. Lu, Investigation of potassium transformation characteristics and the influence of additives during biochar briquette combustion, Fuel, 222 (2018) 407-415.

[98] D. Lynch, A.M. Henihan, W. Kwapinski, L. Zhang, J.J. Leahy, Ash Agglomeration and Deposition during Combustion of Poultry Litter in a Bubbling Fluidized-Bed Combustor, Energy & Fuels, 27 (2013) 4684-4694.

[99] A. Grimm, N. Skoglund, D. Boström, C. Boman, M. Öhman, Influence of Phosphorus on Alkali Distribution during Combustion of Logging Residues and Wheat Straw in a Bench-Scale Fluidized Bed, Energy & Fuels, 26 (2012) 3012-3023.

[100] G. Eriksson, A. Grimm, N. Skoglund, D. Boström, M. Öhman, Combustion and fuel characterisation of wheat distillers dried grain with solubles (DDGS) and possible combustion applications, Fuel, 102 (2012) 208-220.

[101] B.-M. Steenari, A. Lundberg, H. Pettersson, M. Wilewska-Bien, D. Andersson, Investigation of Ash Sintering during Combustion of Agricultural Residues and the Effect of Additives, Energy & Fuels, 23 (2009) 5655-5662.

[102] P. Piotrowska, M. Zevenhoven, K. Davidsson, M. Hupa, L.-E. Åmand, V. Barišić, E. Coda Zabetta, Fate of Alkali Metals and Phosphorus of Rapeseed Cake in Circulating Fluidized Bed Boiler Part 1: Cocombustion with Wood, Energy & Fuels, 24 (2010) 333-345.

[103] P. Billen, B. Creemers, J. Costa, J. Van Caneghem, C. Vandecasteele, Coating and melt induced agglomeration in a poultry litter fired fluidized bed combustor, Biomass and Bioenergy, 69 (2014) 71-79.

[104] P. Billen, J. Van Caneghem, C. Vandecasteele, Predicting Melt Formation and Agglomeration in Fluidized Bed Combustors by Equilibrium Calculations, Waste and Biomass Valorization, 5 (2014) 879-892.

[105] P. Billen, J. Costa, L. van der Aa, L. Westdorp, J. Van Caneghem, C. Vandecasteele, An Agglomeration Index for CaO Addition (as CaCO3) to Prevent Defluidization: Application to a Full-Scale Poultry Litter Fired FBC, Energy & Fuels, 28 (2014) 5455-5462.

[106] C. Bourgel, E. Véron, J. Poirier, F. Defoort, J.-M. Seiler, C. Peregrina, Behavior of Phosphorus and Other Inorganics during the Gasification of Sewage Sludge, Energy & Fuels, 25 (2011) 5707-5717.

[107] J.H. Zeuthen, P.A. Jensen, J.P. Jensen, H. Livbjerg, Aerosol Formation during the Combustion of Straw with Addition of Sorbents, Energy & Fuels, 21 (2007) 699-709.

[108] J. Kaknics, R. Michel, J. Poirier, Miscanthus ash transformation and interaction with bed materials at high temperature, Fuel Processing Technology, 141 (2016) 178-184.

[109] T. Ma, C. Fan, L. Hao, S. Li, W. Song, W. Lin, Biomass-Ash-Induced Agglomeration in a Fluidized Bed. Part 1: Experimental Study on the Effects of a Gas Atmosphere, Energy & Fuels, 30 (2016) 6395-6404.

[110] A.R. Manzoori, P.K. Agarwal, The role of inorganic matter in coal in the formation of agglomerates in circulating fluid bed combustors, Fuel, 72 (1993) 1069-1075.

[111] P.J. van Eyk, A. Kosminski, P.J. Ashman, Control of Agglomeration and Defluidization during Fluidized-Bed Combustion of South Australian Low-Rank Coals, Energy & Fuels, 26 (2012) 118-129.

[112] D.P. McCullough, P.J. van Eyk, P.J. Ashman, P.J. Mullinger, Impact of Sodium and Sulfur Species on Agglomeration and Defluidization during Spouted Bed Gasification of South Australian Lignite, Energy & Fuels, 29 (2015) 3922-3932.

[113] S. Byung Ho, K. Sang Done, Catalytic activity of alkali and iron salt mixtures for steam-char gasification, Fuel, 72 (1993) 797-803.

[114] K.J. Hüttinger, R. Minges, Catalytic water vapour gasification of carbon: Importance of melting and wetting behaviour of the 'catalyst', Fuel, 64 (1985) 491-494.

[115] A. Kosminski, D.P. Ross, J.B. Agnew, Influence of gas environment on reactions between sodium and silicon minerals during gasification of low-rank coal, Fuel Processing Technology, 87 (2006) 953-962.

[116] H.H. Weldes, K.R. Lange, PROPERTIES OF SOLUBLE SILICATES, Industrial & Engineering Chemistry, 61 (1969) 29-44.

[117] R.C. Merrill, Chemistry of the soluble silicates, Journal of Chemical Education, 24 (1947) 262.